Growth of Platinum Clusters in Solution and on Biopolymers: The Microscopic Mechanisms

DISSERTATION

zur Erlangung des akademischen Grades

Doktor im Ingenieurwesen
(Dr. Ing.)

vorgelegt

an der Fakultät Maschinenwesen
der Technischen Universität Dresden

von

Lucio Colombi Ciacchi

geboren am 23. Juli 1973 in Udine (Italien).

Eingereicht am 18. Dezember 2001
Verteidigt am 5. Juli 2002

Antwortsbang der Mensch, antwortsbang die Erkenntnis,
erkenntnisgebunden der Mensch, menschheitsgebunden die Erkenntnis,
sie beide ineinandergebunden und antwortsbang,
überwältigt von der Gotteswirklichkeit des Vor-Wissens,
von der Wirklichkeitsweite der wissenden Frage, die
von keiner irdischen Antwort, von keiner irdischen Erkenntniswahrheit
je zu erreichen ist und doch nur hier
im Irdischen beantwortet werden kann, beantwortet werden muß.

Hermann Broch, aus dem Roman *Der Tod des Vergil*.

Contents

Introduction

Metal clusters are fanciful and unforeseeable molecules. This is why they are extremely fascinating. Clusters have eluded for over a century every attempt of systematic classification and of confinement in a narrow field of science. Rather, chemists, physicists, and material scientists have contributed together to the development of a *transversal* discipline: cluster science [1–3].

The increasing knowledge in cluster science has been supported by the rapid development of novel techniques which have permitted more and more accurate investigations. An impressive acceleration in the understanding of the chemistry of clusters has been promoted by the development of X-ray diffraction and transmission electron microscope techniques. This has made possible the systematic correlation between the chemical reactions leading to cluster formation and the atomic structure of the final product. Many questions related to the cluster synthesis (in particular about the role of different reducing agents and stabilizing polymers) have been successfully investigated. Methods have been developed for the synthesis of clusters with control of their size [4,5] and, with some limitation, of their shape [6]. In the last twenty years, the development of powerful, massively parallel computers has made possible theoretical calculations of various chemical and physical properties of metal clusters by means of ab initio methods, mainly based on the density functional theory [7–9]. However, the microscopic mechanism through which metal clusters form remains difficult to understand [10]. In particular, the elementary steps leading to the nucleation and growth of transition metal clusters upon chemical reduction of metal salts are, at the present time, not yet clear at the atomic scale. This is mainly due to the fast reaction times characterizing the nucleation process and to the variety of oxidation states of the reactants and products, which makes difficult both theoretical and experimental investigations.

This problem is addressed in the present thesis theoretically by means of first-

principles molecular dynamics techniques [11]. Our goal is to propose a microscopic mechanism for the formation of platinum nanoparticles after reduction of Pt(II) complexes, both free in solution and supported by biopolymers. Platinum clusters are of special interest because of their unique electronic and catalytic properties. Precise knowledge about the elementary steps of the Pt cluster formation is needed to achieve a controlled growth of nanoparticles in solution or supported by inorganic and organic substrates.

On the one hand, control on the cluster formation process is fundamental in catalysis where metal clusters find the most important applications. Indeed, the catalytic activity of a colloidal suspension of metal particles depends on the particle size distribution, on the particle morphology, and on the particle composition (in the case of heteronuclear clusters). In principle, all these parameters could be tuned by accurately controlling the process of particle nucleation and growth. On the other hand, in the recent years noble metal clusters have been employed as nanosized building blocks for the "bottom-up" fabrication of nanostructures. In particular, the metal coating of biopolymers is a very promising route to producing complex bio-inorganic structures [12–14]. To achieve a clean metallization process and to obtain a metal coating reflecting the symmetry of the underlying template, a purely heterogeneous nucleation of clusters on the biomolecules appears to be necessary. Otherwise, the spurious homogeneous formation of clusters in the solution invariably leads to irregular and coarse structures [13, 14]. Therefore, it is of great importance to establish a metallization procedure where the nucleation and growth of the clusters are controlled *in situ* by the organic template. To achieve this goal, the knowledge of the mechanisms of cluster nucleation and growth is once again fundamental.

In this work, both the homogeneous cluster formation in solution and the heterogeneous cluster formation on biopolymers (proteins and DNA) after reduction of a dissolved K_2PtCl_4 salt are explored. The primary questions which our investigations will address are: (i) how the reduction process is influenced by the hydrolysis of the metal complexes; (ii) what can be considered a "critical nucleus" for a stable cluster growth; (iii) why the cluster growth appears to be an

autocatalytic process; (iv) which role in the heterogeneous cluster nucleation play organometallic complexes formed between the metal salt and the organic template before the reduction; and finally (v) how can an organic template actively promote the heterogeneous nucleation of clusters. Parallel to the theoretical simulations –which are the main subject of this thesis– metallization experiments performed within our research group will be presented. Through a combined use of theoretical and experimental techniques, our final goal is to develop a novel methodology for a template-controlled metallization of biomolecular substrates.

The first chapter of this thesis deals with a review of fundamental concepts of cluster science and of relevant applications of noble metal clusters. The first-principles molecular dynamics techniques used throughout this work are described in chapter 2. The initial formation of Pt–Pt bonds between dissolved Pt(II) complexes after reduction is studied in chapter 3. In chapter 4, we investigate the addition of Pt complexes to growing clusters. The heterogeneous formation of Pt clusters on DNA molecules is studied in chapter 5. Finally, the results are briefly summarized in the last chapter.

All the computational resources needed for our simulations have been provided by the Center for High Performance Computing at the Dresden University of Technology. The calculations are performed with the highly optimized, massively parallel LAUTREC code [15].

Chapter 1

Metal clusters

1.1 Definitions

1.1.1 Clusters of metal atoms

The term *metal cluster* was introduced in the 1960s by F. A. Cotton [16,17], who proposed the following **definition**:

> A *metal cluster* is a finite group of metal atoms that are held together entirely, mainly, or at least to a significant extent, by bonds directly between the metal atoms, even though some nonmetal atoms may also be intimately associated with the cluster.

This definition states that a group of atom can be classified as a cluster only in the presence of at least one *direct* metal–metal bond. Molecules where metal atoms are only indirectly bound (via, e.g., bridging ligands) are not properly clusters. Notably, for many compounds it is absolutely not trivial to decide whether the atoms are directly bound or not. It was stated that to characterize the nature and the extent of the metal–metal interactions in metal clusters is one of the most challenging problems for theoreticians [18]. It will be shown in chapter 3 that such information can be at least partially obtained by using modern chemical concepts based on quantum mechanical formalisms, and requires the knowledge of the wave-functions of the whole system.

Accordingly to the definition above, a metal cluster may contain non-metallic atoms. *Naked* clusters (containing only metal atoms) are produced by evaporation of metals and condensation of the atoms in noble gas atmosphere [19]. All others chemical or physical synthetical routes lead to *ligated* clusters, where a metallic

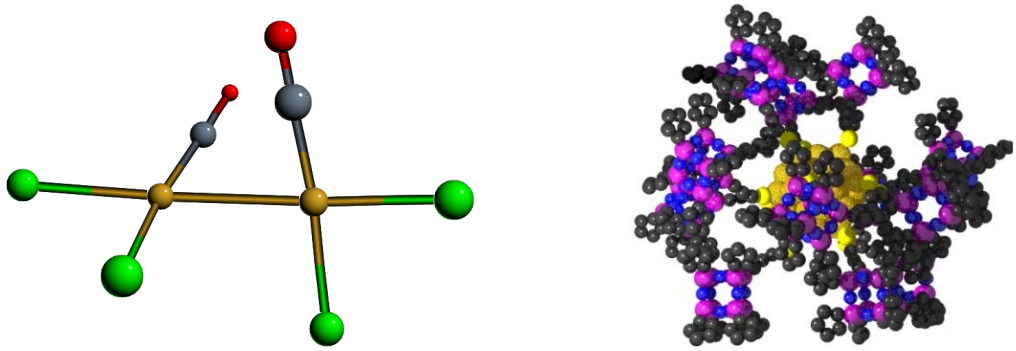

Figure 1.1: Examples of ligated metal clusters. (Left) The $[Pt_2(CO)_2Cl_4]^{2-}$ ion [22]. (Right) An Au_{55} cluster stabilized by silsesquioxane ligands [23].

core is embedded in a non-metallic *ligand shell* [2] (figure 1.1). The electronic (and thus the chemical and physical) properties of a ligated cluster strongly depend on the nature of the ligand shell [18]. This is true both for small clusters of few atoms, such as those in figure 1.1, and for big clusters of some thousand atoms [21] (see figure 1.3).

1.1.2 Colloids

The definition of Cotton does not set a maximum limit for the size of metal clusters. However, if the number of metal atoms reaches the order of magnitude of 10^4, then it is more correct to speak about a small crystal than about a cluster. On the other side, very small crystals have physical and chemical properties different from those of the bulk. For instance, if crystals smaller than 1 μm are immersed in a solvent, even if the solid phase is not soluble in the liquid one, no sedimentation occurs and a stable, *glue-like* suspension is obtained, especially in the presence of organic polymers. This observation led to the concept of *colloidal* suspension, and to the following commonly accepted **definition**:

> A *colloid* is a particle that, if immersed in a liquid phase, cannot sediment spontaneously out of the solution without centrifugation.

In particular, if organic molecules are present in solution in sufficient concentration, they adsorb on the metal surface and can stabilize the particle suspension.

Such molecules are called *surfactants*, *capping agents*, or *stabilizers*. Thus, a metal colloid [24] is composed by a small metal crystal embedded in a shell of surfactants. There is a strict analogy between a colloid (metal particle and surfactant shell) and a cluster (metal core and ligand shell). Indeed, colloids follow perfectly the definition of cluster given by Cotton, and clusters the definition of colloid reported above.

1.1.3 Giant clusters

From a chemical point of view, it is desirable to speak about clusters only in the case of *molecules* which can be thoroughly characterized. That is, cluster must have a defined formula unit and a precise, investigable, structure. To date, very big clusters have been isolated and their structures have been univoquely determined (see figure 1.1, right). Typical examples are $Au_{55}(PPh_3)_{12}Cl_6$ [25] and $[Ni_{38}Pt_6(CO)_{48}]^{6-}$ [26], where the metal cores have dimension of about 1 nm. In addition, on the basis of data from various spectroscopic and microscopic techniques combined with elemental analysis and molecular weight measurements, *giant clusters* have been structurally characterized [21, 27]. Giant clusters consist of a core of noble metal atoms stabilized by a shell of ligands or surfactants. The number of atoms in the metal core follows the series of Chini *magic numbers* [28], which correspond to a FCC close packing of atoms in icosahedral or cuboctahedral shells (figure 1.2). A $Pt_{\sim 2057}$ cluster consisting of 17 (111) layers of atoms found on a protein after metallization (see section 1.3.2 and figure 1.4) is shown in figure 1.3.

Giant clusters form colloidal suspensions in the most common solvents. It is usual to speak about colloids if the size of the metal core lies between 1 and 100 nm, and about clusters for metal cores containing from 2 up to about 5000 atoms. Particles in the size-range 1-10 nm, which are the subject of this thesis, can be considered either clusters or colloids, both definitions being correct. Additionally, the term *nanoparticles* is commonly used especially in the materials science community. This term is a synonym for colloids, but is more generally

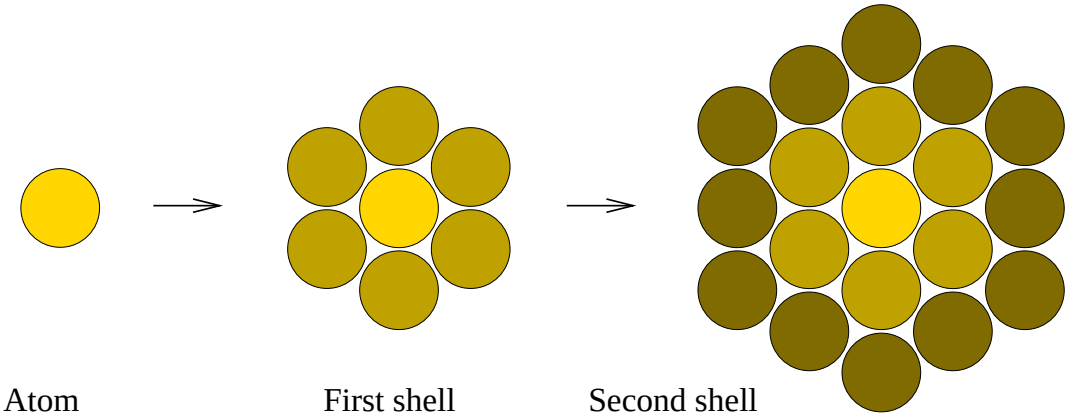

Figure 1.2: Schematic representation of closed shell clusters with nuclearity following the series of Chini magic numbers.

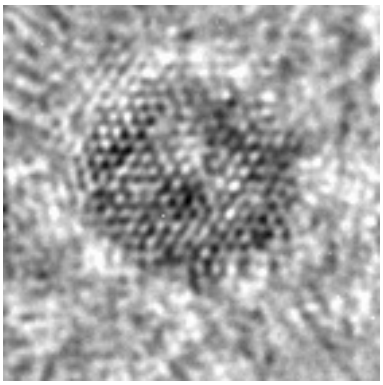

Figure 1.3: A platinum cluster consisting of 8 atomic shells ($Pt_{\sim 2057}$) supported by a protein substrate and imaged by HRTEM [29]. The size of the cluster is about 3.5 nm.

applicable to all cases where the liquid phase is absent, as, e.g., in the case of metallic particles deposited from the gas phase on a solid substrate. Thus, in the following we will speak about clusters, colloids or nanoparticles as equivalent synonyms.

1.2 Physical and chemical properties

It is interesting to investigate how the physical and chemical properties of clusters change with increasing the cluster *nuclearity*, which is defined as the number of metal atoms contained in the cluster. In this way, the transition from the atom to the molecule, to the colloid up to the bulk can be followed in a systematic way. Excellent reviews about this topic have been recently published [7, 8, 18]. In this section, we summarize briefly some fundamental concepts with particular attention paid to structure and energetics of naked clusters, which are important for the investigation of the cluster growth mechanism (chapter 4).

1.2.1 Naked clusters: from the atom to the bulk

Naked clusters can be produced by evaporation of a metal and subsequent condensation of the atoms in an inert gas. By means of a mass spectrometer, clusters of specific nuclearities can be selected and adsorbed on a ceramic surface for further investigations [19]. It should be noted that the underlying surface has a strong influence on the cluster properties [7, 19]. For this reason, it is more correct to speak about *supported* rather than naked clusters. Experimental investigations of really naked clusters should be performed in the gas phase [30]. However, because of the difficulties inherent in this kind of investigations, naked cluster are studied mainly theoretically.

Structure and energetics of naked clusters

Total energy calculations of transition metal clusters have been performed with a variety of techniques, which span from empirical methods up to high-accuracy

quantum mechanical calculations [9]. The results concerning structure and energetics of small metal clusters are generally all in qualitative agreement. An important quantity related to the stability of a cluster is the cohesive energy per atom, which is defined by:

$$E_{coh} = -\frac{1}{N}(E_N - E_{at}) \ , \tag{1.1}$$

where E_N is the total energy of a cluster of N atoms and E_{at} is the total energy of the isolated atom. Generally, E_{coh} increases with the cluster nuclearity, and is roughly proportional to the mean number of metal–metal bonds engaged by each atom (the average coordination number) [18, 31]. Interestingly, clusters with different geometries, but with the same average coordination number, have about the same mean cohesive energy. In order to increase the mean coordination number, and thus to increase the stability, the structure of metal clusters tends to minimize the surface-to-volume ratio. This leads to preferred FCC arrangements of atoms into icosahedral or cuboctahedral structures, or, more generally, into stacked layers of atoms with triangular lattice structures [20].

The mean metal–metal distance in naked clusters increases with the number of atoms. In the case of platinum clusters, the Pt–Pt distance varies between 2.45 Å in the dimer to 2.77 Å in the bulk. Accordingly, the metal–metal bond energy is higher in small clusters than in the bulk. Like the mean cohesive energy, also the mean bond distance is proportional to the average coordination number and not to the number of atoms. Thus, a key factor in the stability of metallic systems is the number of bonds per atoms, regardless of the geometric details of the structure [31].

The electron affinity (EA) is increased passing from the atom to the bulk, and, correspondently, the ionization potential (IP) is decreased. Within the classical spherical droplet model, the EA and the IP of a metallic particle of radius r are:

$$\mathrm{IP}(r) = W + \alpha e^2/r \tag{1.2}$$

$$\mathrm{EA}(r) = W - \beta e^2/r \ , \tag{1.3}$$

where W is the work function of the metal. We note that this classical model

is, in principle, valid only for cluster dimensions where quantum-size effects are negligible. In spite of this, calculated IP and EA values of very small Au clusters (with r ranging from 0.3 to 1 nm) show a clear linear dependence with $1/r$, which leads to an extrapolated value of W very close to the experimental one [7]. Thus, clusters of few tens of atoms already present evident metallic character. Accordingly, the HOMO-LUMO energy gap decreases very fast with the particle nuclearity. For clusters of 13 atoms gaps of about 0.1 eV were calculated [7].

1.2.2 Ligated clusters

All the physical and chemical properties of metal clusters are strongly influenced by the ligand shell. The formation of bonds between the surface atoms of a cluster and the ligands induces a perturbation on the electronic states of the metal core. The effects are strongly dependent on the ligand type, and on the ligand distribution around the metal core. In particular, the same metal atoms can be stabilized by slightly different ligands in a rich variety of structures and isomers. Other typical ligand effects are the quenching of magnetic moments and the changing of optical properties of the metal core [7].

Very common ligands are carbonyl, phosphine, phenantroline, or long polymers such as, e.g., polyacrilate. In addition to the ligand shell, an electric double layer can be present on the cluster surface, due to the presence of free ions (Cl^-, Na^+, etc.) in solution. In general, the metallic cluster surface is very reactive toward physisorption and chemisorption of almost all classes of compounds.

1.3 Application fields

1.3.1 Catalysis

Since a century, the most important application field for noble metal particles is catalysis. The high chemical activity of a colloidal suspension mainly arises from the high number of unsaturated surface atoms. In addition, the reduced particle dimension leads to quantum-size effects due to the breaking of the elec-

tronic band symmetry proper of the bulk. Clusters of few atoms are of special interest, because their chemical activity presents discontinuous changes with unitary variations of the cluster nuclearity [19]. In industrial applications, clusters are either used in colloidal form, or supported by a solid substrate, such as e.g, zeolites and others porous ceramics. The group of chemical reactions in which metal clusters are active catalysts includes especially hydrogenation and related reactions (hydrosilylation, hydration of unsaturated organic molecules et cetera). The catalytic activity of noble metals toward oxidation reactions (a typical example is the oxidation of CO) is the reason why ceramic-supported platinum catalysts are widely used in the automobile industry. The catalytic action of colloidal metals is finally involved in important processes such as photography and electroless metal deposition. For comprehensive reviews we refer to the extensive specialized literature [1, 2].

1.3.2 Nanostructure fabrication

In the recent years, organic nanostructures have been fabricated via a "bottom up" approach, i.e., via the assembly of small structural elements (monomers) into supramolecular complexes [32]. The idea underlying this novel method of nanostructure fabrication is to mime natural processes (occurring, e.g., in living cells) which lead spontaneously to the build-up of complex ordered structures. The spontaneous coalescence of monomers without any external manipulation is called *self-assembly* [32] and is mainly driven by formation of hydrogen bonds and by electrostatic interactions between the monomers. By recreating in vitro the conditions necessary to the self-assembling of isolated structural units, a variety of organic *biomimetic* structures could be obtained [33]. However, the range of technological interest of purely organic structures is small because of their poor mechanical properties and of their limited chemical and thermal stability [34].

On the other hand, it is possible to coat a preformed organic structure (*template*) either with a film of metal or with isolated metallic, nanosized particles [12–14, 29, 35–38]. Both in the case of complete metal coating and in the

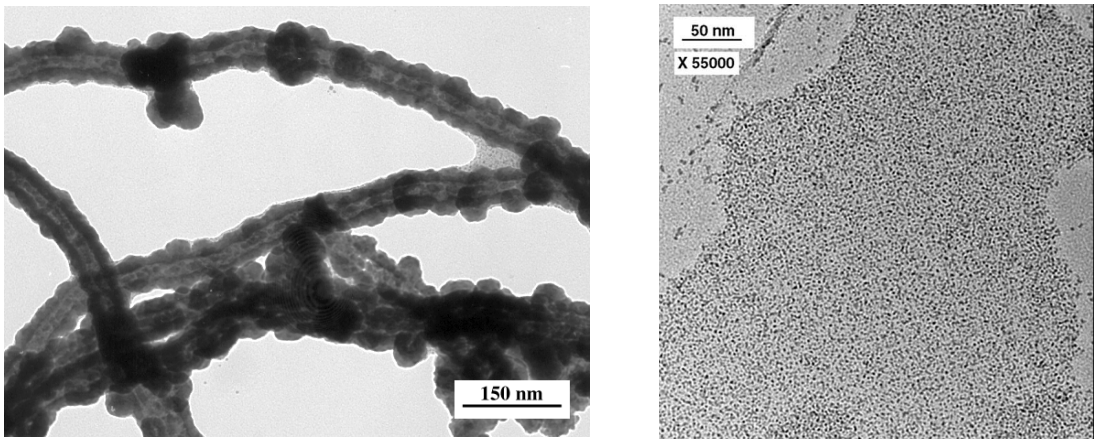

Figure 1.4: (Left) Microtubules coated with a film of nickel grown on the protein surface [36]. (Right) Bacterial S-layer covered with an array of platinum clusters which reflects the fourfold symmetry of the underlying protein template [29]. A HRTEM micrograph of a selected cluster is shown in figure 1.3.

case of deposition of isolated particles, it is common to speak about *metallization* of the template [35]. Biological, self-assembled metallization templates such as bacterial surface layers (S-Layers) [39] are of particular interest because of the periodicity of the protein network. The regular spatial modulation of the physical and chemical properties of the surface makes biotemplates ideal for a space-controlled metallization. Examples of metallized proteins are shown in figure 1.4. However, if metal particles form homogeneously in solution as well as heterogeneously on the template, the obtained metallized structure invariably presents undesired inhomogeneities due to diffusion-driven processes of particle agglomeration. A selectively heterogeneous metallization can be obtained only under the condition that the template itself is able to induce and to control the formation of metal particles. In particular, in order to develop a template-controlled metallization procedure, accurate knowledge about the mechanism of metal cluster formation after the reduction of dissolved metal salts is required. To this aim, the molecular mechanism of homogeneous metal cluster formation in solution will be investigated in chapters 3 and 4, while the heterogeneous metal cluster formation on biological templates (such as, e.g., DNA) will be addressed

in chapter 5. The computational techniques used for these investigations are the subject of the following chapter.

Chapter 2

First Principles Molecular Dynamics

This chapter deals with a brief description of the First Principles Molecular Dynamics (FPMD) technique [11] based on the scheme of Car and Parrinello (CP) [40] which is used throughout this thesis. In the FPMD approach, the forces acting on the atoms are computed from the electronic wave functions obtained within the Density Functional Theory (DFT). The motion of the atomic nuclei is then described by classical Newton equations. In this thesis, a relevant role is played by metallic systems (see chapter 4), which are generally difficult to treat with FPMD techniques. For this reason, the algorithms recently developed to deal with metallic systems in the framework of the CP method will be described with particular care.

2.1 Basics of Density Functional Theory

In this section the fundamental concepts of the Density Functional Theory [41,42] are presented. We refer to fundamental literature [43–46] for accurate descriptions of the formalism.

2.1.1 Adiabatic approximation

Within the Schrödinger picture of quantum mechanics, the temporal evolution of a molecular system is described by the wave equation:

$$\mathcal{H}(\{\mathbf{R}_m\},\{\mathbf{r}_n\},t)\Phi(\{\mathbf{R}_m\},\{\mathbf{r}_n\},t) = i\hbar\frac{\partial\Phi(\{\mathbf{R}_m\},\{\mathbf{r}_n\},t)}{\partial t}\ , \qquad (2.1)$$

where $\mathcal{H}$ is the Hamiltonian operator of the whole system and Φ is the corresponding wave function. Both depends on the coordinates of the nuclei $\{\mathbf{R}_m\}$, on coordinates of the electrons $\{\mathbf{r}_n\}$, and on the time t.

If the evolution of the system under observation is so that no energy is exchanged between nuclei and electrons, then the nuclear and electron dynamics can be considered separately, according to the *adiabatic approximation* [47]. This approximation can be simply justified by the facts that the typical nuclear masses are much larger than the electronic mass, and that in many cases the motion of the electrons is much faster than the typical motion of the nuclei. Thus, the electrons follow instantaneously the nuclei and can be considered any time in their ground state. This approach cannot be applied in non-adiabatic processes such as scattering and electron transfer reactions, but is very useful to simulate a large number of chemical reactions. At fixed nuclei position, the stationary Schrödinger equation of the electrons reads:

$$\hat{H}(\{\mathbf{R}_m\},\{\mathbf{r}_n\})\Psi(\{\mathbf{r}_n\}) = E_0(\{\mathbf{R}_m\})\Psi(\{\mathbf{r}_n\}) \;, \tag{2.2}$$

where the wave function of the electrons, Ψ, depends on the electronic coordinates only, and the Hamiltonian of the electronic system, $\hat{H}$, contains the nuclear coordinates as parameters. The solution of the equation 2.2 leads to the ground state energy E_0, which defines the potential for the motion of the nuclei. E_0 can then be plugged into the Schrödinger equation for the nuclei, or can be used to solve the classical Newton equations of motion:

$$M_I\ddot{\mathbf{R}}_I = -\frac{dE_0(\{\mathbf{R}_m\})}{d\mathbf{R}_I} \;. \tag{2.3}$$

Quantum description of the nuclear dynamics is useful in some particular case (e.g., to describe nuclear tunneling), especially in the case of hydrogen atoms [48]. Otherwise, the nuclei can be treated as classical particles with masses M_I.

2.1.2 The Hohenberg-Kohn and Kohn-Sham approaches

So far, the problem has been reduced to the solution of the many-electrons stationary wave equation 2.2. Considering N electrons, the Hamiltonian of the

electronic system, $\hat{H}$, can be written as[1]:

$$\hat{H} = \hat{T} + \hat{V}_{ee} + \hat{V}, \tag{2.4}$$

where

$$\hat{T} = \sum_{i=1}^{N} -\frac{1}{2}\nabla_i^2 \tag{2.5}$$

is the kinetic energy operator;

$$\hat{V}_{ee} = \sum_{i<j} \frac{1}{|\mathbf{r}_i - \mathbf{r}_j|} \tag{2.6}$$

is the electron-electron repulsion energy operator; and

$$\hat{V} = \sum_{i=1}^{N} v(\mathbf{r}_i) \tag{2.7}$$

with

$$v(\mathbf{r}_i) = -\sum_{\alpha} \frac{Z_\alpha}{|\mathbf{r}_i - \mathbf{R}_\alpha|} \tag{2.8}$$

is the external potential of the nuclei charged Z_α.

The Hohenberg-Kohn theorem

It is important to note that, given N electrons, $\hat{T}$ and $\hat{V}_{ee}$ are univocally defined, so that the Hamiltonian of the system and all its ground state properties depend uniquely on the choice of the external potential v. In particular, the electron density

$$\rho(\mathbf{r}_1) = N \int |\Psi(\mathbf{r}_1, \mathbf{r}_2, \ldots, \mathbf{r}_N)|^2 d\mathbf{r}_2 \ldots d\mathbf{r}_N \tag{2.9}$$

remains defined by the choice of v, or, more precisely, ρ is a unique *functional* of the external potential: $\rho = \rho[v]$. By reversing this approach, the **theorem of Hohenberg and Kohn** [41] states that:

> the ground state density ρ of a many electron system uniquely determines the external potential v (modulo a constant).

[1] From this point, all expression will be written considering atomic units.

The theorem above establishes that N and ρ, instead of N and v, can be chosen as fundamental variables to solve the many-body electronic problem 2.2. Solving the Schrödinger equation is equivalent to minimize the energy functional $E[\Psi] = \langle\Psi|\hat{H}|\Psi\rangle$ with respect to all the wave functions of N electrons:

$$E_0 = \min_{\Psi} \langle\Psi|\hat{H}|\Psi\rangle \ . \tag{2.10}$$

Choosing the density as fundamental variable, the many-body problem can be solved by minimizing the functional $E[\rho]$ with respect to ρ, considering all wave functions having ρ as electron density:

$$\begin{aligned} E_0 &= \min_{\rho} \left\{ \min_{\Psi\to\rho} \langle\Psi|\hat{H}|\Psi\rangle \right\} \\ &= \min_{\rho} \left\{ \int v(\mathbf{r})\rho(\mathbf{r})d\mathbf{r} + \min_{\Psi\to\rho} \langle\Psi|\hat{T}+\hat{V}_{ee}|\Psi\rangle \right\} \\ &= \min_{\rho} \left\{ V[\rho] + F[\rho] \right\} \ , \end{aligned} \tag{2.11}$$

where we have defined:

$$\begin{aligned} V[\rho] &= \int v(\mathbf{r})\rho(\mathbf{r})d\mathbf{r} \\ F[\rho] &= \min_{\Psi\to\rho} \langle\Psi|\hat{T}+\hat{V}_{ee}|\Psi\rangle \ . \end{aligned} \tag{2.12}$$

The Kohn-Sham equations

The functional $F[\rho]$ still contains the complexity of the original many-body problem, which originates from the potential $\hat{V}_{ee}$ (i.e., from the electron-electron interactions), and is still unknown. For a system of *non interacting* electrons in the external potential v, in addition to the functional $V[\rho]$ we would also know the kinetic and electrostatic (Hartree) contributions to the total energy, which are:

$$\begin{aligned} T_0[\rho] &= \min_{\Psi} \langle\Psi|\hat{T}|\Psi\rangle \\ E_H[\rho] &= \frac{1}{2}\iint \frac{\rho(\mathbf{r})\rho(\mathbf{r}')}{|\mathbf{r}-\mathbf{r}'|} d\mathbf{r}d\mathbf{r}' \ . \end{aligned} \tag{2.13}$$

For interacting electrons, the remaining contributions to the total energy can be put together in an *exchange and correlation* functional, defined by:

$$E_{xc}[\rho] = F[\rho] - T_0[\rho] - E_H[\rho] \ . \tag{2.14}$$

From the 2.11 and 2.14, the total energy can be rewritten as:

$$\begin{aligned} E_0 &= \min_{\rho} \{T_0[\rho] + V[\rho] + E_H[\rho] + E_{xc}[\rho]\} \\ &= \min_{\rho} \{T_0[\rho] + V_{KS}[\rho]\} \ , \end{aligned} \tag{2.15}$$

where the *Kohn-Sham* functional V_{KS} has been defined. At this point, looking at the 2.15, it is immediate to recognize that the same minimum condition would be fulfilled by a system of N *non interacting* electrons in the *fictive* Kohn-Sham potential:

$$v_{KS}(\mathbf{r}) = v(\mathbf{r}) + \int \frac{\rho(\mathbf{r}')}{|\mathbf{r} - \mathbf{r}'|} d\mathbf{r}' + \frac{\delta E_{xc}[\rho(\mathbf{r})]}{\delta \rho(\mathbf{r})} \ , \tag{2.16}$$

the last term being the exchange-correlation potential v_{xc}.

In this way, the problem 2.2 for N interacting electrons can be mapped onto a set of N problems for non-interacting electrons, the so-called **Kohn-Sham equations** [42]:

$$\left(-\frac{1}{2}\nabla^2 + v_{KS}(\mathbf{r})\right)\psi_i(\mathbf{r}) = \varepsilon_i \psi_i(\mathbf{r}) \qquad i = 1 \ldots N \ , \tag{2.17}$$

which we are able to solve in a self-consistent way, *given the exchange-correlation potential* v_{xc}. The wave functions ψ_i are the single-particle Kohn-Sham orbitals, from which the density can be calculated as:

$$\rho(\mathbf{r}) = \sum_{i=1}^{N} \psi_i^*(\mathbf{r})\psi_i(\mathbf{r}) \ . \tag{2.18}$$

2.1.3 Solution of the Kohn-Sham equations

Local Density Approximation

Within the adiabatic approximation, the DFT formulation presented above is *exact*. However, in order to practically solve the many-body problem, it is necessary to know the exchange-correlation potential v_{xc}, and there is no way to know it exactly. An approximation that leads to surprisingly small errors in the calculation of ground state properties of a given system is the so-called *local-density approximation* (LDA). The assumptions made within the LDA are that (i) at a point $\mathbf{r}$, $v_{xc}(\mathbf{r})$ only depends on the density at $\mathbf{r}$; and (ii) given locally a density

$\rho(\mathbf{r})$, v_{xc} is equal to the exchange-correlation potential of a *homogeneous electron gas* of density ρ:

$$v_{xc}^{LDA}(\mathbf{r};\rho) = v_{xc}^{hom}(\rho(\mathbf{r})) \ . \tag{2.19}$$

The exchange-correlation potential of a homogeneous electron gas can be splitted in an exchange part, which is calculated exactly, and in a correlation part, which is normally parameterized on values calculated very accurately by Quantum Monte Carlo techniques [49, 50].

A natural, but not trivial, extension of the LDA approximation is to consider also the dependence of v_{xc} on the gradient (and on the Laplacian) of the density:

$$v_{xc}^{GGA}(\mathbf{r};\rho) = v_{xc}\left(\rho(\mathbf{r}), |\nabla\rho(\mathbf{r})|, \nabla^2\rho(\mathbf{r})\right) \ . \tag{2.20}$$

Various form of *generalized gradient approximations* (GGA) have been developed up to now,[2] which in general improve the computed values of bond energies with respect to the simple LDA approach. In particular, the hydrogen bond can be correctly described only within GGA approximations. However, it is to note that there is no *formal* improvement passing from LDA to GGA. The weakness of the DFT formalism, which lies in the approximate description of correlation effects, giving sometimes not negligible errors [53], still remains to be overcome.

Plane-wave expansion of the Kohn-Sham orbitals

In crystalline solids, the Kohn-Sham orbitals ψ_i can be written according to the Bloch's theorem as products of a periodic part u_i and a wavelike part:

$$\psi_i(\mathbf{r}) = u_i(\mathbf{r})\, e^{i\mathbf{k}\cdot\mathbf{r}} \ , \qquad u_i(\mathbf{r}+\mathbf{a}) = u_i(\mathbf{r}) \ , \tag{2.21}$$

where $\mathbf{a}$ is a lattice vector of the crystalline system. It is always possible to expand u_i using a set of plane-waves, whose wave vectors are the reciprocal lattice vectors of the crystal, defined by $\mathbf{G}\cdot\mathbf{a} = 2\pi m$, where m is an integer. Therefore, the orbitals ψ_i can be written as an expansion in plane waves:

$$\psi_i(\mathbf{r}) = \sum_{\mathbf{G}} c_{i,\mathbf{k}+\mathbf{G}}\, e^{i(\mathbf{k}+\mathbf{G})\cdot\mathbf{r}} \ . \tag{2.22}$$

[2] In the calculations of this thesis we use the PW91 GGA functional [51] implemented according to Ref. [52].

It is possible to make use of periodic boundary conditions and plane-wave expansions even if the system to model is not a crystalline solid, but an isolated molecule. In this case the molecule is placed in a periodically repeated *supercell* which must be large enough to prevent any spurious interaction between the system and its repeated images.

The cell vectors $\mathbf{k}$ of the Bloch orbitals are in principle an infinite set. However, it is possible to expand the orbitals ψ_i only over a finite set of $\mathbf{k}$-points (the so-called *special points*). This is allowed because the values of ψ at $\mathbf{k}$-points that are close together is almost identical, so that a whole region of the reciprocal space can be represented by a special point (see for instance Ref. [54]). It is always possible to chose a set of $\mathbf{k}$-points sufficiently dense to compute correctly all electronic properties of the system. In any case, the convergence of the total energy with the number of special points should be checked.

Also the number of coefficient $c_{i,\mathbf{G}}$ is infinite, but in the practical computations the plane-wave summation is performed only over waves with kinetic energy below a limit value $E_{cut} = |\mathbf{k} + \mathbf{G}_{cut}|^2/2$, which is called *cut-off* energy. The error made in the calculation of, e.g., the total energy can be systematically reduced by increasing the value of E_{cut} until convergence is achieved.

Pseudopotentials

The number of waves necessary to correctly expand the Kohn-Sham orbitals can be drasticly reduced by considering in the calculation only the valence electrons, and by including the effect of the core electrons in an appropriate external potential v. Otherwise, the rapid oscillations of the valence orbitals in the core region (necessary to maintain the orthogonality with the low-lying, tightly bound core orbitals) needs a very large number of plane wave components to be correctly described. The wave functions are thus replaced by smooth *pseudo wave functions*, and the true potentials of the nuclei by *pseudopotentials*. The system will then consist of valence electrons and *ions*, i.e., the nuclei with the surrounding core electrons.

A well working pseudopotential should (i) give the same spectrum of valence states as the true potential; (ii) have pseudo wave functions that coincide with the real wave functions at a fixed distance from the nucleus (the *core radius*); (iii) reproduce correctly the chemistry of the atoms in different compounds, oxidation states, or ionization conditions. In particular, the last property is the so-called *transferability* of the pseudopotential, and is related both to the eigenvalue spectrum of the pseudo wave functions and to their absolute magnitude outside the core radius. *Norm conserving* pseudopotentials [3] ensure that the integrals of the squared amplitudes of the real and the pseudo wave functions in the core region (and thus in the valence region) have the same value, and present a very good transferability. In addition, it is necessary to ensure that the pseudopotential is able to reproduce the scattering properties of the nuclei and core electrons for the real valence wave function. In particular, the scattering from the ions is different for each angular momentum component of the valence wave functions, so that the general form for a pseudopotential is:

$$v(\mathbf{r}) = \sum_{lm} |Y_{lm}\rangle \, v_l(\mathbf{r}) \, \langle Y_{lm}| \ , \tag{2.23}$$

where Y_{lm} are the spherical harmonics and v_l is the part of the pseudopotential generated for the wave function component with angular momentum l. In this way, the ionic potential is completely *non local*, and the wave functions have to be projected onto each angular momentum component. To reduce the computational effort, it is very useful to split the ionic potential in a local part and in a non-local part in such a way that every single state can be projected onto a single angular momentum component (separable potential). The form of a norm-conserving, separable pseudopotential given by Kleinman and Bylander [56] is:

$$v = v_{l_{LOC}} + \sum_{lm} \frac{|\Delta v_l \, \mathcal{R}_l^P Y_{lm}\rangle\langle \Delta v_l \, \mathcal{R}_l^P Y_{lm}|}{\langle \mathcal{R}_l^P |\Delta v_l| \mathcal{R}_l^P \rangle} \ , \tag{2.24}$$

where $v_{l_{LOC}}$ is the component of the pseudopotential chosen as local, $\Delta v_l = v_l - v_{l_{LOC}}$, and $\mathcal{R}_l^P$ are the radial parts of the wave functions of the pseudo

[3] In this thesis we use norm-conserving pseudopotential of the type proposed by Troullier and Martins [55].

atom used to construct the ionic potential. Because the wave function is now not projected onto a complete set of spherical harmonics, particular attention should be paid when choosing the locality of the pseudopotential. In some cases, indeed, a not appropriate choice of l_{LOC} leads to "ghost" states in the eigenvalue spectrum of the pseudo atom [57] by passing from a non-local to a separable pseudopotential.

Electrostatic interactions

In periodic boundary conditions, the calculation of the ion-ion and electron-electron electrostatic interactions needs particular care. For this energy terms, the technique of the Ewald summations [58] is commonly used. It is important to note that in the case of cells which contain a net charge, appropriate corrective terms have to be added to the total energy of the system [59, 60]. These corrections take in account the (long range) electrostatic interactions between the system and the periodically repeated images. For instance, the interaction between point charges (PC) q in a simple cubic lattice with edge length L can be computed by a Madelung summation:

$$E_{PC} = -\alpha \frac{q^2}{2\epsilon L} \ , \tag{2.25}$$

where ϵ is the dielectric constant of the system considered, and $\alpha = 2.8373$ is the Madelung constant for a simple cubic lattice. The interaction due to a net charge distribution can be then computed up to $O(L^{-4})$ with a method proposed in Ref. [60].

Minimization of the total energy

In principle, we know how to compute all the contributions to the Kohn-Sham Hamiltonian. The search of the eigenfunctions ψ_i and of the eigenvalues ε_i proceeds through a self-consistent iterative loop over the coefficient $c_{i,\mathbf{k}+\mathbf{G}}$ defined in equation 2.22 (which uniquely define a charge density ρ). The conventional matrix diagonalization methods are generally not as efficient as other techniques for the direct minimization of the Kohn-Sham energy functional $E[\rho]$.

The most simple minimization technique is the *steepest descent* method, where the variable are updated in the direction opposite to the gradient of the function to minimize. In our case, the variables to update are the wave functions ψ_i, (in the practical case, the coefficients $c_{i,\mathbf{k}+\mathbf{G}}$ of the plane wave expansion). The function to minimize is the energy E. Given the wave functions at a step n, the updating to $n+1$ is performed as follows:

$$\bar{\psi}_i^{n+1} = \psi_i^n - \Delta \left(\frac{\delta E}{\delta \psi_i^*} \right)^n \ , \tag{2.26}$$

where Δ is the magnitude of the step, and $(\delta E / \delta \psi_i^*) = \hat{H}\psi_i$. After every minimization step, the orthonormality of the states must be restored, for instance with the Grahm-Schmid algorithm:

$$\bar{\psi}_i^{n+1} \quad \xrightarrow{\text{GS}} \quad \psi_i^{n+1} \ .$$

An extension of the steepest descent method is represented by the *conjugated gradient* method (see, e.g., Ref. [11]). This very efficient algorithm can be used to reach in few steps the electronic ground state, so that it can be implemented in molecular dynamics schemes. In this case, the classical Newton equation of the ions (2.3) is integrated by a numerical algorithm (e.g., the Verlet algorithm). At every MD step, the forces on the ions are calculated after full minimization of the total energy of the electrons within the DFT with the conjugated gradient method.

2.2 The Car-Parrinello method

An alternative scheme to reach the ground state of the electronic system and to perform efficiently MD simulations has been proposed in a seminal paper by Car and Parrinello [40]. The idea is to let the wavefunctions reach the minimum energy *dynamically*, by associating to the Kohn-Sham orbitals a *fictive* mass μ and by integrating the equation of motion:

$$\mu \ddot{\psi}_i = -\hat{H}\psi_i - \eta \, \dot{\psi}_i + \sum_j \Lambda_{ij} \, \psi_j \ , \tag{2.27}$$

where the friction coefficient η is chosen to damp critically the wavefunction motion, and the additional forces $\Lambda_{ij}\,\psi_j$ are necessary to maintain the orbitals orthonormal during the dynamics. The Lagrangian $\mathcal{L}_e$ for the fictitious dynamics of the electronic wave function, from which the equation of motion 2.27 (for the case of $\eta = 0$) can be derived, is:

$$\mathcal{L}_e = \sum_i \mu \langle \dot{\psi}_i | \dot{\psi}_i \rangle - E\,[\{\psi_n\}, \{\mathbf{R}_m\}] + \sum_{i,j} \Lambda_{ij}\,\left[\langle \psi_i | \psi_j \rangle - \delta_{ij}\right]\,, \tag{2.28}$$

where the dependence of E on the orbital set $\{\psi_n\}$ and on the *fixed* ionic coordinates $\{\mathbf{R}_m\}$ has been evidenced.

2.2.1 The Car-Parrinello Lagrangian

Once the electronic ground state is reached, it is possible to associate the same fictitious electron dynamics to the real ionic dynamics, in order to obtain a global equation of motion for the whole system. The complete Lagrangian contains both the electronic and the ionic energetic terms:

$$\mathcal{L} = \sum_i \mu \langle \dot{\psi}_i | \dot{\psi}_i \rangle + \sum_I \frac{1}{2} M_I \dot{\mathbf{R}}_I^2 - E\,[\{\psi_n\}, \{\mathbf{R}_m\}] - E_{II} + \sum_{i,j} \Lambda_{ij}\,\left[\langle \psi_i | \psi_j \rangle - \delta_{ij}\right]\,, \tag{2.29}$$

where E_{II} are the electrostatic ion-ion interactions. The Car-Parrinello Lagrangian 2.29 leads to the following Newtonian equations of motion, which can be solved simultaneously:

$$\begin{cases} \mu \ddot{\psi}_i = -\hat{H}\psi_i + \sum_j \Lambda_{ij}\,\psi_j \\ M_I \ddot{\mathbf{R}}_I = -\dfrac{dE_{tot}}{d\mathbf{R}_I}\,, \end{cases} \tag{2.30}$$

where $E_{tot} = E\,[\{\psi_n\}, \{\mathbf{R}_m\}] + E_{II}$. In this dynamical scheme, the electronic wavefunctions follow the ions remaining close to the ground state, so that no minimization of the electron energy is required at every MD step.

Forces on the ions

In the classical equations of motion, the forces on the ions are calculated as:

$$\mathbf{f}_I = -\frac{dE_{tot}}{d\mathbf{R}_I} = -\frac{d}{d\mathbf{R}_I}\left(\sum_i \langle \psi_i | \hat{H}\,(\{\mathbf{R}_m\})\,|\psi_i\rangle\right)\,. \tag{2.31}$$

That is, any variation of the wave functions during the ionic motion would contribute to the forces on the ions. However, if the wave functions ψ_i are eigenvalues of the Hamiltonian $\hat{H}$, i.e., if the electrons are in their *ground state* for the given ionic configuration, then the theorem of Hellmann-Feynman holds [46], and we can write:

$$\frac{d}{d\mathbf{R}_I}\left(\sum_i \langle\psi_i|\hat{H}\left(\{\mathbf{R}_m\}\right)|\psi_i\rangle\right) = \sum_i \left\langle \psi_i \left| \frac{d\hat{H}\left(\{\mathbf{R}_m\}\right)}{d\mathbf{R}_I} \right| \psi_i \right\rangle = \frac{\partial E_{tot}}{\partial \mathbf{R}_I} \,. \tag{2.32}$$

In this way, the forces on the ions can be easily calculated at every MD step given the ground state Kohn-Sham wave functions.

On the other hand, in the CP dynamical scheme the wave functions are only *near* the Born-Oppenheimer surface, so that the calculated forces on the ions are not exactly the physical ones. However, by accurate choice of the fictitious electron mass μ and of the time-step for the integration algorithm, the errors are statistically canceled out during the dynamics. The result is a microcanonical trajectory which is for fairly long time almost coincident with the "true" Born-Oppenheimer trajectory [61].

Failures of the classical CP scheme

In order to correctly describe with the CP approach the microcanonical evolution of a given system, there must be no energy exchange between the ionic motion and the fictitious wave function dynamics. For this reason, it is fundamental that the frequency spectra of the ionic and electronic degrees of freedom do not overlap. It can be shown [61] that the minimum frequency of the wave function motion ω_e^{min} is related to the fictitious mass μ and to the energy gap of the simulated system E_{gap} by:

$$\omega_e^{min} \simeq \sqrt{\frac{E_{gap}}{\mu}} \,. \tag{2.33}$$

This indicates that the dynamics of systems with no or very small energy gap (such as, e.g., metallic systems) cannot be properly described by the CP Lagrangian 2.29. Instabilities arise also from the so-called "level-crossing", which occurs when an empty energy level reaches, during the dynamical evolution, an

energy value smaller than one of the occupied levels. To overcome these difficulties, it is necessary to go beyond the classical CP scheme.

2.2.2 The Car-Parrinello method for metallic systems

Finite temperature DFT

To correctly perform MD simulations with metallic systems, the DFT formalism has to be extended to the case of finite electronic temperature. In this way, the effect of a fractionary occupation of the states across the Fermi level will be naturally taken in account when calculating the Hellmann-Feynman forces on the ions. The electron density at temperature T is written as:

$$\rho(\mathbf{r}) = \sum_{i=1}^{m} f_i \, \psi_i^*(\mathbf{r}) \psi_i(\mathbf{r}) \ , \tag{2.34}$$

where m is the number of the considered electronic states, and the occupation numbers f_i follow the Fermi-Dirac distribution:

$$f_i(\beta) = \frac{1}{1 + e^{\beta(\varepsilon_i - \varepsilon_F)}} \tag{2.35}$$

where ε_F is the Fermi energy and $\beta = 1/(k_B T)$, k_B being the Boltzmann constant. The total energy functional $E\,[\rho]$ is replaced by the Mermin-Hohemberg-Kohn free energy functional [62]:

$$A\ [T; \{\psi_i\}; \{f_i\}] = \sum_i f_i \langle \psi_i | \hat{T} + \hat{V} | \psi_i \rangle + E_{H,xc}[\rho] - TS[\{f_i\}] \ , \tag{2.36}$$

where the Hartree and exchange-correlation terms (depending only on the density ρ) are put together in the functional $E_{H,xc}\,[\rho]$, and S is the electronic entropy:

$$S\,[\{f_i\}] = \sum_i f_i \ln f_i + (1 - f_i) \ln(1 - f_i) \ . \tag{2.37}$$

The minimization of the free energy functional A can be performed in principle with the same variational approach as in the case of zero temperature.

Definition of an occupation matrix

In the CP MD scheme, it is necessary to maintain the adiabatic separation between the motion of the ions and the fictitious motion of the electrons. This problem can *not* be overcome within the finite temperature DFT neither by choosing the occupation numbers as additional dynamical variables, nor by minimizing A with respect to the f_i at each MD step. Indeed, a fundamental difficulty arises from the fact that the electron density at a finite temperature (as defined in equation 2.34) is *not* invariant upon a unitary transformation of the orbitals $\{\psi_i\}$. Thus, to preserve the commutativity between Hamiltonian and density operator, rotational forces on the orbitals (arising from non-zero off-diagonal terms) necessarily appear in the fictitious CP electronic dynamics. Unfortunately, the associated rotational frequencies are very low [63], so that energy transfer occurs between the ionic and electronic degrees of freedom.

A method to overcome this problem is to introduce, instead of occupation numbers, an occupation *matrix* f of elements f_{ij} varying between 0 and 1, with the constrain that $\mathrm{tr}\, f = N$ [64]. In this case, the free energy functional to minimize has the form:

$$A\,[T,;\{\psi_i\};\{f_{ij}\}] = \sum_{ij} f_{ij}\langle\psi_i|\hat{H}\,|\psi_j\rangle - TS[\{f_{ij}\}]\;, \tag{2.38}$$

with $S\,[\{f_{ij}\}] = \mathrm{tr}\,[f\ln f + (1-f)\ln(1-f)]$. In this case, every unitary transformation acting on ψ_i transform also f so that the electron density (and thus the functional A) remains unchanged. Thus, *if A is at the minimum with respect to f*, it is possible to choose a representation where both f and the Hamiltonian are diagonal, eliminating the low frequency rotation modes from the electronic dynamics. It can be shown that, performing a calculation with m electronic states, if ε_F is the Fermi-level, the minimum frequency of the fictitious electron dynamics is [65]:

$$\omega_e^{min} \simeq \sqrt{\frac{E_{gap}^{artificial}}{\mu}} \tag{2.39}$$

with $E_{gap}^{artificial} = \varepsilon_{m+1} - (\varepsilon_F + \alpha k_B T)$, where α is a constant of the order of 1. The artificial gap is not a physical property of the simulated system, but a

parameter that can be arbitrarily increased by including more electronic states in the calculation.

A dynamical scheme for the occupation matrix

The problem is thus reduced to keep the functional A near the minimum with respect to the occupation matrix f during the dynamics. In a scheme which in principle works, at every step of the ionic dynamics, a full self-consistent minimization of A with respect to $\{f_{ij}\}$ can be performed. However, in the spirit of the CP approach, it is possible to introduce a *dynamical* scheme within the occupation matrix formalism [65,66]

To ensure the adiabatic condition between ionic and electronic motion, the occupation matrix is calculated at every MD step not from the true hamiltonian H but from an *accessory* matrix ξ, with the dimensions of an energy, which dynamically follow the time evolution of H. The diagonal elements of the occupation matrix are computed from the eigenvalue of ξ according to the Fermi-Dirac distribution:

$$f_i = \frac{1}{e^{\xi_i/T}+1} \ . \tag{2.40}$$

A Car-Parrinello Lagrangian for the whole system can be defined as follows [66]:

$$\mathcal{L} = \mathcal{L}\left(\{\psi_i\},\{\dot{\psi}_i\},\xi,\dot{\xi},\{R_I\},\{\dot{R}_I\}\right) + \Delta\mathcal{L}(t) \ . \tag{2.41}$$

The rotationally invariant first term of the Lagrangian is:

$$\begin{aligned} &\mathcal{L}\left(\{\psi_i\},\{\dot{\psi}_i\},\xi,\dot{\xi},\{R_I\},\{\dot{R}_I\}\right) = \\ &\sum_{ij}\mu\, f_{ij}\,\langle\dot{\psi}_i|\dot{\psi}_j\rangle - \frac{1}{2}Q\,\mathrm{tr}(\dot{f}\dot{\xi}) + \sum_I \frac{1}{2}M_I\dot{R}_I^2 - \sum_{ij} f_{ij}\,\langle\psi_i|\hat{H}|\psi_j\rangle + TS(f) \ , \end{aligned} \tag{2.42}$$

where Q is a positive mass constant. The holonomic constraints of orthonormality and of particle conservation to take in account in deriving from $\mathcal{L}$ the equations of motion are: $\langle\psi_i|\psi_j\rangle = \delta_{ij}$ and $\mathrm{tr}\, f = N$. The time-dependent part $\Delta\mathcal{L}(t)$ is added to the Lagrangian 2.42 to eliminate from the equations of motion of the ψ and ξ degrees of freedom any velocity-dependent force term. If we define:

$$H_{ij}^{dyn} = \xi_{ij} - \lambda\delta_{ij} \ , \tag{2.43}$$

where λ is the lagrangian multiplier associated to the constraint of particle conservation, then the equations of motion for H^{dyn}, ψ, and $\mathbf{R}$ are:

$$Q\ddot{H}_{ij}^{dyn} = -(H_{ij}^{dyn} - H_{ij}) \,, \tag{2.44}$$

$$\mu f_{ll} \ddot{\psi}_l = -f_{ll} \hat{H} \psi_l + \sum_k \Lambda_{kl} \psi_k \,, \tag{2.45}$$

$$M_I \ddot{R}_I = -\sum_l \left\langle \psi_l \left| \frac{d\hat{H}}{dR_I} \right| \psi_l \right\rangle \,. \tag{2.46}$$

In this dynamical scheme, at the beginning of the simulation, $H_0^{dyn} = H_0$. At every MD step, the new Hamiltonian H is computed; the Kohn-Sham orbitals are updated according to eq. 2.45; the matrix H^{dyn} is updated according to eq. 2.44, diagonalized, and with its eigenvalues the occupation numbers f_{ll} are computed from eq. 2.40. Finally, ψ is rotated into the reference system where H^{dyn} and f are diagonal.

The mass Q associated to H^{dyn} introduce an inertial shift between the time evolution of H^{dyn} (and thus of the occupation matrix f) and the time evolution of H. The high-frequency oscillatory motion of H^{dyn} maintains the free energy functional A near around the minimum with respect to f during the dynamics. Thus, the energetic coupling between the ionic and electronic degrees of freedom can be avoided with an adequate choice of the mass Q and of the integration time step.

Chapter 3

Nucleation of Pt clusters in solution

In this chapter we describe the mechanism of platinum cluster nucleation upon reduction of the K_2PtCl_4 salt in aqueous solution, as revealed by a series of FPMD simulations. The term *cluster nucleation* is used here as a synonym of *first stage of cluster formation*, no matter through which specific mechanism clusters begin to form. In a classical nucleation mechanism, metal atoms are able to aggregate only in the *metallic*, i.e. zerovalent, oxidation state. However, as we will point out the following, several experimental findings indicate that the initial formation of metal clusters does not necessarily involves zerovalent atoms only. For this reason, we explore the problem of cluster nucleation without assuming the prior complete reduction of the Pt(II) complexes to Pt(0). The main result of our simulations is the observed formation of a Pt–Pt bond between two Pt complexes immersed in the water medium already after a *single* reduction step. In light of this result, we discuss a mechanism of cluster formation where the nucleation stage –in our particular case, the formation of a Pt dimer– involves only partially reduced Pt complexes. The problem of cluster growth will be addressed in chapter 4. The results presented here have been published in reference [67].

3.1 The procedure of cluster preparation

The reduction of Pt(II) to its metallic state can be obtained through a variety of physical and chemical methods [2]. The electron transfer process can be initiated by inorganic and organic reducing agents, via photodecomposition [68], radiolysis [69], sonochemical reduction [70], and other techniques. In particular,

a method for preparing stable colloidal dispersions of platinum particles in solution at room temperature was proposed in a classic paper by Rampino and Nord in the 1940s [71], and is still widely employed. The preparation is quite simple: a Pt(II) or Pt(IV) salt is dissolved in water, the solution is aged overnight and a reducing agent is then added to the solution. This causes the precipitation of platinum colloids according to the formal reaction:

$$\mathrm{Pt(II)} + \mathit{Red} \rightarrow \mathrm{Pt(0)} \downarrow + \mathit{Prod} \tag{3.1}$$

where *Red* indicates the reducing agent and *Prod* other reaction products. The kinetics of the global reaction (3.1) strongly depend on the reactants used and on a few other reaction parameters like pH and temperature. The aging of the salt solution for one or two days before starting the reduction allows the solvolysis of the platinum complexes. In the case of K_2PtCl_4, after dissociation the $PtCl_4{}^{2-}$ ions undergo the following hydrolysis reactions [72]:

$$PtCl_4{}^{2-} + H_2O \rightleftharpoons PtCl_3(H_2O)^- + Cl^- \tag{3.2}$$

$$PtCl_3(H_2O)^- + H_2O \rightleftharpoons PtCl_2(H_2O)_2 + Cl^-. \tag{3.3}$$

At the equilibrium, a 1 mM solution of K_2PtCl_4 consists of 5% $PtCl_4{}^{2-}$, 53% $PtCl_3(H_2O)^-$ and 42% $PtCl_2(H_2O)_2$ [73]. The aging time necessary for reaching the equilibrium is about one day at room temperature. The solution is then stable for some days, after that, decomposition of the complexes starts being noticeable [72]. The aging process has the effect of enhancing the reduction rate. Namely, the reduction of $PtCl_4{}^{2-}$ is considerably faster when the solution has been aged to allow the water substitution of one or two chlorine ligands, according to the reactions (3.2) and (3.3) [69].

To prevent the agglomeration of the formed metal particles, a stabilizing polymer is normally added to the reduction bath [71] (see section 1.1.2). Very efficient stabilizers (or capping agents) are for instance polyacrilate [6] and citrate [74]. Citrate can be used at the same time as capping and reducing agent [75]. It is not yet clear in detail whether the capping agent is directly involved in the mechanism of cluster nucleation or not. If citrate is the reductant, the process of cluster

formation could involve a metallorganic precursor, in which many metal ions are chemically bound to the reducing agent in a polymeric structure. This mechanism was postulated for the first time in the case of the reduction of $AuCl_4^-$ to colloidal gold by citrate [75]. However, the presence of a metallorganic intermediate has been shown to be generally not necessary to promote the nucleation of clusters [76]. In a "classical", generally accepted model, the nucleation of particles is supposed to start after a sufficient number of Pt(II) complexes are reduced to the zerovalent state, i.e., when a critical concentration of Pt(0) atoms is reached. In the next section, this classical mechanism is presented in more detail.

3.2 "Classical" mechanism of cluster nucleation

The mechanism of formation of colloids in solution has been the object of several investigations since the time of Faraday [24]. However, a comprehensive theory for the nucleation of colloidal particles from supersaturated solutions has been formulated by LaMer only in the 1950s [77, 78]. LaMer studied the precipitation of monodispersed sulfur hydrosols by decomposition of thiosulfate in hydrochloric acid, according to the reaction:

$$2\,HS_2O_3^- \rightarrow 2\,HSO_3^- + S_2. \tag{3.4}$$

The model of LaMer can be seen as a particular case of the general nucleation theory in phase-separation reactions, as happens for instance in solidification processes. Basically, when a particle (nucleus) of the new phase is formed, the free-energy variation associated to the formation of a nucleus is:

$$\Delta G = \Delta G_v + \Delta G_s \tag{3.5}$$

where ΔG_v is a *gain* in free energy due to the formation of chemical bonds in the new phase, and ΔG_s is a *loss* in free energy due to the formation of an interface between different phases. If η_v is the free energy per unit of volume of the new phase and γ is the surface tension of the interface, for a spherical nucleus of radius

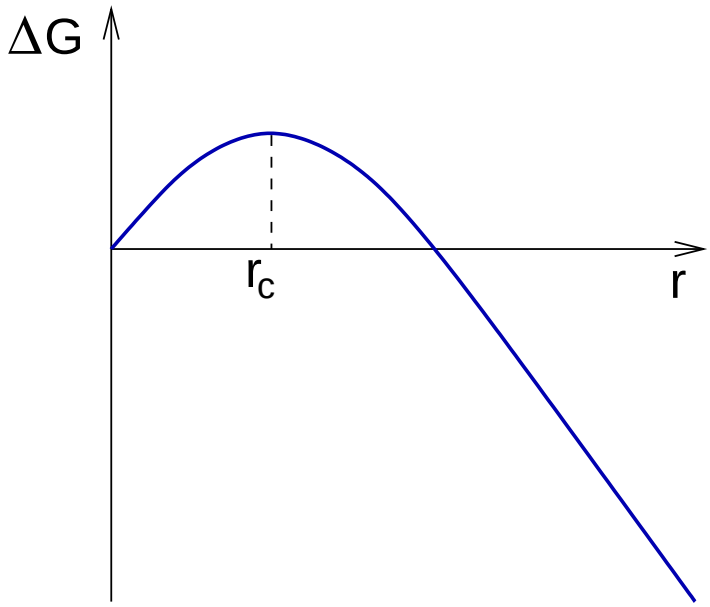

Figure 3.1: Qualitative curve of the variation in free energy vs. particle size for a growing particle according to the "classical" nucleation model.

r the energetic balance can be rewritten as:

$$\Delta G = -\frac{4}{3}\pi r^3 \, \eta_v + 4\pi r^2 \, \gamma. \tag{3.6}$$

The curve of ΔG vs. particle size is represented qualitatively in figure 3.1. The curve presents a maximum at the value r_c of the particle radius, which is called *critical radius*, and is defined by the condition $(\partial \Delta G / \partial r) = 0$ at $r = r_c$. Equation 3.6 can be rewritten in terms of r_c as follows:

$$\Delta G = 4\pi\gamma \left(r^2 - \frac{2r^3}{3r_c} \right). \tag{3.7}$$

According to this model, the formation of particles from supersaturated solutions begins with an energetically unfavoured *nucleation* stage –driven essentially by thermal fluctuations– where by random aggregation of atomic or molecular units a nucleus with critical radius (a critical nucleus) is formed. The nucleation stage is followed by a *growth* stage, where the size of the particle spontaneously increases in a *diffusion-limited* process. Thus, in the case of sulfur hydrosols, after the reaction (3.4) is initiated, the formation of stable particles starts after an induction period, when a *critical concentration* of S_2 in solution is reached. At the

critical concentration, the formation of critical nuclei becomes possible, and the particle growth proceeds by spontaneous aggregation of S_2 units to the formed nuclei.

3.2.1 The case of metal clusters

As already mentioned previously, this classical mechanism of nucleation has been thought to take place also in the case of metal clusters after reduction of metal salts in solution. According to this model, in the case of bivalent platinum salts such as K_2PtCl_4, first Pt(II) complexes are reduced to Pt(0) in a redox reaction:

$$\mathrm{Pt(II)} + 2e \rightarrow \mathrm{Pt(0)}, \tag{3.8}$$

then the atoms aggregate to metallic particles if a critical concentration is reached:

$$\mathrm{N\,Pt(0)} \longrightarrow \mathrm{Pt(0)_N}. \tag{3.9}$$

It should be noted that no evidence of the isolated Pt(0) atoms has ever been given. Their presence is generally inferred from the kinetics of the whole reduction process, which presents in many cases a lag phase. This has been associated with the initial formation of the critical nuclei [76]. However, other investigations [75] have been shown that the appearance of a lag phase in the kinetic curve is due to the slow redox process between reducing agent and isolated metal complexes. In radiation-induced reduction processes, after irradiation of the metal salt solution with γ-ray, radicals and solvated electrons are produced, which *immediately* cause the reduction of the metal complexes. In this case, the whole reduction process does not include any induction period, and the formation of colloids follows immediately after irradiation [74].

In addition, as indicated in several investigations (see, e.g., Ref. [69]) and finally demonstrated by Watzky and Finke in 1997 [79], the formation of transition metal clusters (such as, e.g., Ir, Rh, Pt) is an *autocatalytic* process. This means, once a small nucleus is formed the development of the cluster proceeds through a surface-growth mechanism [79], where the addition/reduction of new metal complexes is catalyzed by the growing cluster. The growth is thus limited by the

rate of incorporation of new atoms into the growing cluster, and not by diffusion, as in the model proposed by LaMer. However, also the kinetic model proposed by Watzky and Finke in Ref. [79] includes a nucleation stage where *completely reduced* atoms react to form a critical nucleus. On the other hand, there are many experimental evidences that the initial formation of a small metal cluster upon reduction of metal salts does not necessarily involve completely reduced atoms only. In the next section, we report a series of experimental findings which will allow us to hypothesize that metal–metal bonds can form between complexes in reduction baths prior to the complete reduction to the zerovalent state.

3.2.2 Failures of the classical nucleation model

The radiation-induced nucleation of metal clusters has been investigated at the atomic scale by ultrafast spectroscopic techniques in the case of silver and other monovalent ions [10]. After radiolytic reduction of Ag^+, Ag(0) atoms have been observed to react with monovalent Ag^+ ions to form $Ag_2{}^+$ dimers [10]. Successive coalescence and reduction steps finally lead to colloidal particles. Interestingly, both the formation of the first metal–metal bonds and the addition of ions to a growing cluster takes place before the complete reduction of the ions to the metallic state. Complete reduction happens only later, and involves the whole cluster during the growth process [10].

The specific mechanism through which platinum colloids nucleate and start growing is still unclear. This is due to the great complexity of the reduction reaction in the case of plurivalent ions such as Pt(II) or Pt(IV). As pointed out in the previous section, platinum colloids are produced via a chain reaction in which the first formed clusters catalyze the further reduction of the metal complexes still present in solution [69]. The autocatalytic process starts at the very beginning of the reaction, when only very few complexes are reduced. In this case, one does not have to wait the induction time necessary to reach a critical concentration of zerovalent atoms, as in the standard nucleation mechanism. In a recent, accurate experimental analysis of the reduction kinetics of $PtCl_4{}^{2-}$ with

hydrogen, monovalent platinum has been postulated to be the first reaction intermediate [74]. In the same work, the appearance of free Pt(0) atom intermediates has been excluded on the basis of simple thermodynamic considerations [74].

In addition, clusters composed of few metal atoms, sometimes in oxidation states higher than zero, have been produced with methods that differ from the standard preparation of colloids only by the presence of ligand molecules like carbonyls or phosphines in the solution. An intriguing example is the production of Pt(I) dimers in a concentrated HCl solution by reduction of K_2PtCl_4 with CO [22], either due to a reaction between partially reduced Pt(I) complexes or to a comproportionation between unreduced Pt(II) and reduced Pt(0) complexes [80]. We note that this is a direct evidence that the formation of metal–metal bonds between platinum complexes in reduction baths does not necessarily involve zerovalent atoms only. This suggest that dimerization may happen in the first step of cluster growth before both metal atoms are reduced to Pt(0), similar to the case of Ag. This possibility is taken in account in the first principles simulations of cluster nucleation presented in the next section.

3.3 FPMD simulations of Pt cluster nucleation

Because of the failures of the classical nucleation model in the case of platinum clusters, we look for a mechanism of Pt–Pt bond formation upon reduction of Pt(II) complexes in solution, without assuming the prior complete reduction of both Pt atoms to their zerovalent state.

3.3.1 Technical details and test calculations

Our electronic and structural optimizations, as well as the FPMD simulations are performed using the Car-Parrinello method [40] in the framework of the spin-polarized density functional theory [43]. The theoretical framework of this technique has been described in chapter 2.

The pseudopotentials used to describe the electron-nuclei interactions have been constructed with the program "fhi98PP" following the scheme of Ref. [81].

In particular, the Pt pseudopotential is generated for the neutral atom considering 18 valence electrons in the configuration $5s^2\,5p^6\,5d^{9.95}\,6s^{0.05}$, the core radius for all three components is 1.60 a.u. and the p component is taken to be local [56]. The accuracy of this pseudopotential is tested for the $PtCl_4^{2-}$ ion and the bare Pt dimer. The computed Pt–Cl bond length in $PtCl_4^{2-}$ is 2.35 Å, which compares well with the experimental value of 2.34 Å [82] and with the value 2.35 Å of a previous calculation [83] based on similar techniques. The electronic configuration of minimal energy for the bare neutral platinum dimer is found to be a triplet, whereas the singlet energy level is found 0.5 eV higher. The Pt–Pt bond length in the dimer is 2.38 Å, to be compared with other DFT values 2.39 Å [84] and 2.40 Å [85]. This is in reasonable agreement with the experimental value 2.45 Å measured by STM techniques on a graphite support [86]. Our computed binding energy for the dimer is 3.34 eV, which should be compared with the theoretical values 2.44 eV [84] and 3.30 eV [85]. There is little agreement between the reported experimental values, which lie in a range between 2.80 and 3.71 eV [86].

In the FPMD simulations, the mass of hydrogen is increased to 2.0 a.m.u., the fictitious electronic mass in the CP method is set to 1100 a.u. and a time step of 6.0 a.u. (about 0.145 fs) is used. These parameters are adequate for CP dynamical simulations of aqueous systems [87]. When necessary, control of the temperature is achieved by a Nose-Hoover thermostat [88] or simply by scaling the atomic velocities.

3.3.2 Preliminary considerations

The results of the investigations are presented throughout the section following the steps which lead to the formation of platinum dimers upon reduction of Pt(II) complexes. Among the Pt(II) salts, we assume as starting point in the FPMD simulations the widely used K_2PtCl_4, which in solution is first dissociated and then hydrolized according to the reactions (3.2) and (3.3). Metal clusters are then obtained by exposing the solvolysis products to a reducing agent. Given the variety of agents used to obtain colloidal platinum from platinum salts, no

attempt has been made to model any particular reduction process. In other words, we do not attempt to investigate here the electron transfer mechanism from a specific reducing agent to a Pt(II) complex. The reducing electron is added each time into the simulation cell containing one or more Pt complexes, assuming that a good model for the system immediately after reduction can be obtained this way after electronic optimization and MD equilibration. This "vertical addition" of an electron to the system followed by ionic motion in the presence of an extra charge may be linked to what happens in radiolytic reduction processes [10,69,70]. Here the electrons produced by γ-ray irradiation of the platinum salt solution can be thought to fall into the LUMO states of the metal complexes present in the solution. More generally, we can address this way all those processes where the reducing agent has only the instrumental role of electron donor, beside which its exact character is little relevant to the subsequent evolution of the reduced fragment. It would seem reasonable to assume that this is the case in many reduction processes involving Pt complexes. We note that in the experiments the final reduction product of a platinum salt is essentially always an ensemble of metal crystallites with diameters ranging between two and three nanometers, in spite of the great number of possible reducing agents. Different size distributions of the metal particles in the colloidal suspension are only due to more or less marked aggregation of the crystallites (Pt clusters bigger than 3 nm are rarely single crystals [89]). Modifications of the colloid morphology are mainly due to different concentrations and types of protective agents [6] and again do not depend on the reducing agent used. Finally, since the presence of a stabilizer is not directly necessary for the reduction (while it helps to control the size and shape of the metal particles [6]) stabilizers are also not directly addressed in this study. Our FPMD simulations are performed on systems which include Pt complexes only, and contain from the beginning the number of electrons which is appropriate to the desired reduction state.

3.3.3 Solvolysis products of K_2PtCl_4 in water solution

A solution of K_2PtCl_4 at the equilibrium (see section 3.1) contains $PtCl_4{}^{2-}$, $PtCl_3(H_2O)^-$, and $PtCl_2(H_2O)_2$ complexes (figure 3.2). We calculated the relaxed geometries and the electronic structure of the three Pt(II) complexes in the gas phase, using a repeated cubic supercell with edge length of 20 Å. The optimized bond lengths and angles of the molecules and the Kohn-Sham eigenvalues are reported in table 3.1 and in the scheme of figure 3.3, respectively.

The vertical electronic affinities (VEA) of the three complexes are computed as the change in total energy upon addition of one electron to the system, at fixed atomic positions. We note that because of the periodic boundary conditions used, the total energies of charged systems must be evaluated including appropriate

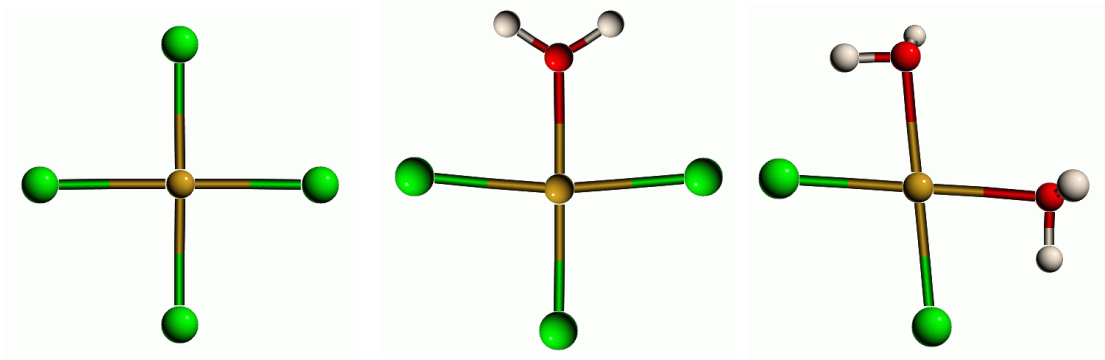

Figure 3.2: The solvolysis products of K_2PtCl_4 considered in the ab initio calculations: $PtCl_4{}^{2-}$ (left); $PtCl_3(H_2O)^-$ (middle); and $PtCl_2(H_2O)_2$ (right).

	$PtCl_4{}^{2-}$	$PtCl_3(H_2O)^-$	$PtCl_2(H_2O)_2$
Pt–Cl	2.35	2.32, 2.27	2.27
Pt–O		2.10	2.13
Cl–Pt–Cl	90.0 °	94.7 °	99.0 °
Cl–Pt–O		85.3 °	80.8 °
O–Pt–O			99.5 °

Table 3.1: Optimized bond lenghts (Å) and angles (deg) of the solvolysis products of K_2PtCl_4.

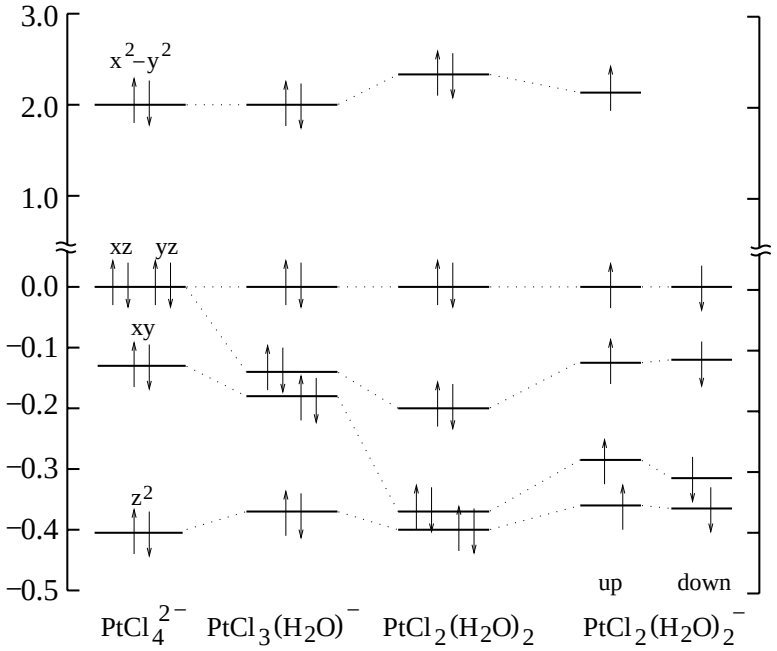

Figure 3.3: Kohn-Sham energy levels (eV) of the solvolysis products of K_2PtCl_4 near the HOMO-LUMO gap. The local spin density of the open-shell reduced complex $PtCl_2(H_2O)_2{}^-$ is also shown.

corrective terms [59, 60]. We do not take into account the contribution to the electron affinity given by the variation of zero point vibration energy upon the reduction, since these zero point corrections are generally smaller than the systematic errors due to other approximations (*e.g.*, the use of pseudopotentials). Our computed electron affinities (EA) for the Cl and O atoms are 3.6 eV and 1.6 eV (expt. 3.6 eV and 1.5 eV, [90] respectively). For the relaxed Pt_2 dimer we obtain an EA of 1.7 eV (expt. 1.9 eV [90]). Of the three Pt(II) complexes, only the neutral complex $PtCl_2(H_2O)_2$ binds an extra electron, giving a positive calculated VEA of 0.7 eV. The reducing electron remains instead delocalized over the whole simulation cell in the case of the negatively charged complexes $PtCl_4{}^{2-}$ and $PtCl_3(H_2O)^-$.[1]

[1]The electron added to investigate a possible reduction state remains delocalized also if the space surrounding $PtCl_4{}^{2-}$ or $PtCl_3(H_2O)^-$ is filled with water molecules, to model the solution environment.

3.3.4 Reduction of $PtCl_2(H_2O)_2$

We now turn to the study of $PtCl_2(H_2O)_2$ upon addition of one electron. First we minimize the electronic structure at fixed atoms. The calculated energy levels for both spin manifolds with respect to the position of the HOMO-1 state are represented in figure 3.3 (right). The atoms are then allowed to move. We report in figure 3.4 **A** the evolution of the particle density associated with the singly occupied orbital during the dynamics. This is obtained as the difference $\varrho_\uparrow - \varrho_\downarrow$ of the electron densities $\varrho_\uparrow$, $\varrho_\downarrow$ associated to the "up" and "down" spin manifolds. At the beginning of the run the additional electron falls as expected into the $d_{x^2-y^2}$ LUMO orbital of the neutral square planar $PtCl_2(H_2O)_2$. However, within $\sim$100 fs, the two water ligands dissociate from the complex. At this point, the Cl–Pt–Cl angle starts increasing from the initial value of about 100°. Within $\sim$ 0.2 ps the angle reaches 180° and a linear $PtCl_2{}^-$ complex is formed, which is then stable in the time scale of the simulation. After quenching the atomic motion, the Pt–Cl distance is 2.25 Å, i.e., only 0.02 Å smaller than the initial value in the $PtCl_2(H_2O)_2$ complex. In $PtCl_2{}^-$, the Pt atom has the exotic d^9 electron configuration, and a d^{10} Pt(0) complex is readily obtained when the reduction is completed by adding one more electron. The $PtCl_2{}^{2-}$ complex is also linear, with a Pt–Cl bond length increased to 2.32 Å. The five highest occupied molecular orbitals of this complex are shown in figure 3.4 **B**. The π_g symmetry of the degenerate HOMOs corresponds to that of the singly occupied orbital of $PtCl_2{}^-$ (cf. figure 3.4 **A**). A σ_g orbital derived from the atomic $5d_{z^2}$ corresponds to an energy level located $\sim$0.5 eV below the HOMO level. As an independent check of these results the electronic structure of $PtCl_2{}^{2-}$ was computed again using a Gaussian basis set [91] and without imposing periodic boundary conditions.[2] The calculation led to the same sequence in the orbital symmetries shown in figure 3.4 **B**. Finally, the linear $PtCl_2{}^{2-}$ complex was obtained also as the final

[2]We used a SDD valence triple zeta basis set [92] together with the corresponding Stuttgart/Dresden pseudopotential for the description of core electrons for the Pt atoms, and a D95 Dunning/Huzinaga valence double-zeta basis set [93] for the remaining atoms. The BPW91 exchange-correlation functional [94] was used.

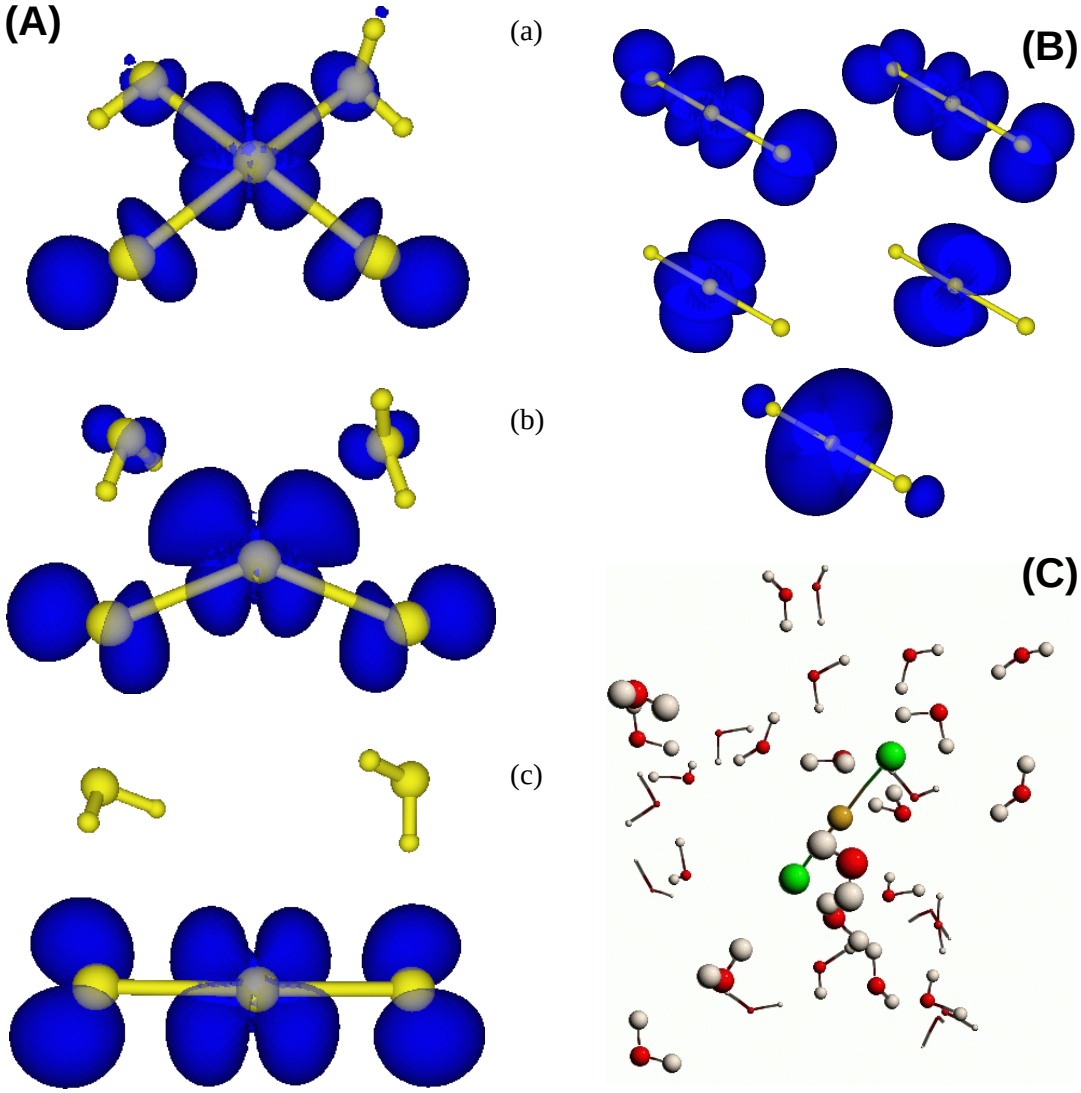

Figure 3.4: (**A**),(a–c) Evolution of $PtCl_2(H_2O)_2$ upon addition of one reducing electron (gas-phase reaction). The particle density associated with the unpaired electron is depicted as iso-value surface at 0.002 au. (**B**) Five highest occupied molecular orbitals of $PtCl_2{}^{2-}$ (iso-density surfaces at 0.003 au). Top rank: the two π_g degenerate HOMOs. Middle rank: the two degenerate δ_g orbitals (their energy level is located ∼0.3 eV below the HOMO level). Bottom rank: σ_g orbital (energy level located ∼0.5 eV below the HOMO level). (**C**) Final configuration of a FPMD simulation of the reduction of $PtCl_2(H_2O)_2$ in a cell filled with water molecule to model the solution environment. After a single reduction step, a linear $PtCl_2{}^{-}$ molecule is obtained, which is further reduced to $PtCl_2{}^{2-}$ in a second reduction step. Note that after the reduction process both chlorine ligands are still bound to the Pt atom.

configuration of a separate FPMD run in which the two extra electrons are added to the $PtCl_2(H_2O)_2$ at the same time at the beginning of the simulation.

In order to investigate the effect of the solution environment on the reduction process, we fill the empty space surrounding the Pt complex with water molecules at bulk water density. The simulated system contains a $PtCl_2(H_2O)_2$ complex and 46 water molecules in a repeated cubic cell of edge 12 Å. The system is first equilibrated for 0.5 ps in a constant temperature (CT) simulation at 300 K, then the reduction is promoted by adding one electron to the system. After minimization of the electronic structure at fixed ionic positions, the dynamics at 300 K is continued. The same pattern of events observed in the gas phase simulation is obtained here in solution, although the rearrangement of the complex is slowed down by the steric hindrance of the surrounding water solution. Namely, the square-planar symmetry of the complex is soon broken by the successive loss of the two water ligands. Once more, the chlorine atoms move off the initial *cis* geometry, and in less than 2 ps of simulated time a linear $PtCl_2{}^-$ complex is obtained, which remains stable in the time scale of the simulation. Further reduction from this point leads to the $PtCl_2{}^{2-}$ complex. Also in this case the complex remains stable, no hydrolysis occurring in 2.5 ps of simulated time. The final configuration of the system after quenching of the atomic motion is shown in figure 3.4 **C**.

3.3.5 Formation of a platinum dimer in water

With the aim of investigating the formation of a Pt–Pt bond upon reduction of platinum salt in solution, we perform MD simulations on a system of two Pt(II) complexes and 36 water molecules contained in a repeated cubic cell of edge 12 Å (figure 3.5 a). The system is first annealed at 300 K for 1.25 ps, after which the Pt–Pt distance is ∼7 Å, then one electron is added and the dynamics is continued. The analysis of the electron density reveals that the additional electron immediately localizes in the LUMO state of one of the two square-planar complexes, which is thus reduced to contain a Pt(I) atom. Once more, in less

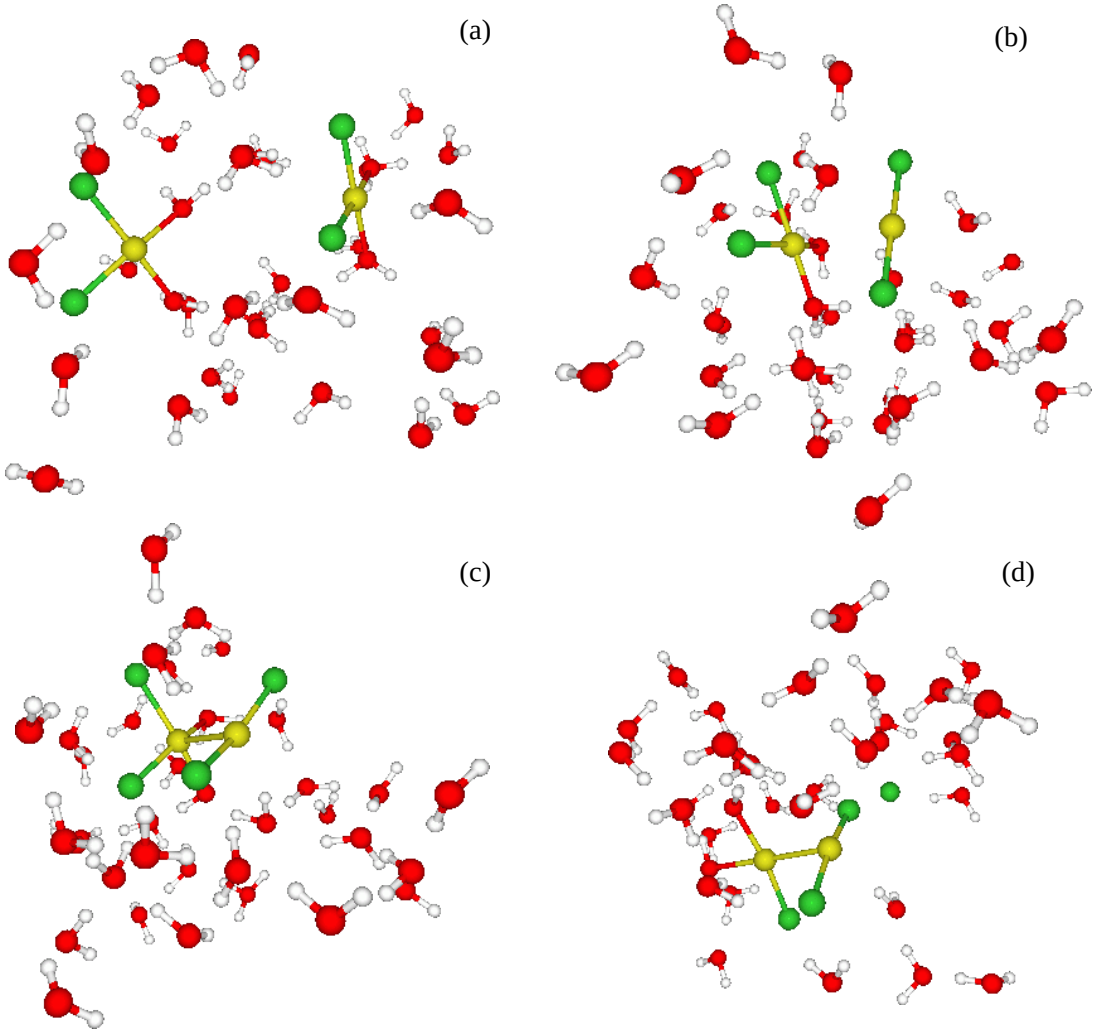

Figure 3.5: Snapshots from a FPMD simulations showing the formation of a Pt dimer from two Pt(II) complexes: (a) two Pt(II) complexes surrounded by 36 water molecules after annealing at 300 K for 1.25 ps. At this point (t = 0) a first reducing electron is added to the system; (b) the formation of a linear $PtCl_2^-$ complex upon reduction is completed (t = 2.2 ps). Soon after, a Pt–Pt bond forms between the complexes; (c) optimized geometry of the Pt(I)–Pt(II) dimer after annealing and quenching (t = 3.5 ps). At this point, a second reducing electron is added to the system, which is annealed at 300 K for 2 ps; (d) final geometry of the Pt(I) dimer after ionic relaxation.

than 2 ps of further simulation time a linear $PtCl_2^-$ develops from this reduced complex after the loss of both water ligands (figure 3.5 b). Remarkably, letting the system evolve after this stage we observe the formation of a Pt–Pt bond between the linear Pt(I) complex and the square-planar Pt(II) complex left intact by the reduction (figure 3.5 c). The Pt(I)–Pt(II) dimer remains then stable for 2 ps more, after which the simulation is stopped. After quenching of the atomic motion, the equilibrium Pt–Pt distance is found to be 2.9 Å. During the dimer formation, the water molecules rearrange so that some empty space is present in the cell at the end of the simulation. This happens because the excluded volume defined by the final Pt_2 complex is significantly smaller than that associated to the two isolated square-planar complexes. To ensure that the observed reaction is not dependent on the lack of water, we performed a novel simulation introducing ten more water molecules in the system, therefore consisting of 46 water molecules, a $PtCl_2(H_2O)_2$ complex and a linear $PtCl_2^-$ complex. The Pt atom of the linear Pt(I) complex was placed on the z axes of the square planar Pt(II) complex, with its two Cl^- ligands on top positions with respect to a Cl^- ligand and an H_2O ligand of the square planar complex. The initial distance between the Pt atoms of the two complexes was set to 4.8 Å. The simulation led as before to the formation of a bond between the platinum atoms. To investigate if the observed bond formation process is affected by the initial value of the twist angle between the two complexes, we performed two more FPMD simulations of a system containing a Pt(I) complex, a Pt(II) complex and 37 randomly placed water molecules, setting the initial Pt–Pt distance to 4.0 Å. In these simulations, the initial torsion angle defined by the two Pt atoms and two Cl^- ligands (one per Pt atom) was varied by $+45^\circ$ and -45° with respect to the value used for the 46 water molecule system in the previous simulation. Both simulations led, as before, to the formation of a Pt–Pt bond of equilibrium length 2.9 Å .

Finally, we add a second reducing electron to the annealed configuration of the Pt(I)–Pt(II) dimer surrounded by 36 water molecules, and start a FPMD-CT simulation at 300 K from this point. In this case a chlorine ligand is immediately lost, and the structure of the dimer gradually changes so that after about 1.5 ps

the Pt–Pt bond is in the same plane of the bonds with the other ligands for both Pt atoms (figure 3.5 d). The angle between the two ligand planes is $\sim 75\,^{\circ}$. The final geometry resembles very closely that of the $[Pt_2Cl_4(CO)_2]^{2-}$ ion, as obtained by reduction of K_2PtCl_4 with CO [22, 95]. The Pt–Pt equilibrium distance is 2.6 Å, which is a typical value for Pt(I) dimers [80].

3.3.6 Characterization of the Pt–Pt bond

To understand the mechanism of bond formation leading to the Pt(I)–Pt(II) dimer, we perform a series of electronic structure minimizations on frozen gas-phase atomic geometries. Our purpose is to isolate the evolution of the particle density associated to the unpaired electron during the bond formation (figure 3.6 a–d). The geometry of the two Pt complexes is extracted from the system shown in figure 3.5 b, and the Pt–Pt distance is varied moving the complexes by successive rigid translations. When the $PtCl_2{}^-$ molecule is far from $PtCl_2(H_2O)_2$ (figure 3.6 a), the isolated electron occupies the π_g orbital, as expected (cf figure 3.4 **A**). When the Pt–Pt distance is reduced to about 4 Å, the σ_g energy level

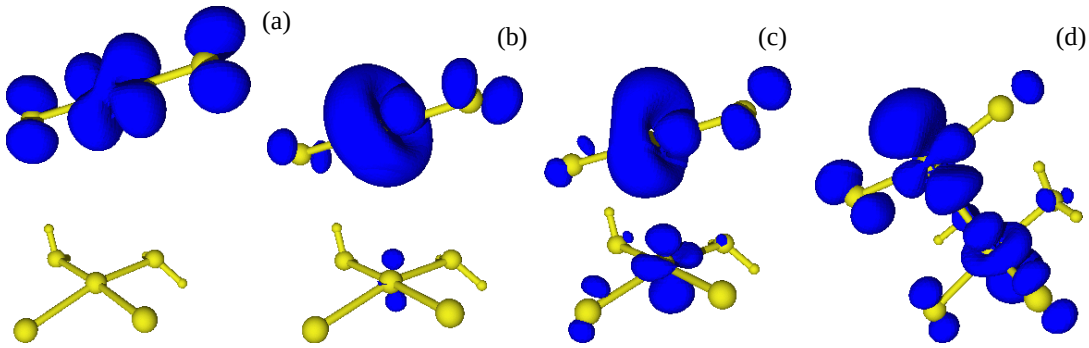

Figure 3.6: Evolution of the particle density associated to the unpaired electron during the formation of a Pt–Pt bond between a Pt(II) complex and a Pt(I) complex (iso-density surfaces at 0.002 au); (a–c) results from the electronic structure optimization for three fixed gas phase geometries. The Pt–Pt distances are 5.4 Å (a), 4.0 Å (b) and 3.3 Å (c); (d) fully optimized geometry of the Pt(I)–Pt(II) dimer with the antibonding half-filled HOMO state. The equilibrium Pt–Pt distance is 2.87 Å.

	Plane-wave basis set			Gaussian basis set		
Atom	x (Å)	y (Å)	z (Å)	x (Å)	y (Å)	z (Å)
Pt(1)	3.741	1.997	1.938	3.907	2.081	2.138
Pt(2)	0.868	1.993	1.936	0.975	2.086	2.143
Cl(3)	4.121	3.636	3.486	4.360	3.354	4.092
Cl(4)	3.871	0.374	0.257	4.075	0.838	0.027
Cl(5)	0.424	3.118	3.859	0.463	3.205	4.168
Cl(6)	0.000	0.000	2.619	0.000	0.000	2.764
O(7)	1.032	1.005	0.082	1.157	1.156	0.251
O(8)	1.566	3.884	1.227	1.787	3.957	1.495
H(9)	1.490	4.391	2.080	1.665	4.578	2.262
H(10)	2.566	3.580	1.248	2.821	3.603	1.499
H(11)	2.033	0.758	0.000	2.147	1.027	0.000
H(12)	0.602	0.150	0.345	0.700	0.283	0.340

Table 3.2: Final geometry of the Pt(I)–Pt(II) dimer obtained in the simulations after adding one electron to a system containing two $PtCl_2(H_2O)_2$ complexes. The two coordinate sets are the result of two structural relaxations using a plane-wave basis set and a Gaussian basis set.

(cf figure 3.4 **B**) becomes higher than the π_g one, and is thus the one occupied by the unpaired electron (figure 3.6 b). At this point we observe hybridization between the σ_g orbital and the occupied d_{z^2} state of $PtCl_2(H_2O)_2$ (figure 3.6 b,c), indicating the formation of a bond. The fully relaxed structure of the Pt(I)–Pt(II) dimer with the antibonding half-filled HOMO state is shown in figure 3.6 d, and the atomic coordinates are reported in table 3.2. In the gas-phase, the Pt–Pt equilibrium distance is 2.87 Å. The analysis of the electron density of the formed dimer in the equilibrium structure reveals the existence of a bond critical point between the Pt atoms (figure 3.7), as should be the case if a Pt–Pt chemical bond is present. Our computed binding energy for the Pt(I)–Pt(II) dimer system is 1.52 eV, obtained as the difference between the total energy of the dimer system in the gas phase and the sum of the energies of the two isolated complexes.[3]

[3]The computed total energies of charged systems must be corrected for the spurious electrostatic interactions induced by the periodic boundary conditions adopted in the plane-wave

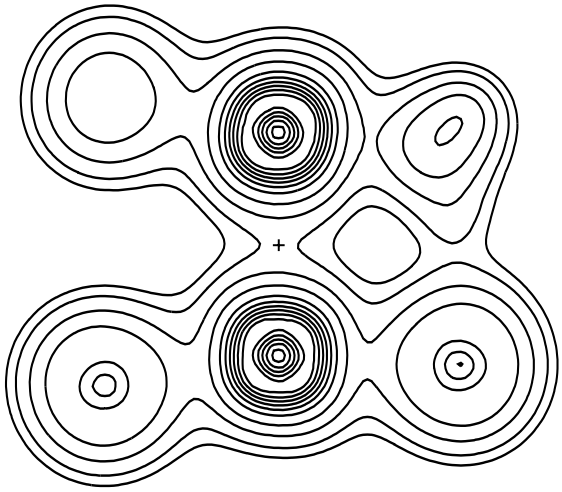

Figure 3.7: Contour plot of the electron density ϱ of the Pt(I)–Pt(II) dimer $[PtCl_2(H_2O)_2][PtCl_2{}^-]$ in the plane containing the two Pt atoms and one Cl^- ligand of the Pt(I) unit (right-bottom in the plot). The outer contour is at $\varrho = 0.0030$ au. The small cross indicates the $(3,-1)$ bond critical point ($\varrho = 0.0054$ au) between the Pt atoms. On the right side, the hydrogen bond between a Cl^- ligand of the Pt(I) unit and a water ligand of the Pt(II) unit is visible.

A further optimization of the Pt(I)–Pt(II) dimer structure was performed as an additional check, using a Gaussian basis set and without imposing periodic boundary conditions [91–94]. The system remained in the dimer geometry of figure 3.6 d, with the slightly higher Pt–Pt distance of 2.93 Å. The coordinate set of the structure after this additional optimization is reported in table 3.2. The 3N−6 non-zero eigenvalues of the Hessian matrix associated to the final optimized geometry are all positive, implying that this structure corresponds to a potential energy minimum.

To further characterize the structure, we analyze the motion of the Pt(I)–Pt(II) and the Pt(I)–Pt(I) dimers during 3 ps of unconstrained dynamical simu-

formalism. A simple way to compute the correction terms up to order $O(L^{-4})$ in the case of cubic supercells of edge-length L is reported in refs. [59] and [60]. We note that in solution the computed total energy values depend strongly on the instantaneous configuration of the water molecules surrounding the complex, so that computing a reliable binding energy in the water environment would be a much more difficult task.

lation in the gas phase. In both cases, the initial Pt–Pt distance is 0.1 Å bigger than its equilibrium value. As expected, the systems oscillate freely around their minimum energy configuration. In particular, for each dimer, a good approximation of the bond vibrational frequency can be readily obtained from the observed oscillations of the Pt–Pt distance. For the Pt(I) dimer, the resulting Pt–Pt oscillation frequency is 176 cm^{-1}, i.e. a value close to the value 170 cm^{-1} assigned to the Pt–Pt stretching mode of the $[Pt_2Cl_4(CO)_2]^{2-}$ ion [22]. In the case of the Pt(I)–Pt(II) dimer, the estimated Pt–Pt stretching frequency is 106 cm^{-1}. This value is intermediate between the 176 cm^{-1} value we obtain for the Pt(I)–Pt(I) dimer and the 81 cm^{-1} frequency of the Pt–Pt stretching mode of the Magnus' green salt $[Pt(NH_3)_4][PtCl_4]$ [96], where two square planar units formally containing a Pt(II) atom are linked along the z axes by a weak Pt–Pt interaction. We interpret this result as an indication that the Pt–Pt bond in the Pt(I)–Pt(II) dimer considered in this work is stronger than the typical bonding of Pt(II)·Pt(II) complexes.

To further investigate the Pt–Pt bond, we use the "Theory of Atoms in Molecules" originally introduced by Bader [97]. According to this theory, information about the chemical bonds in a molecule can be extracted from the topological analysis of the Laplacian $L = \nabla^2\varrho$ of the (positive) electron density ϱ. In transition metal complexes, the outer shell of the metal atom core presents zones of electron density depletion and accumulation, revealed by maxima and minima of L, respectively. These density distortions arise from the formation of bonds in the complex and reflect the geometrical disposition of the ligands [98]. We compute L for the Pt(I)–Pt(II) dimer, for the Pt(I)–Pt(I) dimer and, as reference, for the $[Pt_2Cl_4(CO)_2]^{2-}$ dimer. The iso-value surfaces of L at the value of 0.03 au, representative of depletion regions, are presented in figure 3.8. In the case of the Pt(I) dimers two maxima of L are located along the Pt–Pt axes and the other maxima points toward the Cl^-, CO and H_2O ligands (figure 3.8 b,c), as expected [98]. In the case of the Pt(I)–Pt(II) dimer, the Laplacian presents a single maximum in the region between the Pt atoms, located close to the linear Pt(I) unit (figure 3.8 a), indicating a weaker chemical bond between the two

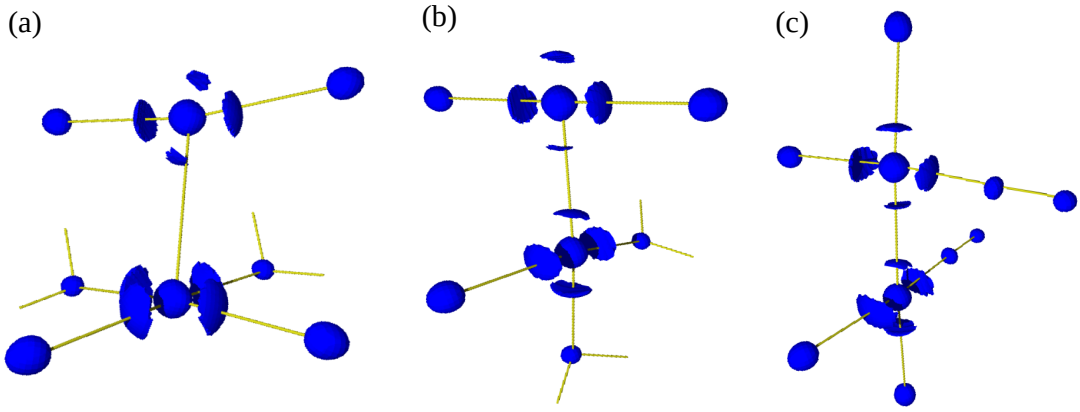

Figure 3.8: Iso-value surfaces of the Laplacian of the electron density $L = \nabla^2\varrho$ at $L = 0.03$ au for three platinum dimers: (a) The Pt(I)–Pt(II) dimer $[PtCl_2(H_2O)_2][PtCl_2{}^-]$ obtained in the simulations after adding one electron to a system containing two $PtCl_2(H_2O)_2$ complexes; (b) the Pt(I)–Pt(I) dimer $Pt_2Cl_3(H_2O)_2{}^-$ obtained after the addition of a second electron; (c) the Pt(I)–Pt(I) dimer $[Pt_2Cl_4(CO)_2]^{2-}$ (experimentally isolated in Ref. [22]). One maximum of L between the Pt atoms in the Pt(I)–Pt(II) dimer (a) and two maxima between the Pt atoms in the Pt(I)–Pt(I) dimers (b,c) are evident, indicating that the metal–metal bond formed after the first reduction step is strengthened after the addition of a second reducing electron.

metal atoms.

To summarize, a stable Pt(I)–Pt(II) dimer is obtained in the calculations. The topological analysis of the charge density (figures 3.7 and 3.8), and the results concerning the bond distance, energy and stretching motion clearly indicate that a Pt–Pt bond forms between the two Pt complexes already after a single reduction step. The Pt–Pt interaction is then strengthened when an additional electron is acquired by the dimer during the second reduction step.

3.4 Discussion of a novel nucleation mechanism

The electroless growth of platinum clusters in solution is a nucleation-dominated, [79, 89] autocatalytic [69, 74, 79] process. The nucleation of platinum particles is generally believed to follow a two-step mechanism: i) reduction of Pt(II) to

isolated Pt(0) atoms and ii) subsequent aggregation of the zerovalent atoms to form metal clusters. This corresponds to the "classical" mechanism of nucleation described in section 3.2. However, as we pointed out in section 3.2.2, there are experimental observations that cannot be explained by this nucleation model alone, like *e.g.* the possibility of producing dimers which present higher oxidation states [22]. In addition, the presence of Pt(0) atoms as reaction intermediates in the reduction of $PtCl_4^{2-}$ with hydrogen leading to colloidal Pt particles has been recently ruled out [74]. In the series of FPMD simulations presented in the previous section, we observe the formation of a Pt–Pt bond after the reduction from Pt(II) to Pt(I) of a single Pt complex. By addition of a second electron, a Pt(I) dimer is obtained, which closely resembles the Pt dimer experimentally obtained upon reduction of K_2PtCl_4 with CO in HCl solution [22]. These results are obtained both in gas phase and in solution, starting from different initial conditions (varying *e.g.* the relative position of the two complexes and the number and arrangement of the water molecules separating them). Within the predictive power of the DFT-GGA functional used, this is a sufficient condition to establish the existence of a novel reaction path to dimer formation in which, surprisingly, only *one* reducing electron is needed to initiate cluster formation, whereas *four* would be needed in the standard mechanism. The microscopic mechanism provided by our simulations suggests a simple and consistent picture within which the existing experimental evidence can be interpreted. In the following, we discuss the essential features of the complete nucleation process which in the standard experimental procedures leads to the formation of colloidal nanoparticles, taking in account the possibility of forming metal–metal bonds already after the first reduction step.

3.4.1 Role of the hydrolysis in the reduction process

It is known that the reduction of $PtCl_4^{2-}$ is faster when the solution has been aged to allow the water substitution of one or two chlorine ligands, according to the reactions (3.2) and (3.3) of section 3.1 [69]. Thus, hydrolysis facilitates in some

way the electron transfer from the reducing agent to the metal complexes. The investigation of the electron transfer mechanism is beyond our scopes. Consistent with the experimental observations, we may assume that electrons are transferred to the Pt(II) metal complexes only after hydrolysis. Our gas phase electronic structure calculations support this assumption, giving a positive VEA only for the hydrolyzed diaqua-complex $PtCl_2(H_2O)_2$.

3.4.2 Reduction of a Pt(II) complex to the monovalent and zerovalent state

In all our simulations, both in the gas phase and in water solution, the addition of one electron to $PtCl_2(H_2O)_2$ leads to a well characterized linear Pt(I) complex $PtCl_2{}^-$. The $PtCl_2{}^{2-}$ complex, where the Pt(0) atom is in the d^{10} electronic configuration, is obtained both by adding one further electron to $PtCl_2{}^-$ and by adding two electrons to $PtCl_2(H_2O)_2$ at one time.

We note that many examples exist of twofold-coordinated linear complexes of transition metal atoms in the d^{10} electronic configuration, *e.g.* $Hg(CN)_2$, $Au(NH_3)_2{}^+$ and $AgCl_2{}^-$ [73]. In addition, whereas, to our knowledge, no examples of complexes containing one Pt(I) atom have been reported, linear $Pt(0)L_2$ complexes, where L is generally a phosphine, are known [99]. Phosphines are able to stabilize Pt(0) atoms through the overlap of their lone pair with the empty $6s$ Pt orbital, whose associated energy level raises relative to the $5d$ level if the atom is complexed [100]. Chlorine ligands, however, are not really effective in stabilizing atoms of late transition elements in low oxidation states, so that the $PtCl_2{}^{2-}$ complexes cannot presumably survive for a long time in the solution. This may explain why they have not been reported experimentally as stable species. If H_2O and Cl^- are the only available ligands (*e.g.*, in the present case of a K_2PtCl_4 solution), Pt(0) has been experimentally reported only in the form of metal particles. The Pt(I) and Pt(0) dichloro-complexes $PtCl_2{}^-$ and $PtCl_2{}^{2-}$ should be thus thought as metastable reaction intermediates. Interestingly, during the simulations it was always the water ligands and never the chlorine ones which were

observed to dissociate upon reduction of the $PtCl_2(H_2O)_2$ complex. After this, the dichloro complexes remained stable for all the time of the MD simulations and no water substitution was observed. These results indicate that the Pt atom in the d^9 and in the d^{10} electronic configuration is better stabilized by chlorine than by water.[4] We note that this does not exclude the possibility of water/chlorine exchanges, which are certainly possible in the experimental time scale, inaccessible to our simulations. Indeed, the linear dichloro-complex $AgCl_2^-$, very similar to $PtCl_2^{2-}$, is known to undergo partial hydrolysis [101]. However, it is a reasonable assumption that, for a fairly long time since the beginning of the reduction, negatively charged Pt(I) and Pt(0) linear dichloro-complexes are present in the solution.

3.4.3 Formation of the first Pt–Pt bonds

After some of the Pt(II) complexes are reduced to Pt(I), the nucleation of clusters may take place by various mechanisms, namely (i) further reduction to Pt(0) and formation of bonds with other zerovalent atoms; (ii) formation of bonds with other Pt(I) complexes and (iii) formation of bonds with Pt(II) complexes. The first mechanism corresponds to the classical nucleation model, while the second is reminiscent of a reaction mechanism which has been proposed to explain the formation of Pt(I) dimers after reduction of platinum salts in solution [80]. The third mechanism is the one suggested by the results of our simulations. In the case of K_2PtCl_4 we expect both the first and the second mechanisms to be limited by a further hydrolysis of the reduced complexes. Hydrolysis is necessary since reactions between negatively charged complexes would otherwise have to occur which are presumably hindered by long-range repulsive electrostatic forces. As discussed in the former section, the hydrolysis of $PtCl_2^-$ or $PtCl_2^{2-}$ never occurred in the simulations, so that these processes are likely to be associated to non-negligible energy barriers. As a consequence, both the first and the second mechanisms imply an activation energy for the nucleation of the cluster.

[4] Similarly, an adsorbed layer of chlorine ligands is always present on the surface of colloidal Pt(0) metal particles [2].

On the other hand, the reaction between $PtCl_2{}^-$ and $PtCl_2(H_2O)_2$ occurs spontaneously within a few ps in our room temperature simulations. This indicates that when a reducing agent is added to an aged solution of K_2PtCl_4, and as soon as a Pt(II) complex is reduced to Pt(I), there is a reaction path leading to a Pt–Pt bond which does not require an appreciable activation energy and does not imply bonding of negatively charged complexes. This reaction may thus play an important role in the formation of Pt dimers, and more generally in the nucleation of Pt colloidal particles.

3.4.4 Formation of a Pt(I) dimer

In our simulations, after a bond between a Pt(II) complex and a Pt(I) complex is formed, the addition of a further electron leads to a Pt(I) dimer after the loss of a chlorine ligand. Some indirect evidence of the existence of a Pt(I) dimer intermediate in the reduction of a K_2PtCl_4 solution is related to one of the first isolated monovalent platinum dimers [22], the $[Pt_2Cl_4(CO)_2]^{2-}$ ion. This complex, structurally very similar to the Pt(I) dimer obtained in our simulations, can be produced with a method which closely resembles the standard colloid preparation, when a suspension of the K_2PtCl_4 salt in concentrated hydrochloric acid solution is stirred with carbon monoxide at atmospheric pressure [22]. The main difference between this procedure and the standard preparation of colloids lies in the high concentration of Cl^- ions and in the presence of CO (the latter being both a reducing agent and a stabilizing ligand for platinum). Under these conditions, further reduction and growth accompanied by loss of the ligands is simply not possible, because of the strong metal–CO interaction and of the high concentration of Cl^- ions present in solution. However, if extracted from the solution and dipped in water, the dimeric salt is not stable and a black precipitate is obtained, which is presumably formed by aggregation of metallic particles [22].

Thus, the preparation of $[Pt_2Cl_4(CO)_2]^{2-}$ may be seen as a reduction process "frozen" at an intermediate step by the presence of stabilizing ligands in sufficient concentration, which would otherwise proceed until colloidal particles are formed.

3.4.5 Nucleation of colloidal particles

When no stabilizing ligands are present in the solution, a dimer may represent an intermediate step toward the formation of bigger clusters. In particular, in the earliest stage of the reduction process, the concentration of unreduced Pt(II) ions is much higher than that of the reduced complexes. If the reduction rate is not too high, the formation of a bond between Pt(II) and Pt(I) complexes, which according to our results does not imply an activation energy, is thus a likely event.[5] Once the Pt(II)–Pt(I) bond is formed, our results indicate that the addition of a second electron can promote the loss of a chlorine ligand (cf. figure 3.5 d). This way, the negative charge localized on the dimer is not increased when the formal valence state of the whole complex is reduced.

An iterated reduction/dechlorination mechanism could be important in the following stages of the reaction, favouring the reduction while the cluster grows by addition of Pt atoms which can be in a reduction state higher than zero. This model growth mechanism is remindful of what we observe in our calculations, where a bond forms between a Pt(II) atom in the stable d^8 electronic configuration and a second Pt atom in the unstable open-shell d^9 electronic configuration. Trying to generalize this result, we can ask if similar reactions may happen at the surface of an open-shell cluster, playing the role of our d^9 Pt atom. This would imply that not only the addition of reduced Pt(0) atoms to a growing cluster is possible, but also that of unreduced Pt(II) ions. This issue will be the subject of the next chapter.

A key point of the present nucleation model is the formation of a Pt(I) complex reaction intermediate. We note that the existence of a Pt(I) intermediate has been already postulated [70] in the context of the sonochemical reduction of $PtCl_4{}^{2-}$ to colloidal platinum.[6] Additionally, when Pt(II) is reduced by hydrogen,

[5] On the other hand, if a very high number of reducing electrons are available, the complete reduction to Pt(0) may presumably occur before the aggregation of atoms starts, as in the classical nucleation model.

[6] Similarly, it has been suggested that the electrochemical reduction of Pt(IV) on graphite involves the formation of a Pt(III) intermediate [102].

a mechanism where Pt(I) is the first intermediate can explain well the kinetics of the whole reduction process [74]. We note that a mechanism similar to the one proposed here has been proposed [10] to explain the nucleation of clusters upon radiolytic reduction of monovalent ions like Ag^+ and Au^+. Formation of dimers after aggregation of reduced Ag(0) atoms with excess Ag^+ ions as well as addition of monovalent ions to growing clusters has been observed [10]. According to our FPMD results also bivalent platinum ions can form dimers after a single reduction step, suggesting that this may be a more general property of late transition metals.

Chapter 4

Growth of Pt clusters in solution

The subject of this chapter is the growth of platinum clusters after the reduction of K_2PtCl_4 in aqueous solution. The formation of the first Pt–Pt bonds after the start of the reduction process has been investigated by means of first principles molecular dynamics in chapter 3. We observed that a Pt(II) complex is able to react with a partially reduced Pt(I) complex, in which the Pt atom is in the open-shell electronic configuration d^9 [67]. Here, we generalize this reaction mechanism investigating the addition of free Pt(II) complexes to Pt_2, Pt_{12}, and Pt_{13} clusters in various oxidation states. The results allow us to suggest that both the nucleation and the growth of platinum clusters proceed through the same molecular mechanism. Namely, cluster form from the very beginning via steps of Pt(II) addition to a partially reduced cluster followed by further reduction of the whole growing seed. This is consistent with the observed autaoccelerating kinetics of the formation process of metal nanoparticles [79] and suggests a stable growth path of platinum clusters in the presence of very mild reducing agents.

4.1 Possible mechanisms of cluster growth

The formation of metal clusters upon reduction of a dissolved metal salt is a process that involves two different chemical reactions: (1) A reduction reaction where the metal ions are reduced to the metallic (zerovalent) state, and (2) an aggregation reaction, which leads to enlargement of the cluster by addition of metal atoms to a growing nucleus. Other more complex growth processes, such as the coalescence of two small clusters to form a bigger one, are not considered at this stage of the study. The formation of clusters can be thought to occur through several mechanisms, which differ one from the other by how the reduction and the

aggregation reactions are separated in time. According to the classical nucleation mechanism proposed by LaMer [77, 78], the reduction reaction occurs in a first stage of the process and leads to the formation of zerovalent atoms. In a second stage, the zerovalent atoms aggregate to form a metal cluster (see section 3.2). Thus, the global process of particle formation can be separated in a *nucleation* stage, where the reduction reaction occurs, and a *growth* stage, where a diffusion-limited aggregation reaction takes place. A different model has to be considered when the presence of growing clusters has a direct influence on the kinetics of the reduction reaction. In fact, the formation of transition metal clusters is known to occur in an *autocatalytic* way, where the first formed clusters catalyze the further reduction of dissolved complexes [69, 89]. In a proposed mechanism [79], the autocatalysis starts after a first reaction stage, where small clusters are formed by aggregation of previously reduced zerovalent atoms. The subsequent growth takes place via the reduction of ions in situ, on the catalytic cluster surface. Thus, in this second stage the reduction and the aggregation reactions cannot be considered as two separate processes. Like in the classical mechanism of LaMer, in this model the global process of particle formation can be splitted in two well distinct stages of nucleation and growth. In particular, the formation of a critical nucleus still requires the complete reduction of complexes followed by the aggregation of the zerovalent atoms.

On the other hand, we have shown in the previous chapter that the formation of a Pt dimer does not necessarily requires the complete reduction of the two Pt complexes involved in the reaction. Already after a *single* reduction step, a chemical bond can form between the Pt atoms. In other words, during the reduction of a dissolved platinum salt the aggregation process can start without waiting for a critical concentration of zerovalent atoms. Furthermore, we have hypotisized that also the growth process may occur via addition of *unreduced* Pt(II) complexes to open-shell growing clusters. According to this model mechanism, which is investigated in the following, the growth of platinum particles proceeds in a way that minimizes the overall reduction barrier. Indeed, while the electron transfer process from the reducing agent to the metal ions is often

the limiting stage of the whole cluster formation process [10], metal colloids are observed to form starting from bivalent platinum salts even in the presence of very mild reducing agents. Like in the previous chapter, the electron transfer from a specified reducing agent to the growing cluster is not directly addressed in our study. The system contains from the beginning the number of electrons necessary for the desired reduction state. Among the possible Pt(II) complexes, we consider in the simulations only the $PtCl_2(H_2O)_2$ complex. This is the hydrolysis product of $PtCl_4^{2-}$ which is supposed to participate actively in the process of cluster formation upon reduction [67, 74].

4.2 FPMD simulations

We report here the results of our FPMD simulations. First, the formation of a Pt trimer after addition of Pt(II) complexes to the dimers obtained in chapter 3 is simulated. Then, we turn to the investigation of the reaction between a Pt(II) complex and clusters of 12 and 13 atoms in various oxidation states. For these investigations, we used a CP algorithm which is appropriate to simulate metallic systems [65, 66], as described in chapter 2.

4.2.1 Formation of a Pt trimer

In chapter 3, we have found that after one electron is added to a $PtCl_2(H_2O)_2$ complex, the two water ligands are lost, and the Cl^- ligands rearrange so that a linear $PtCl_2{}^-$ complex is obtained. The Pt(I) complex is able to react with a second $PtCl_2(H_2O)_2$ complex with formation of a Pt–Pt bond along the z axis of $PtCl_2(H_2O)_2$. In this way, a Pt(I)–Pt(II) dimer is formed after a single reduction step (figure 4.1 **A**). At this point, this dimer could either receive a second reducing electron from the reducing agent, or react again with a Pt(II) complex. The addition of a further electron has been studied in chapter 3, and leads to the loss of a chlorine ligand with strengthening of the Pt–Pt bond. The obtained Pt(I)–Pt(I) dimer is shown in figure 4.1 **B** In the following, we investigate the reactions of the Pt(I)–Pt(II) dimer and of the Pt(I)–Pt(I) dimer with further

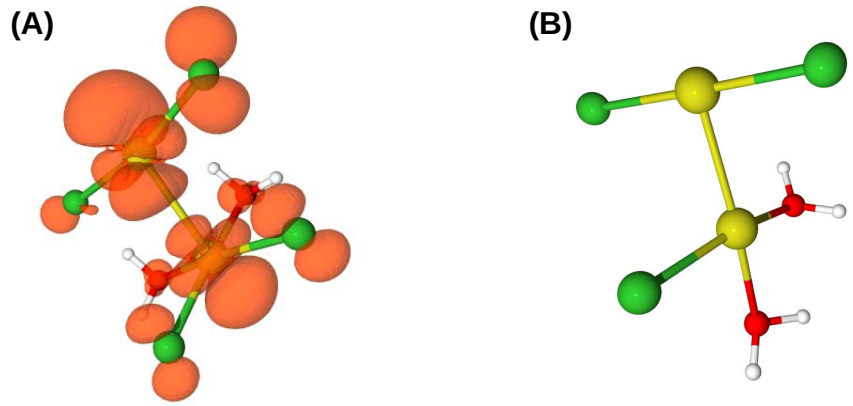

Figure 4.1: (**A**) The dimer obtained in chapter 3 after addition of one electron to a system containing two Pt(II) complexes. The particle density associated with the unpaired electron is shown as an iso-surface at the value of 0.002 au. (**B**) The dimer obtained after addition of a second electron to the dimer in **A**.

Pt(II) complexes.

A trimer formed after a single reduction step

The particle density associated with the unpaired electron of the Pt(I)–Pt(II) dimer presents an unbounded orbital lobe located on the Pt(I) unit, which is expected to be a reactive site (figure 4.1 **A**; see also figures 3.6 and 3.8 of chapter 3). A FPMD simulation is thus started considering a system where a Pt(II) complex approaches the Pt(I)–Pt(II) dimer from the side of the Pt(I) unit (figure 4.2 **A**). The initial Pt–Pt distance between the free Pt(II) complex and the Pt(I) atom of the dimer is set to about 3.6 Å. After about 0.2 ps of simulated time this distance is decreased to about 3.0 Å, then the system oscillates around the equilibrium for about 1.5 ps and the simulation is stopped. After quenching the atomic motion, a structure corresponding to a minimum of the potential energy surface is reached. In the final configuration (figure 4.2 **B**) the Pt(I) unit is bound to two Pt(II) units forming a linear Pt trimer, where the Pt–Pt distances are 3.01 and 3.10 Å. The same reaction could be observed in a simulation cell filled with water molecules to model the solution environment. In this case, the

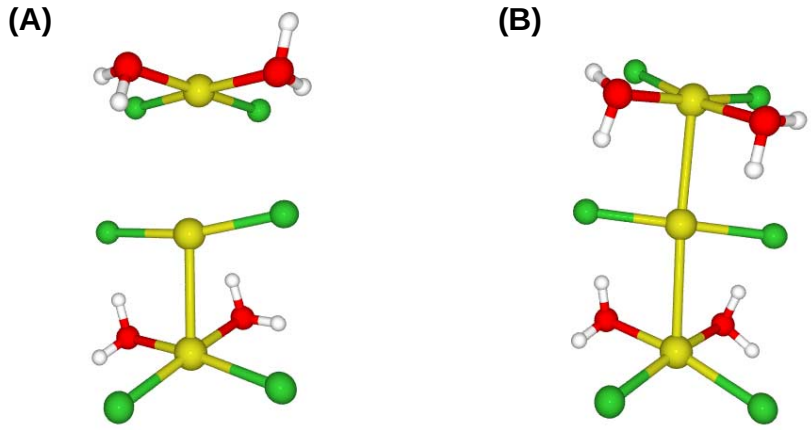

Figure 4.2: Snapshots of a FPMD simulation showing the formation of a Pt trimer after a single reduction step. (**A**) A Pt(II) complex approaches the Pt(I)–Pt(II) dimer shown in figure 4.1 A. (**B**) The final trimer structure.

final Pt–Pt distances in the trimer are both reduced to ~ 2.9 Å. The final trimer geometry is shown in figure 4.3 together with the particle density associated with the unpaired electron.

A trimer formed after two reduction steps

The formation of a Pt(I)–Pt(I)–Pt(II) trimer is simulated considering a system where a Pt(II) complex approaches the Pt(I)–Pt(I) dimer of figure 4.1 **B**. The initial Pt–Pt distance between the Pt(II) complex and the threefold-coordinated Pt(I) atom of the Pt(I)–Pt(I) dimer is set to ∼4.0 Å (figure 4.4 **A**). After about 0.5 ps of simulated time a Pt–Pt bond is formed between the Pt(II) complex and the Pt(I)–Pt(I) dimer, and after quenching of the atomic motion the Pt(II)–Pt(I) distance is 2.80 Å (figure 4.4 **A**). Interestingly, a water molecule detaches from the Pt(I)–Pt(I) dimer during the formation of the bond with the Pt(II) complex. Thus, the trimer presents a new reactive site for further addition and/or reduction reactions.

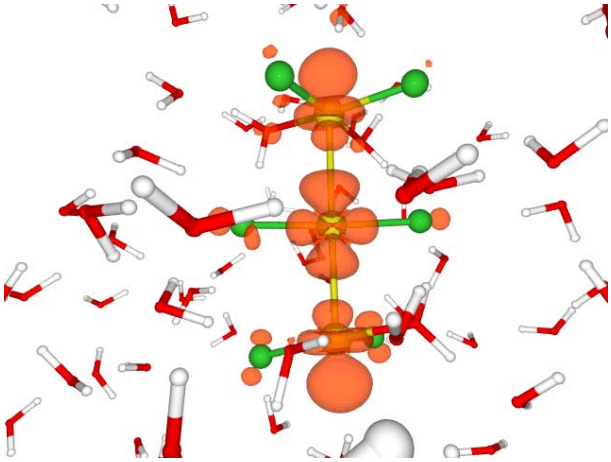

Figure 4.3: A Pt(II)–Pt(I)–Pt(II) trimer immersed in water obtained in a FPMD simulation. The orange isosurface at 0.002 au depicts the particle density associated with the unpaired electron.

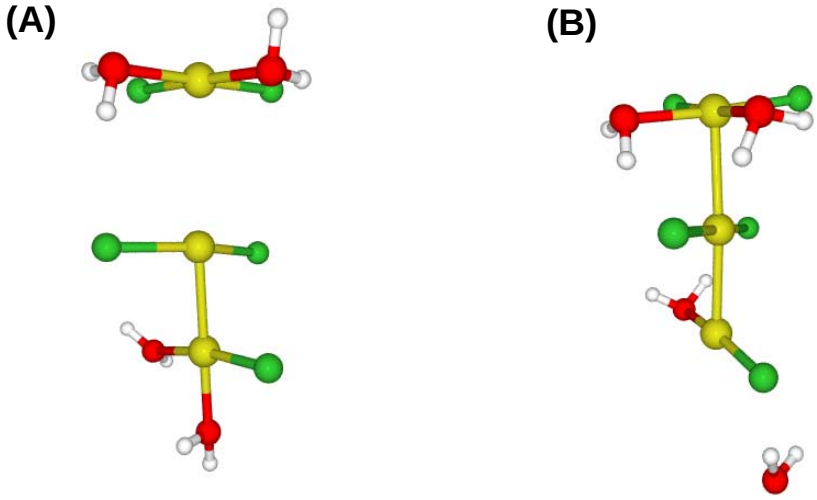

Figure 4.4: Snapshots of a FPMD simulation showing the formation of a Pt trimer after two reduction steps. (**A**) A Pt(II) complex approaches the Pt(I)–Pt(I) dimer shown in figure 4.1 B. (**B**) The final trimer structure.

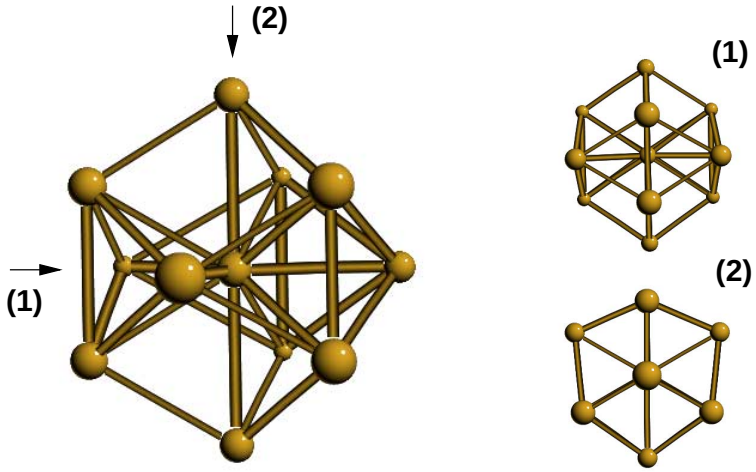

Figure 4.5: The naked Pt_{12} cluster obtained after annealing of 12 Pt(0) atoms starting from an arbitrary BCC structure. One of the three twofold-symmetry axis present in the cluster is labeled with **(1)**, and a twofold-symmetry axis is labeled with **(2)**. Views along both axis are shown on the right side.

4.2.2 Growth of a Pt_{12} cluster

We turn now to study the growth of a bigger cluster, modeling the addition of a complex to a Pt_{12} cluster. This simulation system is chosen because the reaction product is the first atomic closed-shell cluster Pt_{13}, according to the series of Chini magic numbers (see section 1.1.3).

A naked Pt_{12} cluster

To find a structure of Pt_{12} corresponding to a local minimum of the potential energy surface, we start with a configuration of 12 Pt(0) atoms in a BCC structure, with minimum Pt–Pt distances of 3.3 Å. The system is first annealed for ∼2 ps in a FPMD simulation at 600 K, then the atomic motion is slowly quenched down until the equilibrium geometry of figure 4.5 is reached. The cluster consists of a central Pt atom surrounded by the other 11 atoms. The presence of three twofold-symmetry axis and of one threefold-symmetry axis in the cluster structure is evidenced in figure 4.5. 32 Pt–Pt bonds are present in the cluster, with a mean Pt–Pt distance of 2.73 Å.

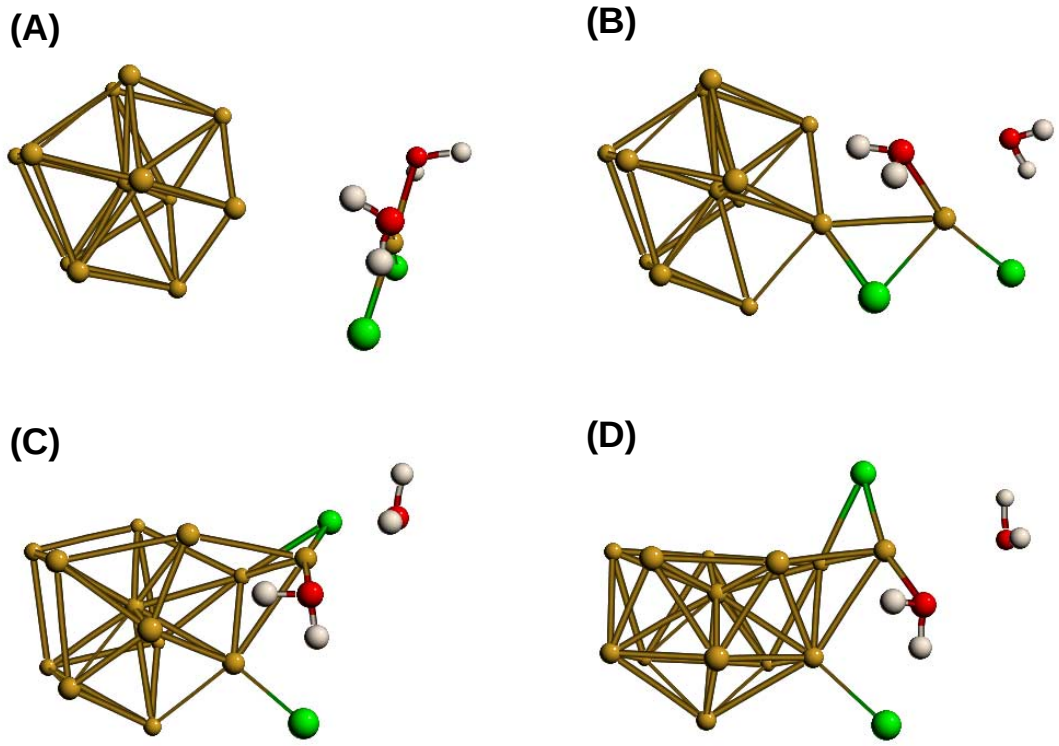

Figure 4.6: Snapshots from a FPMD simulation showing the reaction of a $PtCl_2(H_2O)_2$ complex with a naked Pt_{12} cluster. (**A**) Initial configuration. (**B**) After ∼0.5 ps of simulated time, the Pt(II) complex adsorbs on the cluster surface with formation of a direct Pt–Pt bond and of a bridge through one of the Cl^- ligands. (**C**) After about 2 ps, the Pt(II) atom has formed three bonds with atoms of the cluster, and one of the Cl^- ligands is left on the cluster surface. (**D**) Final configuration, after about 5 ps of simulated time.

Reaction of $PtCl_2(H_2O)_2$ with the naked Pt_{12} cluster

The reaction of the naked Pt_{12} cluster with an unreduced $PtCl_2(H_2O)_2$ complex is studied in a FPMD simulation at constant energy (figure 4.6). During the dynamics, the temperature oscillates between ∼250 and ∼350 K. The Pt(II) complex is initially placed on top of one of the Pt(0) atoms forming the cluster, and the Pt(II)–Pt(0) distance is set to about 3.7 Å (figure 4.6 **A**). Immediately, the Pt(II) complex approaches the Pt_{12} cluster, and adsorbs on its surface. At this point, one of the Cl^- ligands moves toward the underlying cluster and forms

a bridge between one atom of the cluster and the Pt(II) atom (figure 4.6 **B**). In the rest of the dynamics, the Pt atom initially belonging to the Pt(II) complex forms up to three bonds with other Pt atoms (figure 4.6 **C**). During the formation of the new Pt–Pt bonds, the whole structure of the cluster changes, consistently with the high mobility of the surface atoms in small transition metal clusters at room temperature [105]. After about 5 ps of simulated time, the atomic motion is quenched and the system reaches the equilibrium structure of figure 4.6 **D**.

Reaction of $PtCl_2(H_2O)_2$ with a $Pt_{12}Cl_4$ cluster

In the previous simulation, we observed the reaction of an unreduced Pt(II) complex with a fully reduced Pt_{12} clusters. This shows that unreduced metal ions can be incorporated into small metal clusters at room temperature without noticeable energy barriers. With the aim of simulating more closely a process of cluster growth under mild reducing conditions, we increase the global oxidation state of the Pt_{12} cluster by addition of chlorine ligands arbitrarily distributed on its surface, keeping the whole system neutral. Minimization of the $Pt_{12}Cl_4$ structures leads to a minimum energy configuration where the symmetry of the metal core remains unaltered upon addition of the chlorine ligands. The equilibrium Pt–Cl distances are all equal to 2.24 Å. The relaxed structure is shown in figure 4.7 together with the empty orbital states above the Fermi level, which are mainly localized on the Pt atoms free of ligands. These empty orbital lobes are expected to be reactive sites for bond formation via electron acception from closed shell complexes in aggregation reactions.

The reaction of $Pt_{12}Cl_4$ with a $PtCl_2(H_2O)_2$ complex is investigated in a FPMD simulation at the mean temperature of ∼300 K (figure 4.8). The initial distance between the Pt(II) atom and the nearest Pt atom of the cluster is set to ∼3.7 Å. (figure 4.8 **A**) As expected, the $PtCl_2(H_2O)_2$ complex is soon adsorbed on the cluster surface (figure 4.8 **B**) forming a Pt–Pt bond along the z axis of the square-planar complex. Later, also the chlorine ligands bind to Pt atoms of the cluster (figure 4.8 **B,C**). Like in the previous simulation, the Pt(II) atom starts

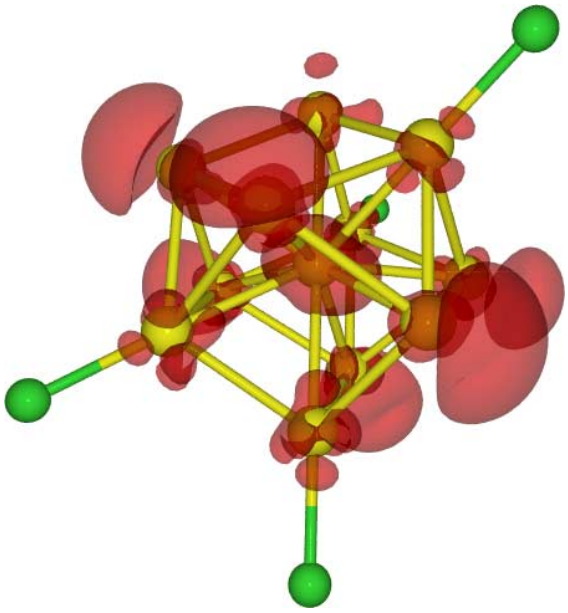

Figure 4.7: Relaxed structure of the $Pt_{12}Cl_4$ cluster considered in the simulations. The empty states above the Fermi level are depicted with a red semitransparent isosurface.

forming several bonds with the other Pt atoms. After about 2 ps of simulated time, the Pt atom originally belonging to the Pt(II) complex is completely incorporated into the cluster structure and cannot be distinguished from the other Pt atoms composing the cluster. This consists at this point of a central Pt atom coordinating the other surrounding 12 Pt atoms (figure 4.8 **D**). Six chlorine ligands are adsorbed on the cluster surface. Remarkably, in spite of the *magic number* nuclearity of the formed cluster (Pt_{13} is the first atomic closed-shell cluster), this structure is *not* a local minimum of the potential energy surface. Indeed, letting the system evolve spontaneously from this point, the central atom moves off its position (figure 4.8 **E**). The whole cluster structure changes completely, and a structure consisting of three stacked (111) slabs of Pt atoms is obtained after $\sim$3.2 ps of simulated time. The system remains in this configuration for $\sim$1.8 ps more, then the atomic motion is slowly quenched down. The final equilibrium structure is shown in figure 4.8 **F**.

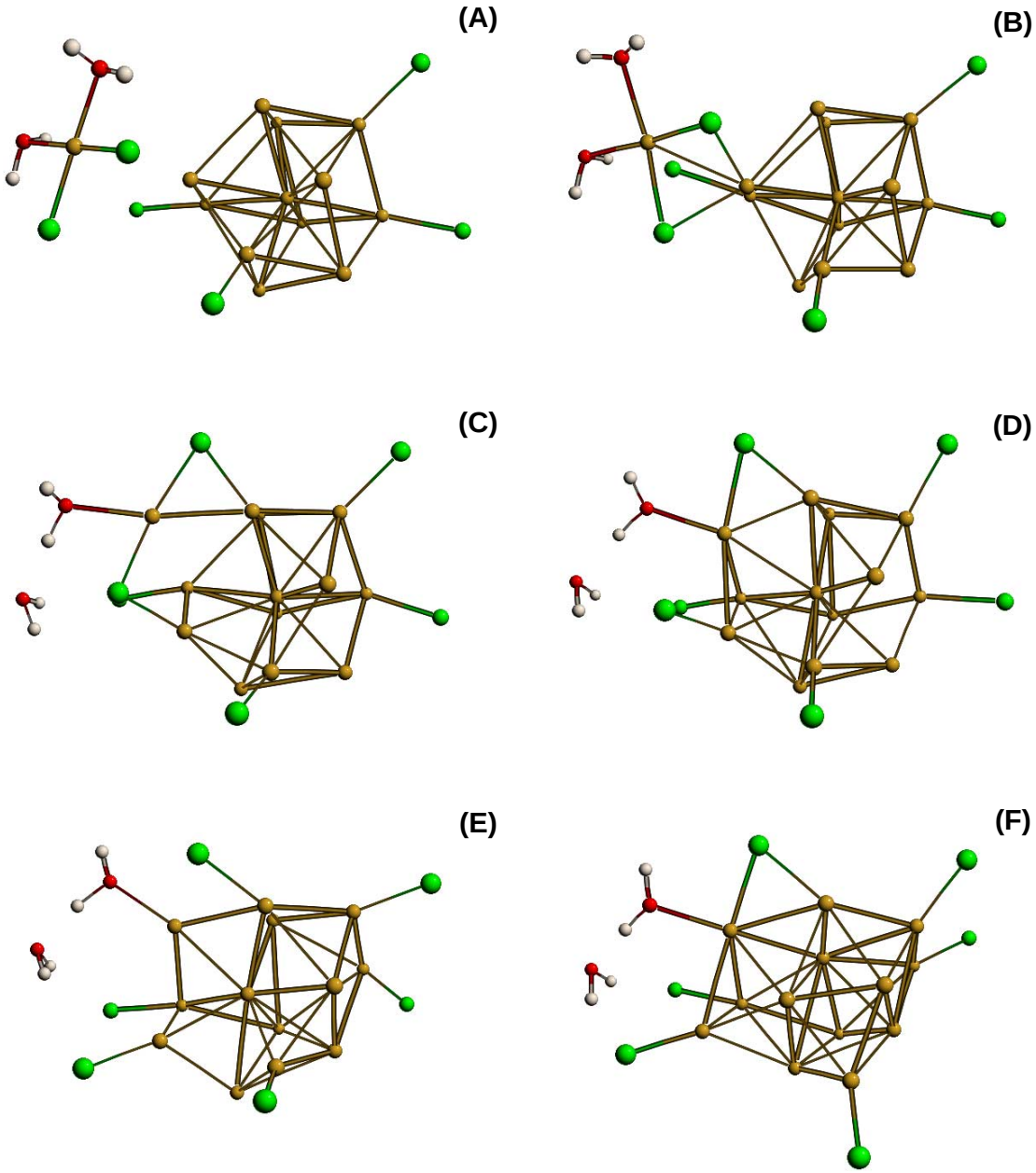

Figure 4.8: Snapshots from a FPMD simulation showing the reaction of a $PtCl_2(H_2O)_2$ complex with a ligated cluster $Pt_{12}Cl_4$. (**A**) 0.0 ps of simulated time; (**B**) 0.6 ps; (**C**) 1.3 ps; (**D**) 2.0 ps; (**E**) 3.2 ps; (**F**) 5.0 ps.

Reaction of $PtCl_2(H_2O)_2$ with a $Pt_{13}Cl_6$ cluster

A further addition step of Pt(II) complexes to the growing cluster is observed in a new FPMD simulation. A $PtCl_2(H_2O)_2$ complex is placed near to the optimized cluster structure $Pt_{13}Cl_6$ obtained in the previous simulation (figure 4.9 **A**). The distance between the Pt(II) atom and the nearest Pt atom of the Pt_{13} cluster is set to ∼3.6 Å. Once again, soon the Pt(II) complex is adsorbed on the cluster surface, and the Pt(II) atom is fully incorporated into the cluster structure (figure 4.9 **B**–**D**). During the simulation, three chlorine ligands move in phase from "on top" positions (figure 4.9 **B**) to "bridge" positions (figure 4.9 **C**) with respect to the Pt atoms composing the cluster. Later, one of the ligand moves again to an "on top" position on a Pt atom nearby (figure 4.9 **D**). This demonstrates the ability of the ligands to freely diffuse on the cluster surface at room temperature [103, 104]. The FPMD simulation is stopped after about 5 ps of simulated time. The final structure is shown in figure 4.9 **D**.

4.3 Discussion of the results

The structure and energetics of transition metal clusters have been so far investigated theoretically by means of empirical [105], semiempirical [31], and recently ab initio [9, 85, 106] static calculations. From the results of these investigations, some considerations have been made about possible cluster growth paths [31,105]. In this thesis, the specific problem of cluster growth is addressed for the first time by means of ab initio dynamical simulations. As starting point, we assume as a fundamental feature of the cluster formation mechanism the observed reactivity of unreduced Pt(II) complexes toward bond formation with open-shell Pt atoms [67]. In an attempt to generalize this reaction mechanism, we have studied the adsorption of $PtCl_2(H_2O)_2$ complexes on Pt_2, Pt_{12} and Pt_{13} clusters in various oxidation states.

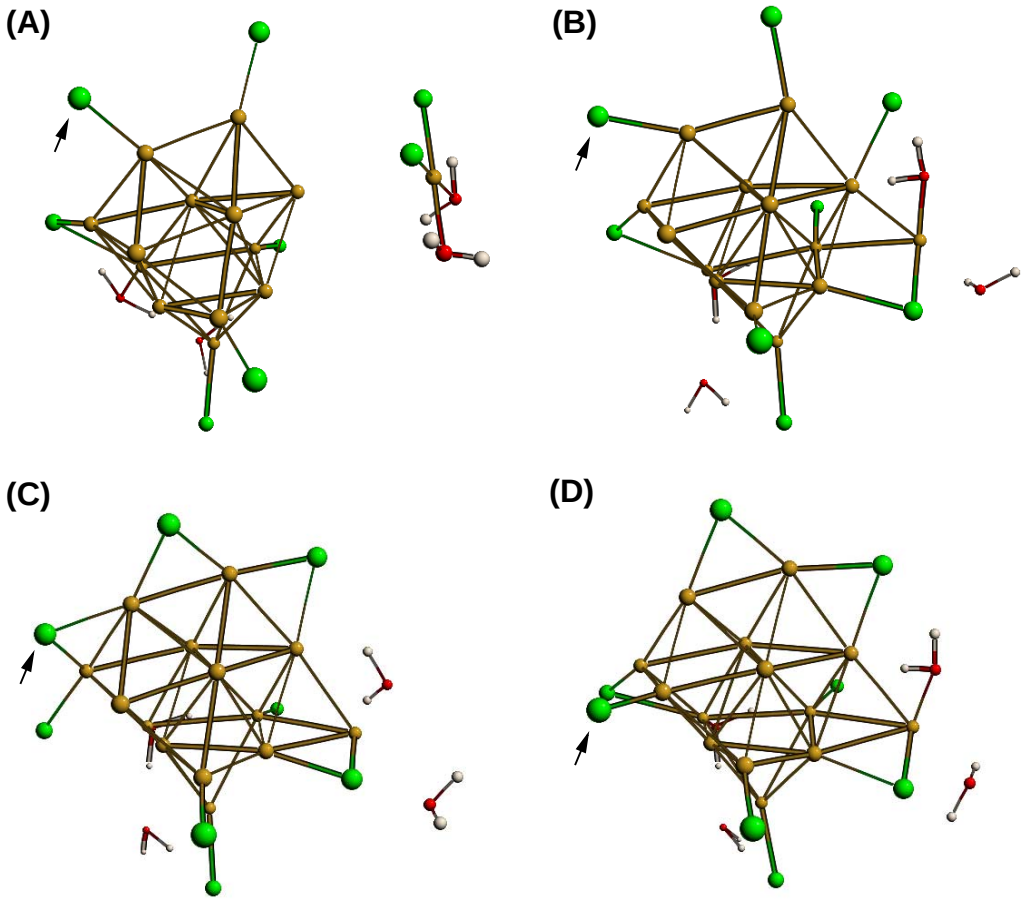

Figure 4.9: Snapshots from a FPMD simulation showing the reaction of a $PtCl_2(H_2O)_2$ complex with a ligated cluster $Pt_{13}Cl_6$. (**A**) 0.0 ps of simulated time; (**B**) 1.4 ps; (**C**) 3.5 ps; (**D**) 5.2 ps. The arrow indicates a chlorine ligand which changes adsorption site during the simulation.

4.3.1 Aggregation of complexes to growing clusters

In general, the reaction $Pt_{n-1} + Pt \rightarrow Pt_n$ is expected to be exothermic, if the atoms are all in the zerovalent state [31]. From static calculations of a big number of different naked Pt cluster structures, no obvious pattern appears for the metallic growth according to this reaction [31]. This means, the aggregation of atoms to a growing cluster is expected to imply a large reorganization of the metallic structure. Namely, first the atoms are adsorbed onto reactive sites of the cluster surface (as, e.g., edges or steps), then low energy rearrangements of the cluster

skeleton lead to the minimum energy structure for the given nuclearity [105].

The results of our FPMD investigations are all consistent with the statements above. In room temperature simulations, we observe that the addition of a new atom to a stable cluster leads to a complete rearrangement of the cluster structure without noticeable energy barrier and within a few ps of simulated time. However, here we do not assume a complete reduction to the zerovalent state prior to the aggregation reduction. In all simulations presented in the previous section, an unreduced Pt(II) complex first adsorbs on the cluster surface. Then, without adding any reducing electron to the system, the Pt(II) atom is completely incorporated into the cluster structure.

The aggregation reaction occurs via electron donation from the occupied d_{z^2} orbital of the square planar complex into the empty orbital lobes localized on free atoms of the cluster surface (see fig. 4.7). Interestingly, the reaction proceeds in the same way even if the cluster is not completely reduced to the metallic state. Thus, addition of Pt(II) complexes should be possible as long as reactive sites are present on the cluster surface, and is *not* dependent on the overall oxidation state of the cluster.

4.3.2 An autocatalytic growth mechanism

Through addition of Pt(II) complexes, both the oxidation state and the nuclearity of a cluster increase with the effect of enhancing its electron affinity. Thus, the reduction becomes more and more favourable during the growth process. On the other side, the reduction process is expected to cause desorption of chlorine ions from the cluster surface, as observed in the case of the Pt(II)–Pt(I) dimer in chapter 3. Thus, new reactive sites for further addition of complexes are created after reduction. In other words, the reduction and the aggregation processes take advantage one from the other, and both become easier and easier during cluster growth. This explains why the growth of platinum cluster is an autocatalytic process [69, 79], and suggests a stable growth pathway under minimal reducing conditions (see figure 4.10).

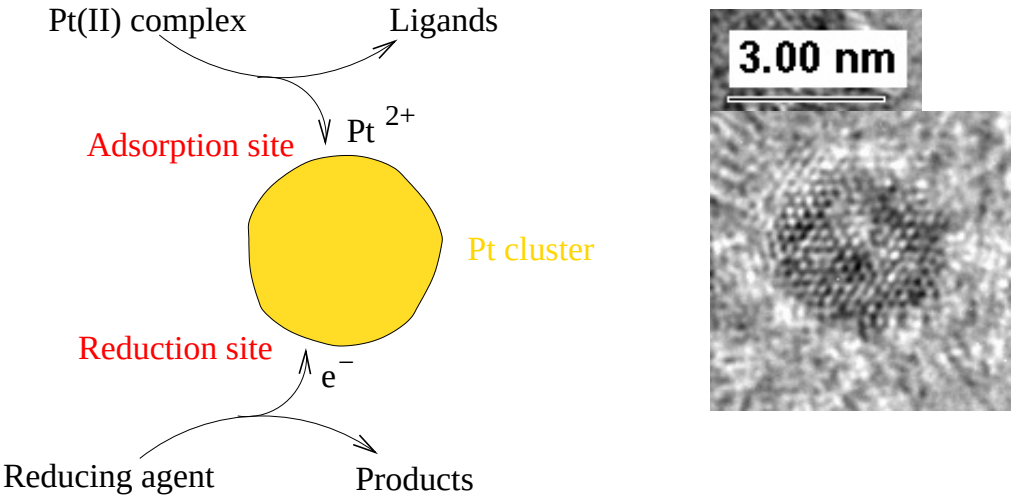

Figure 4.10: Scheme of the autocatalytic mechanism proposed in this thesis (left), leading to formation of platinum nanoparticles (right).

Noteworthy, the formation of platinum cluster proceeds through this mechanism from the very beginning of the reduction process. Already the formation of dimers and trimers can occur, in principle, after a single reduction step and without noticeable energy barrier. For this reason, we suggest that a *nucleation* stage cannot be distinguished from a *growth* stage on the basis of a molecular mechanism of atom aggregation. The overall cluster formation process is expected to be limited by the barriers encountered in the electron transfer process, in particular in the early stages. However, in the presence of a sufficiently strong reducing agent, the growth of cluster is expected to occur spontaneously already from the initial reduction step. In other words, a singly reduced Pt(I) complex can be considered as a (degenerate) "critical nucleus" for the cluster growth.

4.3.3 Role of the ligands during cluster growth

In our simulations, the oxidation state of the clusters is defined by the number of chlorine ligands adsorbed on the cluster surface. This choice of the simulated system is consistent with the growth mechanism described above, where chlorine

ligands leave the clusters only after reduction. We observe a high mobility of the chlorine ligands on the cluster surface at room temperature. Indeed, the *fluxionality* of the ligands is a known phenomenon in the physics of metal clusters [103, 104, 107]. In our simulations, the ligands are able to move from on-top to bridge adsorption sites and vice versa without encountering any noticeable energy barrier. Three ligands are observed to move "in phase", at the same time (see figure 4.9). This observed behaviour is promoted by the addition of new chlorine ligands to the cluster during the reaction with a $PtCl_2(H_2O)_2$ complex. This leads to a cascade effect driven by the steric and electrostatic repulsions between the ligands.

It is known that ligands play a fundamental role in stabilizing the structure of small metal clusters. The presence of only few chlorine ligands is not enough to "freeze" the growing metal cores in a stable geometry. In particular, the $Pt_{13}Cl_6$ cluster obtained in one of the simulations (figure 4.8) does not present a spherical close-packed geometry of the metal atoms, as is the case for naked Pt_{13} clusters [18] and of other strongly ligated M_{13} clusters [107]. On the contrary, starting from a geometry where a central Pt atom is surrounded by the other atoms, a compact structure consisting of three stacked layers of atoms arranged in a triangular lattice is obtained after the central atom has moved off its position. This open cluster geometry offers further reactive sites for the addition of unreduced complexes, as we observed in a successive simulation (figure 4.9). Small *magic number* Pt clusters consisting of 13 and 55 noble metal atoms are indeed very difficult to isolate, and are stable only in the presence of complex ligand systems [23]. In conclusion, a growth process involving mild reducing agents and low concentration of chlorine ligands is not expected to stop after formation of small clusters. This is consistent with the fact that size distributions of clusters obtained after reduction of dissolved K_2PtCl_4 in the presence of surfactants weakly bounded to the cluster surface are normally centered on much bigger nuclearities [89].

Chapter 5

Formation of Pt clusters on DNA

In this chapter, the mechanism of formation of metallic nanoparticles on biological substrates is investigated. In particular, we focus on the nucleation and growth of metal clusters on DNA molecules.[1] Under particular conditions, the formation of Pt cluster takes place *selectively* on DNA templates upon reduction in K_2PtCl_4 solution. This means that the homogeneous nucleation of clusters in solution is kinetically suppressed and heterogeneous nucleation exclusively occurs at the DNA. This condition is accomplished by allowing Pt(II) complexes to bind to the DNA bases before starting the reduction process. The formed Pt(II)·DNA adducts act then as preferred sites for the nucleation of clusters, where the initial Pt–Pt bond formation involves *unreduced* Pt(II) complexes (see chapter 3). Theoretical modeling reveals that the heterogeneous nucleation is promoted by the strong donor character of the nucleotides, which stabilize and strengthen newly formed Pt–Pt bonds already after the first reduction step. A clean *in situ* metallization of DNA substrates becomes possible as a result, as demonstrated by the fabrication of ultra-thin necklaces of nanoparticles extending over the whole DNA length (figure 5.1).

The results presented here are published in reference [108], and are obtained in close collaboration with other colleagues from the bio-nanotechnology group of our institute. The TEM and AFM images of this chapter were recorded by Ralf Seidel [109] with a Philips CM 200 TEM at 200 keV, and with a Digital Instrument NanoScope IIIA AFM working in tapping mode, respectively.

[1] Note that, as in chapter 3, *nucleation* is thought as a synonym of *initial cluster formation*, both nucleation and growth occurring through the same molecular mechanisms (see chapter 4).

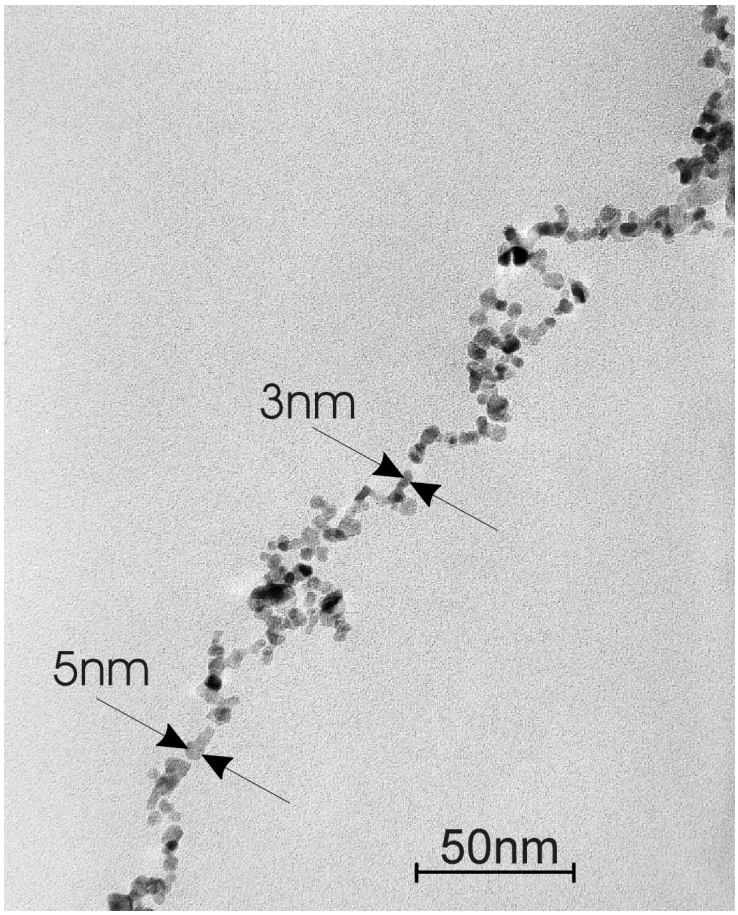

Figure 5.1: "Necklace" of platinum nanoparticles selectively grown on a single DNA molecule string. Note the absence of homogeneously nucleated clusters in the background.

5.1 The procedure of DNA metallization

In a typical experiment [109], the DNA molecules are "activated" by incubation of a DNA solution with an aged solution of K_2PtCl_4 (1 mM) for at least $\sim$ 20 h at room temperature, keeping a complex-to-nucleotide ratio (C/N) of 65:1. During the incubation, some of the Pt(II) complexes bind covalently to the DNA bases. The complexation of Pt(II) with DNA has been intensively investigated, especially in the case of the antimitotic anticancer drug cisplatin, which binds to DNA strands in a sequence-specific way [110]. The most favourable binding site is the N_7 position of guanine, to which hydrolyzed Pt complexes coordinate already

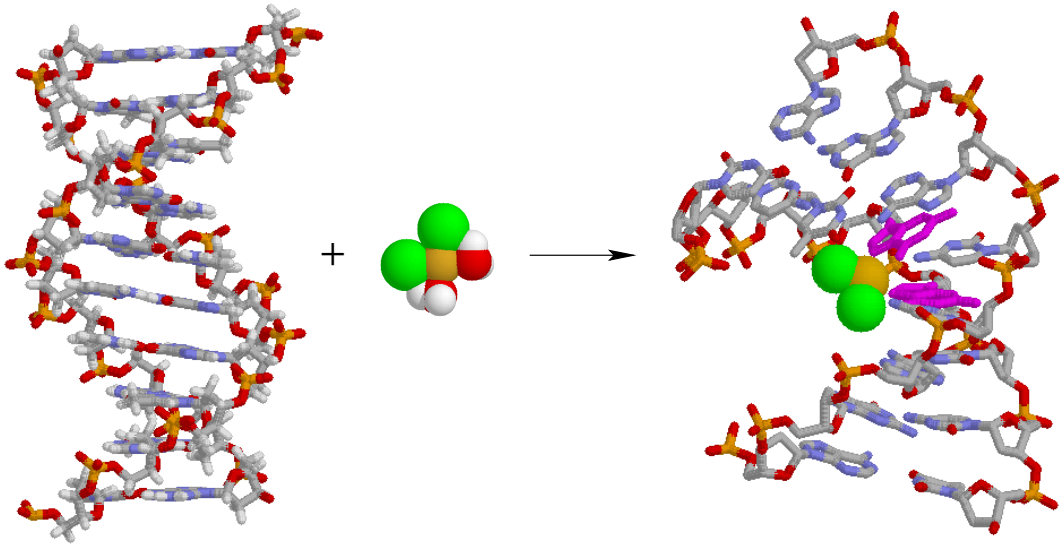

Figure 5.2: Reaction of a $PtCl_2(H_2O)_2$ complex with a DNA decamer. The X-ray structure of the Pt·DNA decamer (on the right side) is taken from reference [111].

after a few minutes of incubation (figure 5.2). Accordingly, the initial reaction of tetrachloroplatinate with DNA takes place preferentially at (GC) planes [112]. However, at high C/N ratios and after ∼20 h of incubation, all other possible metal-binding sites along the biopolymer become occupied, and a saturation value of six Pt complexes per (AT,GC) unit is reached [112]. After the activation step, dimethylamine borane (DMAB) is added to the solution to reduce Pt(II) to metallic platinum. In the absence of DNA or any additional capping agent, the reduction of an aged solution of K_2PtCl_4 would lead to the formation of clusters which readily aggregate to form a colloidal suspension of relatively large Pt agglomerates (figure 5.3 **A**). In the presence of activated DNA we obtain regular, continuous chains of nanoparticles of about 5 nm diameter extended over the whole DNA length (figures 5.1 and 5.3 **B**). The lattice plane distances within the particles are identical to those of bulk platinum in high resolution TEM images (figure 5.4).

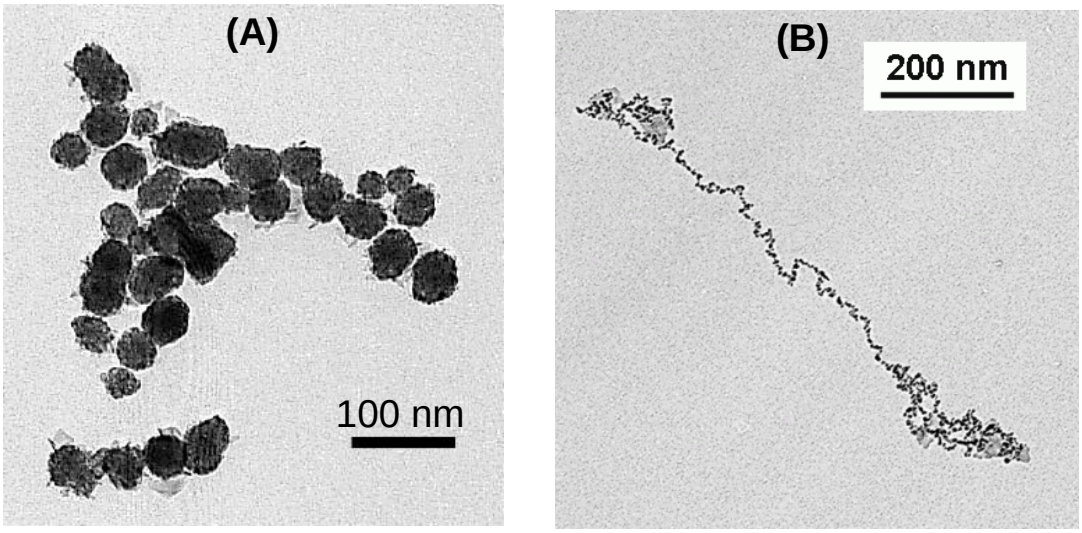

Figure 5.3: (**A**) Aggregates of platinum particles formed homogeneously after reduction of an aged solution of K_2PtCl_4. (**B**) Platinum particles nucleated selectively on a λ-DNA molecule (from reference [113]), after incubation of DNA with an aged solution of K_2PtCl_4 and subsequent reduction.

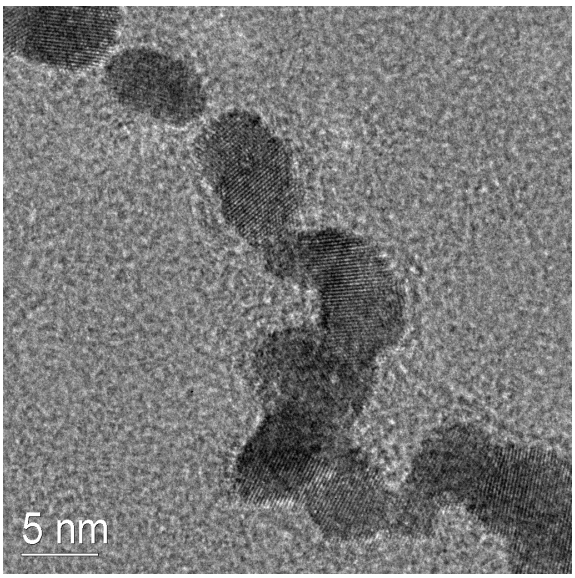

Figure 5.4: HRTEM image of platinum nanoparticles grown selectively on a DNA molecule (see figures 5.1 and 5.3 **B**). Fourier transform analysis of these particles reveals peaks corresponding to the lattice-plane spacing of bulk platinum.

5.1.1 Cluster formation governed by DNA activation

The reduction/aggregation mechanism of complexed metal ions in the presence of DNA has never been systematically investigated. More generally, the heterogeneous nucleation of clusters in the presence of organic polymers –a process of primary importance in the production of metal catalysts– is not yet understood in detail [6]. In particular, the role of organometallic complexes which might be formed before the metal atoms are reduced to the metallic state is not clear [76, 114]. Here, we show that cluster nucleation upon reduction of $PtCl_4{}^{2-}$ ions in the presence of DNA is governed by Pt(II)·DNA adducts formed before the reduction in the base-specific activation step. This is the result of two series of observations, which are shown to correspond to two ways of tuning the properties of DNA as a metallization template. Firstly, adjusting the activation time prior to reduction enables control of the balance between the heterogeneous nucleation at the DNA template and the homogeneous nucleation occurring in the solution. Secondly, the reaction kinetics can also be controlled by varying the content of guanine-cytosine (G–C) vs. adenine-thymine (A–T) base-pairs in the DNA sequence at fixed activation time. Both observations are reported in detail in the following.

Homogeneous vs. heterogeneous nucleation

The rate of the nucleation process and the balance between heterogeneous and homogeneous nucleation can be controlled by varying the activation time t_a, that is, by altering the number of Pt(II) complexes covalently bound to DNA before the reduction is started. This is revealed by monitoring the reduction kinetics by UV-VIS spectroscopy in the non-specific light absorption range ($\lambda = 600$ nm) and by imaging the morphology of the final structures with AFM. By increasing t_a, the kinetics of the process *accelerates* (figure 5.5), and the observed nucleation behavior changes dramatically (figure 5.6). Large aggregates of homogeneously nucleated particles form after short activation times ($t_a \sim 0$), although some small clusters grown on the DNA strands are also visible (figure 5.6 **A**). However,

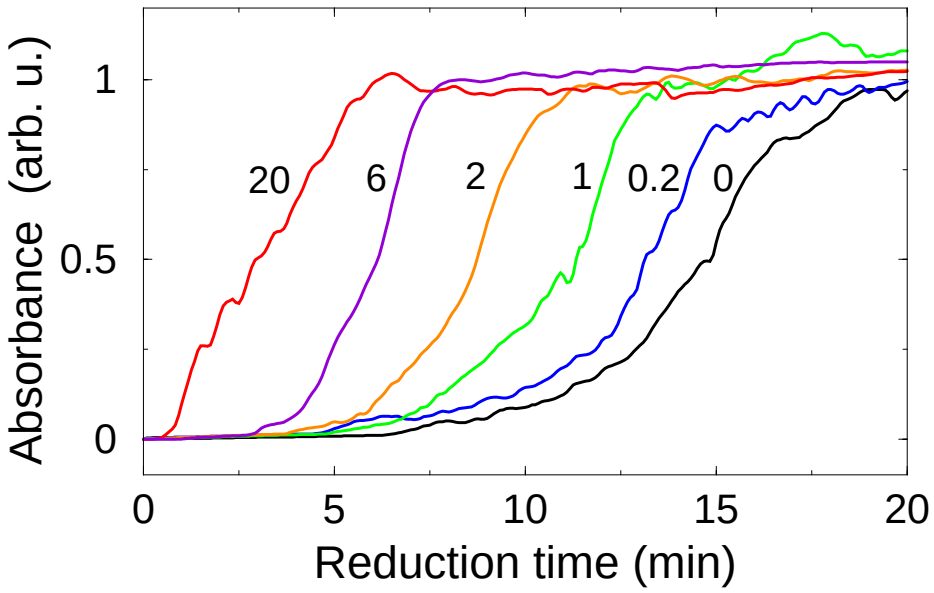

Figure 5.5: Time evolution of the absorbance (at $\lambda = 600$ nm) of a 1 mM aged solution of K_2PtCl_4 during reduction in the presence of DNA molecules. The DNA was kept in the platinum salt solution for different activation times t_a (indicated in hour units beside each curve) before starting the reduction with DMAB. The development of absorbance in the non-specific absorption region of the UV-VIS-spectrum of Pt complexes indicates the formation of colloidal platinum and the aggregation of small colloidal particles into bigger structures during the reduction process.

only heterogeneous nucleation takes place after long activation times ($t_a \sim 20$ h, figures 5.6 **B**, 5.1, and 5.3 **B**).

Sequence-dependent reduction kinetics

The *in situ* metallization process is thus selectively promoted by the activation of the DNA substrate before the reduction. This suggests that Pt(II)·DNA adducts formed during the activation step strongly promote heterogeneous cluster nucleation, enhancing the reaction rate. Such a mechanism would imply a faster reduction process after a short activation time for a higher content of (GC) base pairs in the DNA, since for short interaction times Pt(II) complexes are known to bind primarily to guanine bases [112]. We can therefore investigate the role of

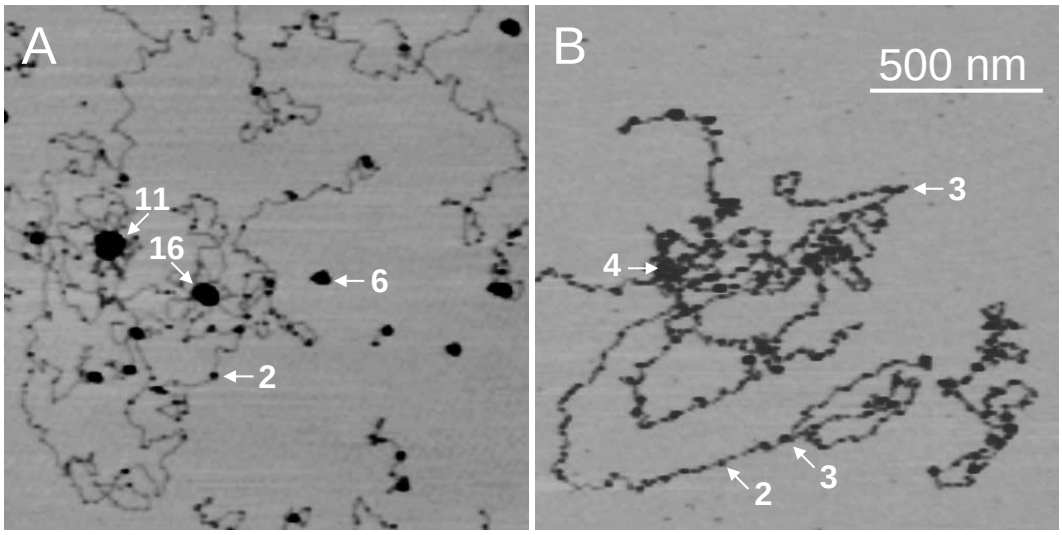

Figure 5.6: Products of the metallization process of non activated (**A**) and activated DNA (**B**), immobilized onto mica and imaged by SFM in tapping mode. The scan size is 1.5 μm x 1.5 μm for both images. The height of selected particles, indicated by arrows, is reported in nm units.

Pt(II)·DNA adducts by performing metallization experiments at variable DNA composition. We used three different types of DNA as templates, containing 26 %, 41 % and 72 % of (GC) planes. Before starting the reduction, activation of DNA with Pt(II) complexes was accomplished for times ranging from 10 min to 48 h. The characteristic reduction time t_r, defined as the reaction time at which the absorbance is half its saturation value, is reported in table 5.1 for each DNA type. As expected, at short and intermediate t_a, we observe a faster reduction process for higher G contents. Moreover, the dependence of t_r on the (GC) content levels out for long t_a, i.e. when all possible binding-sites along the molecule are occupied.

5.2 FPMD simulations

The formation of Pt clusters is a nucleation-limited process [79], which means that once a small nucleus is formed, cluster growth proceeds autocatalytically [69,79]. Since in the experiments presented in the previous section heterogeneous nucle-

Activation time	26 % (GC)	41 % (GC)	72 % (GC)
10 min	13.5	13.0	12.7
30 min	12.6	11.4	11.0
1 h	11.1	10.7	8.8
2 h	10.2	8.7	7.8
16 h	5.9	5.5	5.1
48 h	3.4	3.1	3.4

Table 5.1: Variation of the characteristic reduction times t_r (in minutes) of the metallization process with the activation time t_a for three different DNA types containing different amounts of (GC) base pairs. DNA from *Clostridium perfringens* (containing 26.5 % of (GC) base pairs), salmon testes (41.2 % (GC)) and *Micrococcus luteus* (72 % (GC)) purchased from SIGMA-ALDRICH was used.

ation dominates over homogeneous nucleation, the presence of Pt(II) complexes bound to the DNA must favour the initial stages of cluster growth. In particular, the first step of cluster growth –the formation of a Pt dimer after a single reduction step [67]– is expected to be easier if at least one of the Pt atoms is covalently bound to a DNA base. To investigate this issue, we model the Pt dimer formation at DNA by means of first-principles molecular dynamics (FPMD) simulations [40]. The competing process –homogeneous cluster nucleation upon reduction of K_2PtCl_4 in solution– has been extensively studied with the same techniques in chapter 3.

5.2.1 Choice of the simulation system

During the incubation of the DNA with the platinum salt solution, Pt(II) complexes react with the nucleotides to form both monofunctional and bifunctional adducts, that is, the Pt atom binds to one or to two DNA bases. The K_2PtCl_4 solution used has been previously aged to allow hydrolysis of the tetrachloroplatinate ions according to the reactions (3.2) and (3.3), as discussed in chapter 3. After reaction of Pt(II) with the DNA bases, further hydrolysis of the Pt(II)·DNA adducts is expected to occur in the time scale of our experiments.

To model the Pt(II)·DNA adducts we consider two representative systems: a partially hydrolyzed complex bound to a guanine, G·$PtCl_2(H_2O)$ [**GP**], and a fully hydrolyzed complex bound to two stacked guanines, GG·$Pt(H_2O)_2$ [**GGP**]. These complexes are chosen to model two limit cases in our experimental process: The monofunctional **GP** complex is representative for adducts formed in the early activation stages, while a bifunctional and completely hydrolyzed **GGP** complex represents adducts formed after a long activation time.

In the simulations, two stacked bases model the whole DNA substrate. The steric constraint exerted by the DNA molecule is modeled by binding the N_9 atom of each guanine to a methyl group, which is kept fixed. We assume that neither the complementary strand nor the backbone qualitatively influence the mechanism of dimer formation. This is justified by the observed selective affinity of Pt complexes for the *bases* of DNA [110], and is consistent with the localization of the LUMO state of a Pt(II)/*d*(pGpG) system on the metal/guanine center [115]. In addition, the reactions to simulate –occurring in the major groove of DNA– are expected not to be sterically hindered by the DNA structure. All the static and dynamical simulations are performed in a cubic cell with edge-length 18 Å, which prevents any significant interaction between the simulated system and its periodically repeated images.

5.2.2 Reduction of the Pt(II) complexes

In this study, we do not attempt a direct calculation of the electronic affinity of the complexes considered. This would be a very difficult task due to the complexity of the system to simulate and the net charge present in some cases in the simulation cell. More simply, we study *qualitatively* the reduction properties of the considered systems by calculating the energy gap between the highest occupied molecular orbital (HOMO) and the lowest unoccupied molecular orbital (LUMO) in each model system. The computed HOMO-LUMO energy gap values of the $PtCl_2(H_2O)_2$ [**P**], the **GP** and the **GGP** complexes are 2.34 eV, 2.25 eV and 1.13 eV, respectively. This indicates that the reduction of fully hy-

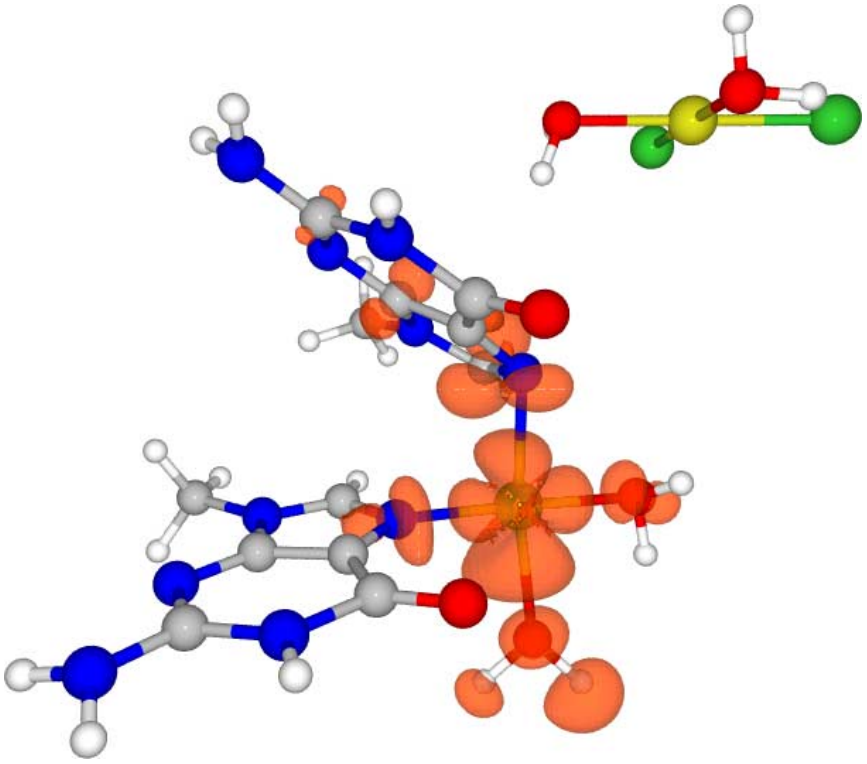

Figure 5.7: Localization of a reducing electron added to a system containing a Pt·DNA adduct and a free Pt(II) complex. The particle density associated with the additional electron is depicted as an orange semi-transparent iso-surface at the value of 0.002 au.

drolyzed bifunctional Pt·DNA adducts is favoured over the reduction of free **P** complexes. This is consistent with the observed localization of a reducing electron in a system containing a **GGP** and a **P** complex. After electronic minimization at fixed atomic positions, the additional electron is completely localized on the Pt(II)·DNA complex (figure 5.7). Within the plane-wave formalism used in this study, this ensures that the most favourable reduction sites of the whole system are the Pt·DNA adducts formed during the activation step of the experimental procedure.

After addition of one electron to the **GP** or the **GGP** complex, in dynamical simulations we observe the detachment of a water molecules from the Pt atom, in both cases. We note that in solution the reduction of a **P** complex causes the detachment of both water ligand with rearrangement of the geometry, leading

to the linear molecule $PtCl_2{}^-$. In the case of Pt(II)·DNA complexes, a whole geometry rearrangement is hindered by the steric confinement of the bases in the DNA helix structure. This has the effect of precluding the loss of both water ligand, and a threefold-coordinated complex with an empty orbital lobe is obtained (see figure 5.8 (A1)). The following step of the Pt dimer formation –the reaction with a second Pt complex– is investigated in the next section.

5.2.3 Formation of a Pt dimer at the DNA

In the presence of both free Pt complexes in solution and Pt·DNA complexes, the most favoured reduction sites are the Pt atoms bound to DNA. Pt dimers may thus form via the reaction of reduced Pt·DNA adducts with unreduced **P** complexes approaching from the solution (reaction path **(1)**). However, under our experimental conditions only less than 3% of the total Pt(II) complexes are bound to the nucleotides. Thus, a second reaction path (reaction path **(2)**) should be considered, where a **P** complex is reduced in solution to $PtCl_2{}^-$ before binding to an unreduced Pt·DNA adduct. FPMD simulations at 300 K are performed to investigate both reaction paths (figure 5.8). The observed pattern of events in reaction path **(1)** is essentially the same whether the system includes a **GGP** adduct (figure 5.8, top) or a **GP** adduct (not shown). First, a water molecule detaches from the Pt atom complexed to DNA immediately after one electron is added to the system. The reduced Pt·DNA complex and an approaching unreduced **P** complex then start forming a Pt-Pt bond oriented along the **P** complex z axis after ∼0.5 ps of simulated time (figure 5.8 A1–B1). At this point, a water ligand detaches from the **P** complex and the geometry of the Pt dimer gradually changes, until a structure consisting of two tilted Pt/ligands half-plane units connected by the Pt–Pt bond is reached (figure 5.8 C1). The equilibrium Pt–Pt distance after structural relaxation is 2.57 Å in both the **GP** and the **GGP** systems, with Pt–Pt bond energies of 1.82 eV and 2.25 eV, respectively.[2] For

[2]The reported gas-phase bond energy values are calculated for each Pt dimer as the absolute value of the difference between the total energy of the fully relaxed dimer structure and the total energy of the same system after increasing the Pt–Pt distance to 12 Å and relaxing the

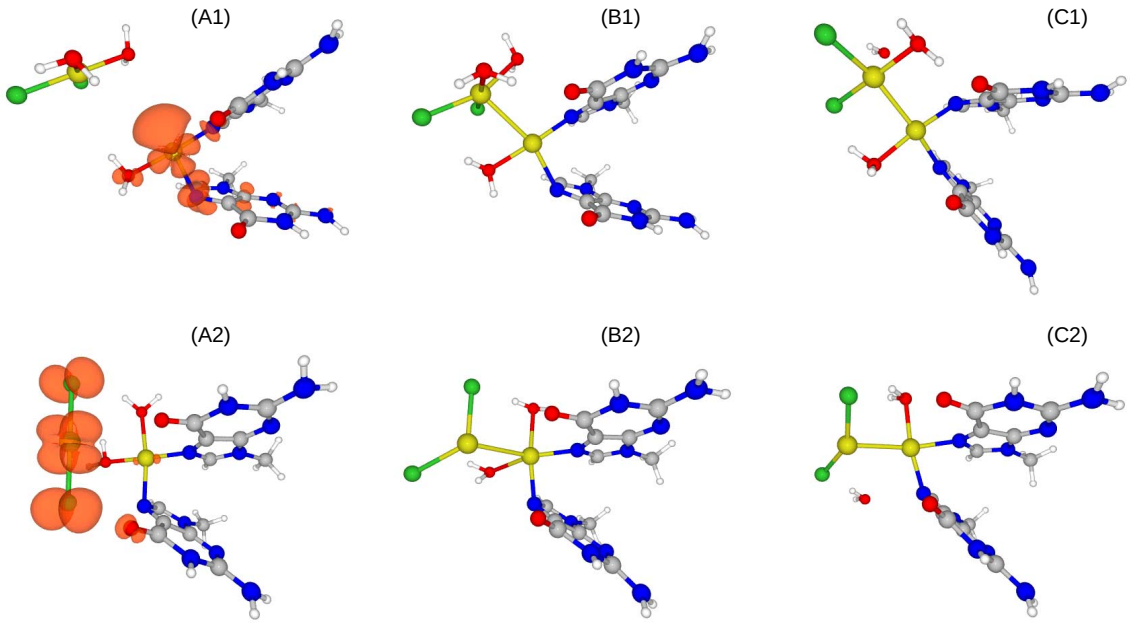

Figure 5.8: Snapshots of two FPMD simulations of the formation of platinum dimers bound to two stacked DNA bases, following the reaction paths **(1)** (top) and **(2)** (bottom) described in the text. Pt: yellow, Cl: green, O: red, N: blue, C: grey, H: white. The orange iso-density surface at 0.002 au is associated with the unpaired orbital state of the reactant species reduced before dimer formation.

comparison, in the Pt_2^{hom} dimer obtained upon single reduction of a system of two $PtCl_2(H_2O)_2$ free complexes in solution, the equilibrium Pt–Pt distance is 2.87 Å and the Pt–Pt bond energy is 1.52 eV (see section 3.3 and reference [67]). Thus, reduction at DNA and heterogeneous dimer formation following path **(1)** are energetically favoured and lead to stronger Pt–Pt bonds than the corresponding processes which lead to homogeneous dimer formation in solution.

FPMD simulations of path **(2)** yield the reaction of a reduced $PtCl_2^-$ complex with a **GGP** complex (figure 5.8, bottom) or a **GP** complex (not shown). Once more, the two reactions proceed in a similar way. A Pt–Pt bond initially forms along the z axes of the Pt·DNA adduct (figure 5.8 A2–B2). This leads to a configuration (figure 5.8 B2) analogous to the stable Pt_2^{hom} dimer structure

other atomic positions. These calculations are performed in a cubic cell with 18 Å edge length, the Pt atoms lying along the cube diagonal.

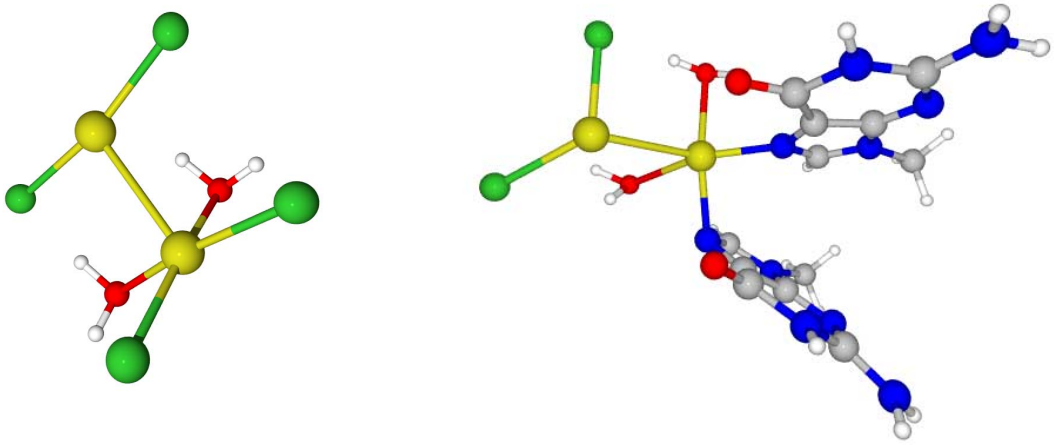

Figure 5.9: Comparison between two dimers obtained after a single reduction step of a system containing two Pt(II) complexes. (**A**) A Pt dimer formed homogeneously in solution (chapter 3), and (**B**) a snapshot from a FPMD simulation of the heterogeneous formation of a dimer at the DNA (cf. figure 5.8 B2).

obtained during homogeneous nucleation in solution (figure 5.9). Here, however, two guanine ligands replace the two *cis* Cl atoms of Pt_2^{hom}, and a further reaction step is observed. Namely, the top $PtCl_2^-$ unit displaces and substitutes one of the water molecules of the square planar Pt·DNA complex (figure 5.8 B2–C2). The equilibrium Pt–Pt distance after structural relaxation is 2.54 Å and 2.59 Å in the **GP** and the **GGP** systems, with bond energies of 1.74 eV and 2.38 eV, respectively. Thus, although in path (**2**) a free complex is initially reduced in solution, the more stable Pt dimers are once more those forming from Pt·DNA adducts.

5.2.4 The water substitution process

The reaction processes shown in figure 5.8 for paths (**1**) and (**2**) present various similarities. In both cases we initially observe the formation of a Pt–Pt bond aligned with the z axis of the square-planar Pt(II) reactant complex, which has one or two water ligands. Immediately after this, and without encountering any

appreciable energy barrier, the Pt(I) complex substitutes one of these water ligands, a reaction which is completed within 1.5 ps of simulation time at room temperature. A strong Pt–Pt bond whose length is typical of Pt(I) dimers [80] is obtained as a result in both cases, suggesting that the presence of nucleotide ligands is a sufficient condition to yield such bond geometry irrespective of the details of the reduction process. Interestingly, we find that this condition is also necessary; i.e., the water substitution process does not spontaneously occur in the absence of nucleotide ligands. Indeed, forcing the water substitution process in the $Pt_2{}^{hom}$ dimer produces a relaxed structure analogous to the one of figure 5.8 C2, with the Pt–Pt bond shortened to 2.52 Å. However, the process is now associated with a *positive* energy variation. In particular, switching the positions of the top $PtCl_2{}^-$ unit and a water ligand within the $Pt_2{}^{hom}$ dimer leads to a total energy increase of ∼0.2 eV. This indicates that the water substitution and the formation of a strong Pt–Pt bond are forbidden during homogeneous nucleation, and only become possible in the presence of the DNA substrate. We interpret this effect as a consequence of the strong donor character of the guanine ligands, which leads to charge density accumulation on the metal atom and weakening of its bonds with the other ligands located in both *trans* and *cis* positions [116, 117].

This issue is investigated by analysis of the electronic structure of a Pt(II)/imidazole complex. The imidazole ring is considered here as a good model both for DNA bases as, e.g., guanine and for heterocyclic aminoacids as, e.g., histidine. In figure 5.10 the orbital states of imidazole across the Fermi level are shown. Note the presence of both a σ-donor state (0.55 eV below the HOMO level) and of a π-donor state (1.21 eV below HOMO). A π-acceptor state is present, but is located very high in energy (5.11 eV) with respect to the HOMO level. Thus, imidazole is expected to be a strong donor ligand for late transition metal atoms. The optimized structure of an Im·$PtCl_2(H_2O)$ complex is shown in figure 5.11, and the bond distances are compared with the ones of a $PtCl_2(H_2O)_2$ (**P**) complex. In particular, the Pt–O distance between the central Pt atom and the water ligand in *cis* position with respect to the Imidazole ring is considerably larger in

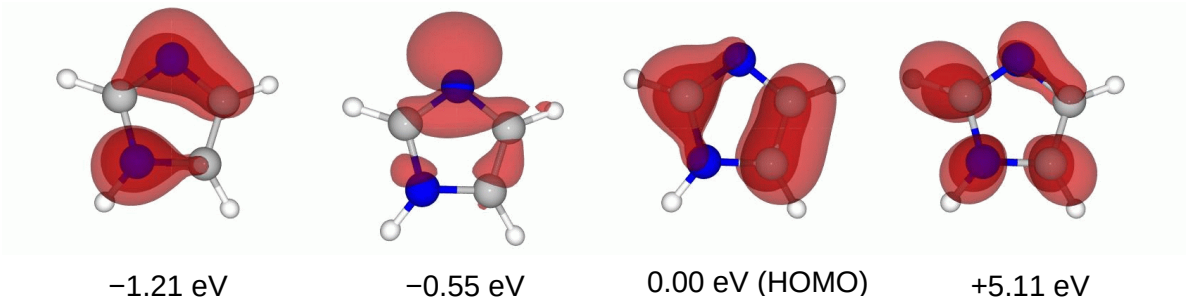

Figure 5.10: The orbitals of imidazole and their associated Kohn-Sham eigenvalues across the Fermi level. For each state, the associated particle density is depicted as an iso-surface at 0.003 au.

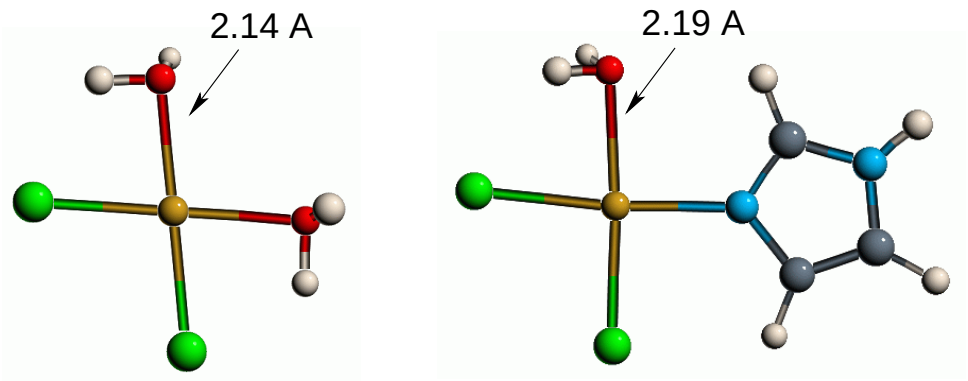

Figure 5.11: Comparison between the structures of a Im·$PtCl_2(H_2O)$ complex (right) and a $PtCl_2(H_2O)_2$ complex (left). Note the increased Pt–O distance when imidazole is present as a ligand.

the Im·Pt complex than in the **P** complex. This indicates a weakening of the Pt–O bond due to the presence of the heterocyclic ligand. Therefore, the water ligand is expected to be easily displaced in nucleophilic substitution processes, as observed during the formation of a Pt dimer bound to guanine ligands. This is consistent with the theoretical mechanism of substitution reactions in square planar complexes [117], where a ligand in *cis* position with respect to a strong σ-donor or π-donor group is expected to be displaced by the entering ligand.

The same water substitution process is observed during the formation of a Pt dimer after reduction of a **P** complex and reaction of the $PtCl_2{}^-$ unit with a

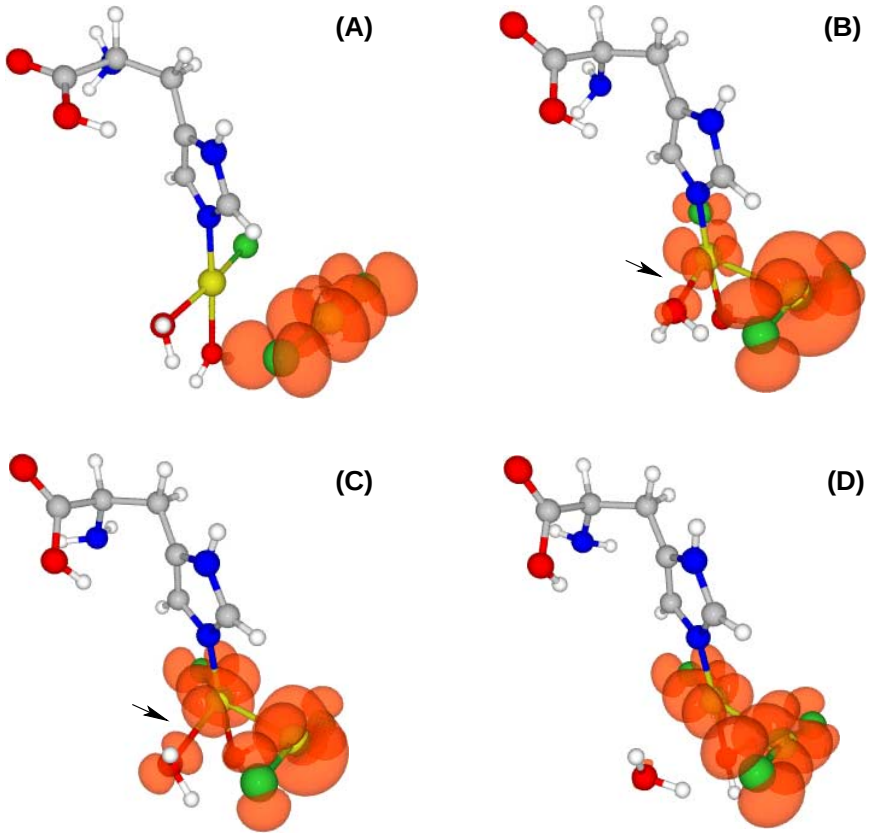

Figure 5.12: Snapshots of a FPMD simulation showing the formation of a strong Pt–Pt bond during the reaction of a reduced $PtCl_2^-$ complex with an unreduced His·Pt(II) complex (**A**–**D**). The electron density associated with the singly occupied orbital is depicted as an iso-surface at 0.002 au. A σ antibonding interaction (indicated with an arrow in **B** and **C**) localizes on a Pt–O bond and causes the detachment of a water ligand from the His·Pt(II) complex.

Pt(II) complex coordinated to a histidine ligand (figure 5.12). After the formation of the Pt–Pt bond along the z axes of the Pt(II) complex (figure 5.12 **B**), a σ antibonding interaction localizes between the Pt atom and the water ligand located in *cis* position with respect to the histidine ligand (figure 5.12 **C**). This causes the break of the Pt–O bond, and the water substitution process takes place (figure 5.12 **D**).

5.2.5 Further reduction steps

We have seen that, at the very beginning of the reduction reaction, the heterogeneous dimer formation at a DNA –involving stronger Pt–Pt bonds– is preferred over the homogeneous dimer formation in solution. In addition, the dimers formed at the DNA are expected to be preferential sites for further reduction processes leading finally to cluster formation. This arises from two observations: (i) Similarly to the Pt·DNA adducts discussed above, because of the presence of the heterocyclic guanine ligands, the heterogeneously nucleated Pt dimers can be expected to possess higher electron affinity than corresponding dimers in solutions. (ii) The process of water substitution during the formation of a strong Pt–Pt bond has an influence on the reduction properties of the formed dimer. In particular, our calculations indicate that the electron affinity of the Pt dimer is *enhanced* by the water substitution process taking place only at DNA. For instance, the computed electron affinity along reaction path (**2**) (section 5.2.3) increases by 0.4 eV when going from the B2 to the C2 geometry of the system in figure 5.8 (bottom). Thus, the metal dimers formed at DNA are expected to be preferential sites for further reduction processes allowing easier and easier incorporation of Pt atoms from the solution, consistent with the observed autocatalytic nature of the cluster formation [69, 79].

5.3 Discussion of the nucleation mechanism at the DNA

Building regular patterns of inorganic nanoparticles associated with DNA [13, 14, 38, 118–121] or proteins [29, 36, 37, 122] is an increasingly important field of materials science research. The main goal is to combine the self-assembly capabilities of biomolecules with the quantum properties (e.g., optical and electronic) of small particles, to fabricate a new generation of devices at the nanometer scale [14, 38]. A peculiarity of DNA as a biological macromolecule is the specificity of the Watson-Crick base pairing, which allows the programming of its

intra- and intermolecular associations and thus the building of supramolecular structures and networks [123]. Furthermore, DNA is an ideal template for the assembly of metal [13, 14, 38] and semiconductor [120, 121] clusters into wire-like structures, offering a variety of binding sites for several metal ions [124] and exhibiting remarkable mechanical properties [125].

Here we observe that DNA is also a substrate capable of selectively promoting the heterogeneous nucleation of metallic nanoparticles upon chemical reduction of a dissolved platinum salt. This provides a reaction channel for a clean metallization process, and thus reveals a novel functionality of DNA-based structures. Namely, we find that the competing homogeneous nucleation channel, where large metal clusters form in the solution and subsequently adsorb on the biomolecule, is kinetically suppressed under appropriate conditions. This is because cluster nucleation from a Pt complex seed is exceedingly faster if the complex contains one or two DNA bases as ligands, while cluster growth is a nucleation-limited process. By theoretical modeling, we demonstrated that the formation of Pt dimers at activated DNA is catalyzed by the local nucleotide/platinum chemistry. Thus, if Pt atoms are previously complexed to DNA, metallization nuclei form preferentially at activated DNA rather than homogeneously in solution. Going through an autocatalytic growth process, the first-formed heterogeneous nuclei quickly develop into bigger particles, consuming the metal complex feedstock present in the solution. In this way, metallic structures will nucleate and grow *exclusively in situ* during the reduction process, the DNA substrate acting thereby as a very effective catalyst for cluster formation.

Selective *in situ* nucleation appears to be necessary to grow thoroughly predefined metal nanostructures on a biomolecular template such as DNA. Under this conditions, thin, regular chains of platinum nanoparticles with an average diameter of 4 nm could be produced (figure 5.1) using a simple metallization procedure involving *activated* DNA but no other stabilizing ligands or surfactants. We suggest that other strong donor ligands than DNA, bound to metal ions before (or during) the reduction process to form organometallic complexes, may induce cluster nucleation in a similar way. This would be consistent with a mech-

anism which was proposed to explain the nucleation of gold colloidal particles after reduction of Au(III) complexes by citrate [114]. Furthermore, we expect that the nucleation of Pt nanoparticles on the surface of proteins [29, 36, 37, 122] may proceed as on DNA substrates, if heterocyclic aminoacids (e.g., histidine) are present.

Finally, we find that the heterogeneous nucleation is nucleotide-specific, with enhanced kinetics for higher guanosine content (table 5.1). These findings reveal a useful link between the chosen base sequence of the DNA template and the spatial distribution of active metallization seeds. Namely, heterogeneous cluster nucleation and tailored substrate design may be used to develop space-resolved metallization techniques in which metal structures are grown selectively on predefined portions of biological templates.

Conclusions

Homogeneous formation of Pt clusters in solution

In the FPMD simulations described in chapter 3, we observed the formation of a Pt(I) dimer after reduction of K_2PtCl_4 in aqueous solution. In a simulation cell filled with water molecules to model the solution environment, one electron was added to two $PtCl_2(H_2O)_2$ complexes. The reduction of one of the square planar complexes proceeds by loss of both water ligands, while the remaining chlorine ligands move far away one from the other until a linear $PtCl_2^-$ complex is formed. The reduced Pt(I) complex is able to react with the unreduced Pt(II) complex, forming a Pt–Pt bond along the z axes of the square-planar complex. The addition of a further electron promotes the loss of a chlorine ligand and a Pt(I) dimer is obtained. In chapter 4, we showed that both the Pt(II)–Pt(I) dimer and the Pt(I)–Pt(I) dimer are able to react again with $PtCl_2(H_2O)_2$ to form platinum trimers.

The addition of unreduced Pt(II) complexes to growing clusters has been investigated in chapter 4. We observed that $PtCl_2(H_2O)_2$ is able to react with Pt_{12}, $Pt_{12}Cl_4$, and $Pt_{13}Cl_6$ clusters. In all cases, a Pt–Pt bond is first formed between $PtCl_2(H_2O)_2$ and the cluster along the z axes of the Pt(II) complex. Then the chlorine ligands are adsorbed on the cluster surface, and the water ligand are either detached from the Pt(II) atom or remain bound to it. In a few picoseconds, the atom initially belonging to the Pt(II) complex is incorporated into the cluster structure and becomes indistinguishable from the other Pt atoms. Considerable rearrangement of the whole cluster structure is observed in all cases after the reaction with the Pt(II) complex.

The microscopic mechanism of Pt cluster formation

We have suggested that the formation of metal–metal bonds between complexes in oxidation states higher than zero is a key step in the nucleation mechanism of colloidal particles after the reduction of a platinum salt. The results of our FPMD simulations allowed us to formulate a mechanism of cluster growth which proceeds through addition of *unreduced* Pt(II) complexes to *only partially* reduced clusters and/or complexes. The following reduction to the zerovalent state requires an electron exchange between the reducing agent and a whole cluster. This is favoured over the reduction of single complexes prior to aggregation to the cluster. Indeed, due to the delocalization of the metallic orbitals, the electron affinity of the cluster is higher than that of the single Pt atom complexes [2] (cf. section 1.2). This is consistent with the autocatalytic nature of the reduction process [79], in which the presence of already formed clusters catalyzes the reduction of Pt(II) complexes [69, 76].

The growth process is expected to continue at least until a closed-shell configuration is reached. Indeed, the size distributions of monocrystalline colloidal particles of transition metals are often determined by series of *magic numbers* of atoms in the cluster corresponding to atomic and electronic closed-shell configurations (cf. section 1.1.3).

Only the very first reduction step is strictly necessary to start the aggregation process. Indeed, in the mechanism proposed here, a Pt(I) complex provides the starting point for the autocatalytic growth of a metallic cluster. That is, every Pt(II) complex which receives one electron from the reducing agent and is reduced to Pt(I) can be a nucleation center for the growth of platinum particles. This is in agreement with the experimental observation that, in most reduction methods, the formation of metal particles is a nucleation-dominated process [79, 89, 126].

Substrate-controlled cluster formation on DNA templates

According to the mechanism described above, the fundamental step of the whole cluster formation process is the initial reduction of Pt(II) complexes with forma-

tion of Pt dimers. Pt(II) complexes are able to bind covalently to biopolymers, and in particular form stable adducts with DNA molecules. In chapter 5 the heterogeneous formation of clusters on DNA molecules has been investigated. We found that if a Pt(II) complex is covalently attached to the DNA bases, then its reduction is favoured over the reduction of free Pt(II) complexes in solution. In addition, Pt dimers formed heterogeneously at DNA molecules after a single reduction step present a stronger Pt–Pt bond and are expected to possess higher electron affinity than the corresponding homogeneously formed dimers. Going through an autocatalytic growth mechanism, the first-formed heterogeneous nuclei may quickly develop into bigger particles, consuming the metal complex feedstock present in solution and thus completely hindering the homogeneous particle formation.

On the basis of this idea, in a team work with the experimentalists of our research group, we developed a procedure which led to purely heterogeneous metallization of DNA molecules (see figure 5.1). We consider this result as the first application of a new coating methodology where the biological metallization template actively promotes the deposition of metal under particular conditions. In this way, any inhomogeneity arising from spurious particle formation in solution is avoided. Because the kinetics of heterogeneous particle formation depends on the DNA base sequence, we suggest that selectively heterogeneous cluster nucleation and tailored substrate design may be combined to develop space-resolved metallization techniques in which metal structures are grown selectively on predefined portions of biological templates.

References

[1] P. Braunstein, L. A. Oro, P. R. Raithby editors, *Metal Clusters in Chemistry*; Wiley-VCH: Weinheim (1999).

[2] G. Schmid editor, *Clusters and Colloids*; VCH: Weinheim (1994).

[3] W. Ekardt editor, *Metal Clusters*; Wiley: Chichester (1999).

[4] A. Henglein, D. Meisel, *Langmuir* **14**, 7392 (1998).

[5] J. D. Aiken III, R. G. Finke, *J. Am. Chem. Soc.* **120**, 9545 (1998).

[6] T. S. Ahmadi, Z. L. Wang, T. C. Green, A. Henglein, M. A. El-Sayed, *Science* **272**, 1924 (1996).

[7] G. Pacchioni, S. Krüger, N. Rösch, in [1], pp.1392–1433.

[8] P. Ballone, W. Andreoni, in [3], pp.71–144.

[9] D. R. Jennison, P. A. Schultz, M. P. Sears, *J. Chem. Phys.* **106**, 1856 (1997).

[10] J. Belloni, M. Mostafavi, in [1], pp. 1213–1247.

[11] M. C. Payne, M. P. Teter, D. C. Allan, T. A. Arias, J. D. Johannopoulos, *Rev. Mod. Phys.* **64**, 1045 (1992).

[12] M. Mertig, R. Wahl, M. Lehmann, P. Simon, W. Pompe, *Eur. Phys. J. D* **16**, 317 (2001).

[13] J. Richter *et al.*, *Adv. Mater.* **12**, 507 (2000).

[14] E. Braun, Y. Eichen, U. Sivan, G. Ben-Yoseph, *Nature* **391**, 775 (1998).

[15] De Vita, A.; Canning, A.; Car, R. *EPFL Supercompt. J.* **6**, 22 (1994).

[16] F. A. Cotton, *Inorg. Chem.* **3**, 1217 (1964).

[17] F. A. Cotton, *Quart. Rev.* **20**, 389 (1966).

[18] N. Rösch and G. Pacchioni, in [2], pp. 5–88.

[19] U. Heiz, A. Sanchez, S. Abbet, W.-D. Schneider, *J. Am. Chem. Soc.* **121**, 3214 (1999).

[20] O. Rossell, M. Seco, G. Segalés, in [1], pp. 1053–1072.

[21] G. Schmid, N. Klein, B. Morun, A. Lehnert, *Pure & Appl. Chem.* **62**, 1175 (1990).

[22] P. L. Gogging, R. J. Goodfellow, *J. Chem. Soc. Dalton Trans.*, 2355 (1973).

[23] G. Schmid, R. Pugin, J.-O. Malm, J.-O. Bovin, *Eur. J. Inorg. Chem.*, 813 (1998).

[24] M. Faraday, *Phil. Trans. Roy. Soc.* **147**, 145 (1857).

[25] U. Simon, G. Schön, G. Schmid, *Angew. Chem.* **105**, 264 (1993); *Angew. Chem. Int. Ed. Engl.* **32**, 250 (1993).

[26] A. Ceriotti, F. Demartin, G. Longoni, M. Manassero, M. Marchionna, G. Piva, M. Sansoni, *Angew. Chem. Int. Ed. Engl.* **24**, 697 (1985).

[27] M. N. Vargaftik, N. Y. Kozitsyna, N. V. Cherkashina, R. I. Rudy, D. I. Kochubey, I. I. Moiseev, in [1], pp. 1364–1391.

[28] P. Chini, *Gazz. Chim. Ital.* **109**, 225 (1979); *Organomet. Chem.* **200**, 37 (1980).

[29] M. Mertig, R. Kirsch, W. Pompe, H. Engelhardt, *Eur. Phys. J. D* **9**, 45 (1999).

[30] M. Schmidt, R. Kusche, B. von Issendorf, H. Haberland, *Nature* **393**, 238 (1998); M. Schmidt, R. Kusche, W. Kronmüller, B. von Issendorf, H. Haberland, *Phys. Rev. Lett.* **79**, 99 (1997).

[31] B. Bigot, C. Minot, *J. Am. Chem. Soc.* **106**, 6601 (1984).

[32] G. M. Whitesides, J. P. Mathias, C. T. Seto, *Science* **254**, 1312 (1991).

[33] V. Percec, C.-H. Ahn, G. Ungar, D. J. P. Yeardley, M. Möller, S. S. Sheiko, *Nature* **391**, 161 (1998).

[34] K. Mc Grath, D. Kaplan editors, *Protein-Based Materials*; Birkhäuser: Boston (1997).

[35] M. Markowitz, S. Baral, S. Brandow, A. Singh, *Thin Solid Films* **224**, 242 (1993).

[36] R. Kirsch, M. Mertig, W. Pompe, R. Wahl, G. Sadowski, K. J. Böhm, E. Unger, *Thin Solid Films* **305**, 248 (1997).

[37] M. Mertig, R. Kirsch, W. Pompe, *Appl. Phys. A* **66**, S723 (1998).

[38] J. Richter *et al.*, *Appl. Phys. Lett.* **78**, 536 (2001).

[39] W. B. Sleytr, M. Sára, P. Messner, D. Pum, *J. Cell. Bionchem.* **56**, 171 (1994).

[40] R. Car, M. Parrinello, *Phys. Rev. Lett.* **55**, 2471 (1985).

[41] P. Hohenberg, W.Kohn, *Phys. Rev. B* **136**, 864 (1964).

[42] W. Kohn, L. J. Sham, *Phys. Rev. A* **140**, 1133 (1965).

[43] Gunnarsson, O.; Lundqvist, B. I. *Phys. Rev. B* **1976**, *13*, 4274–4298.

[44] R. G. Parr, W. Yang, *Density-Functional Theory of Atoms and Molecules*, Oxford University Press: Oxford (1989).

[45] J. M. Seminario editor, *Recent Developments and Applications of Modern Density Functional Theory*; Elsevier: Amsterdam (1996).

[46] E. Merzbacher, *Quantum Mechanics*; Wiley: New York (1970).

[47] M. Born, J. R. Oppenheimer, *Ann. Phys.* **84**, 457 (1927).

[48] A. Gross, *Surf. Sci. Rep.* **32**, 291 (1998).

[49] D. M. Ceperly, B. J. Alder, *Phys. Rev. Lett.* **45**, 566 (1980).

[50] J. P. Perdew, A. Zunger, *Phys. Rev. B* **23**, 5048 (1981).

[51] Perdew, J. P.; Wang, Y. *Phys. Rev. B* **45** 13244 (1992).

[52] White, J. A.; Bird, D. M. *Phys. Rev. B* **50**, 4954 (1994).

[53] P. J. Feibelman, B. Hammer, J. K. Nørskov, F. Wagner, M. Scheffler, R. Stumpf, R. Watwe, J. Dumesic, *J. Phys. Chem. B* **105**, 4018 (2001).

[54] H. J. Monkhorst, J. D. Pack, *Phys. Rev. B* **13**, 5188 (1976).

[55] Troullier, N.; Martins, J. L. *Phys. Rev. B* **43**, 1993 (1991).

[56] Kleinman, L.; Bylander, D. M *Phys. Rev. Lett.* **48**, 1425 (1982).

[57] X. Gonze, R. Stumpf, M. Scheffler *Phys. Rev. B* **44**, 8503 (1991).

[58] P. P. Ewald, *Ann. Phys. (Leipzig)* **54**, 519 (1917); *Ann. Phys. (Leipzig)* **54**, 557 (1917); *Ann. Phys. (Leipzig)* **64**, 519 (1921);

[59] M. Leslie, M. J. Gillan, *J. Phys. C* **18**, 973 (1985).

[60] G. Makov, M. C. Payne, *Phys. Rev. B* **51**, 4014 (1995).

[61] G. Pastore, E. Smargiassi, F. Buda, *Phys. Rev. A* **44**, 6334 (1991).

[62] N. D. Mermin, *Phys. Rev.* **137**, A1441 (1964).

[63] M. P. Grumbach, D. Hohl, R. M. Martin, R. Car, *J. Phys. Condens. Matter* **6**, 1999 (1994).

[64] N. Marzari, D. Vanderbilt, M. C. Payne, *Phys. Rev. Lett.* **79**, 1337 (1997).

[65] J. VandeVondele, A. De Vita, *Phys. Rev. B* **60**, 13241 (1999).

[66] M. Stengel, A. De Vita, *Phys. Rev. B* **62**, 15283 (2000).

[67] L. Colombi Ciacchi, W. Pompe, A. De Vita, *J. Am. Chem. Soc.* **123**, 7371 (2001).

[68] N. Toshima, K. Nakata, H. Kitoh, *Inorg. Chim. Acta* **265**, 149 (1997).

[69] A. Henglein, B. G. Ershov, M. Malow, *J. Phys. Chem.* **99**, 14129 (1995).

[70] Y. Mizukoshi, R. Oshima, Y. Maeds, Y. Nagata, *Langmuir* **15**, 2733 (1999).

[71] L. D. Rampino, F. F. Nord, *J. Am. Chem. Soc.* **63**, 2745 (1941).

[72] C. I. Sanders, D. S. Martin Jr., *J. Am. Chem. Soc.* **83**, 807 (1961).

[73] F. A. Cotton, G. Wilkinson, C. A. Murillo, M. Bochmann, *Advanced Inorganic Chemistry*, 6th ed.; John Wiley: New York (1999).

[74] A. Henglein, M. Giersig, *J. Phys. Chem. B* **104**, 6767 (2000).

[75] J. Turkevich, P. C. Stevenson, J. Hillier, *J. Discuss. Faraday Soc.* **11**, 55 (1951).

[76] D. G. Duff, P. P. Edwards, B. F. G. Johnson, *J. Phys. Chem.* **99**, 15934 (1995).

[77] V. K. LaMer, R. H. Dinegar, *J. Am. Chem. Soc.* **72**, 4847 (1950).

[78] V. K. LaMer, *Ind. Eng. Chem.* **44**, 1270 (1952).

[79] M. A. Watzky, R. G. Finke, *J. Am. Chem. Soc.* **119**, 10382 (1997).

[80] T. E. Müeller, F. Ingold, S. Menzer, D. M. P. Mingos, D. Williams, *J. Org. Chem.* **528**, 1163 (1997).

[81] Fuchs, M.; Scheffler, M. *Comput. Phys. Commun.* **119**, 67 (1999).

[82] Atoji, M.; Ritchardson, J. W.; Rundle, R. E. *J. Am. Chem. Soc.* **79**, 3017 (1957).

[83] Carloni, P.; Andreoni, W.; Hütter, J.; Curioni, A.; Giannozzi, P.; Parrinello, M. *Chem. Phys. Lett.* **234**, 50 (1995).

[84] Cui, Q.; Musaev, D. G.; Morokuma, K. *J. Chem. Phys.* **108**, 8418 (1998).

[85] Yang, S. H.; Drabold, D. A.; Adams, J. B.; Ordejón, P.; Glassford, K. *J. Phys.: Condens. Matter* **9**, L39 (1997).

[86] Gupta, S. K.; Nappi, B. M.; Gingerich K. A. *Inorg. Chem.* **20**, 966 (1981). Miedema, A. R.; Gingerich, K. A. *J. Phys. B* **12**, 2081 (1979).

[87] Sprik, M.; Hütter, J.; Parrinello, M. *J. Chem. Phys.* **105**, 1142 (1996).

[88] Nose, S. *Molec. Phys.* **52**, 255 (1984). Hoover, W. G. *Phys. Rev. A* **31**, 1695 (1985).

[89] P. R. Van Rheenen, M. J. McKelvy, W. S. Glausinger, *J. Solid State Chem.* **67**, 151 (1987).

[90] D. R. Lide, Ed., *CRC Handbook of Chemistry and Physics*; CRC Press: Boca Raton, FL, (1996).

[91] M. J. Frisch et al., *Gaussian 98*, Revision A.2; Gaussian, Inc., Pittsburgh, PA (1998).

[92] T. Leininger, A. Nicklass, H. Stoll, M. Dolg, P. Schwerdtfeger, *J. Chem. Phys.* **105**, 1052 (1996).
(Web address: http://theochem.uni-stuttgart.de/pseudopotentials).

[93] T. H. Dunning, Jr., P. J. Hay, in *Modern Theoretical Chemistry*, H. F. Schaefer, III, Ed.; Plenum: New York (1976), pp 1–28.

[94] J. P. Perdew, *Electronic Structure of Solids '91*; P. Ziesche and H. Eschrig, Eds.; Akademie Verlag: Berlin (1991). A. D. Becke, *Phys. Rev. A* **38**, 3098 (1988).

[95] A. Modinos, P. Woodward, *J. Chem. Soc., Dalton Trans.*, 1516 (1975).

[96] D. M. Adams, J. R. Hall, *J. Chem. Soc., Dalton Trans.*, 1450 (1973).

[97] R. F. W. Bader, *Atoms in Molecules—A Quantum Theory*; Oxford University Press: Oxford (1990).

[98] R. J. Gillespie, I. Bytheway, T.-H. Tang, R. F. W. Bader, *Inorg. Chem.* **35**, 3954 (1996).

[99] S. Otsuka, T. Yoshida, M. Matsumoto, K. Nakatsu, *J. Am. Chem. Soc.* **98**, 5850 (1976).

[100] J. J. Low, W. A. Goddard, III, *J. Am. Chem. Soc.* **106**, 6928 (1984). S. Obara, K. Kitaura, K. Morokuma, *J. Am. Chem. Soc.* **106**, 7482 (1984). J. O. Noell, P. J. Hay, *J. Am. Chem. Soc.* **104**, 4578 (1982). A. C. Balazs, K. H. Johnson, G. M. Whitesides, *Inorg. Chem.* **21**, 2162 (1982).

[101] A. Alexander, E. C. F. Ko, Y. C. Mac, A. J. Parker, *J. Am. Chem. Soc.* **89**, 3703 (1987).

[102] J. L. Zubimendi, L. Vázquez, P. Ocón, J. M. Vara, W. E. Triaca, R. C. Salvarezza, A. J. Arvia, *J. Phys. Chem.* **97**, 5095 (1993).

[103] R. J. Lawson, J. R. Shapely, *J. Am. Chem. Soc.* **98**, 7433 (1976).

[104] L. J. Farrugia, A. Guy Orpen, in [1], pp. 1001–1027.

[105] D. J. Wales, A. I. Kirkland, D. A. Jefferson, *J. Chem. Phys.* **91**, 603 (1989).

[106] N. Rösch, L. Ackermann, G. Pacchioni, *Chem. Phys. Lett.* **199**, 275 (1992).

[107] Allevi, C.; Heaton, B. T.; Seregni, C.; Strona, L.; Goodfellow, R. J.; Chini, P.; Martinengo, S. *J. Chem. Soc. Dalton Trans.* **1986**, 1375.

[108] M. Mertig, L. Colombi Ciacchi, R. Seidel, W. Pompe, A De Vita, *Nano Letters* **2**, DOI:1021/nl025612r (2002).

[109] R. Seidel, PhD thesis (in preparation).

[110] B. Lippert, Ed., *Cisplatin: chemistry and biochemistry of a leading anticancer drug* (Wiley-VCH, Weinheim, 1999).

[111] P. M. Takahara, A. C. Rosenzweig, C. A. Frederick, S. J. Lippard, *Nature* **377**, 649 (1995); P. M. Takahara, C. A. Frederick, S. J. Lippard, *J. Am. Chem. Soc.* **118**, 12309 (1996).

[112] J.-P. Macquet, T. Theophanides, *Biopolymers* **14**, 781 (1975).

[113] R. Seidel, M. Mertig, W. Pompe, *Surf. Interface Anal.* **33**, 151 (2002).

[114] J. Turkevich, P. C. Stevenson, J. Hillier, *J. Phys. Chem.* **57**, 670 (1953).

[115] P. Carloni, M. Sprik, W. Andreoni, *J. Phys. Chem. B* **104**, 823 (2000).

[116] T. G. Appleton, H. C. Clark, L. E. Manzer, *Coord. Chem. Rev.* **10**, 335 (1973).

[117] A. R. Rossi, R. Hoffmann, *Inorg. Chem.* **14**, 365 (1975).

[118] C. A. Mirkin, R. L. Letsinger, R. C. Mucic, J. J. Storhoff, *Nature* **382**, 607 (1996).

[119] A. P. Alivisatos *et al.*, *Nature* **382**, 609 (1996).

[120] J. L. Coffer *et al.*, *Appl. Phys. Lett.* **69**, 3851 (1996).

[121] T. Torimoto *et al.*, *J. Phys. Chem. B* **103**, 8800 (1999).

[122] W. Shenton, D. Pum, U. B. Sleytr, S. Mann, *Nature* **389**, 585 (1997).

[123] N. C. Seeman, *Trends in Biotechnology* **17**, 437 (1999).

[124] T. G. Spyro, Ed., *Nucleic Acid - Metal Ion Interactions* (Wiley, New York, 1980).

[125] S. B. Smith, Y. Cui, C. Bustamante, *Science* **271**, 795 (1996).

[126] J. V. Zoval, J. Lee, S. Gorer, R. M. Penner, *J. Phys. Chem. B* **102**, 1166 (1998).

Acknowledgments

This thesis has been written at the end of four years I spent in Dresden at the University of Technology in the material science and nanotechnology group directed by Prof. Wolfgang Pompe. He is the first I would like to thank because he convinced me to start my PhD in his group, gave me a wonderful theme to work out, and supported my work all these years with fruitful suggestions and original ideas. But not only for the scientific inputs I am indebted to Prof. Pompe. I will never forget his generous human impulses, his enormous charge of energy, and his sense of humor. If you saw Prof. Pompe singing "Es saßen die alten Germanen" on the guitar or playing old Christmas songs with the flute, you didn't work in Dresden in vain.

The atmosphere in the group and my colleagues were as friendly and special as the boss. Especially acknowledged is Dr. Michael Mertig, who followed my day-to-day research on DNA with passion and patience, and directed the combination of the theoretical simulations with the metallization experiments. Large part of the work of this thesis was planned and carried out together with him. I would like to thank Michael also for innumerable discussions about art, music, politics and cookery, and because he always remembered me that God made enough time for all of us.

I am very indebted to Ralf Seidel for the TEM pictures of chapter 5 of this thesis and for his marvellous work in the lab. He is the first man in the world who forged a platinum necklace by coating a DNA string with 5 nm small pearls of metal. Remo Kirsch, Jan Richter, Reiner Wahl, Alexander Kirchner worked hard on metallization of biomolecules, too, and all contributed to this work. They are kindly acknowledged.

An impressive contribution to this work has been given by Dr. Alessandro De Vita. I don't have enough words to thank him for all he did for me in these four years. Sandro introduced me to the first-principles molecular dynamics techniques, gave me his parallel code LAUTREC, followed and motivated every

step of my work with constant engagement, taught me how to write a scientific paper, invited me three times a year to Lausanne (often receiving me as a guest in his home), and above all he has been a very good friend. Having worked and discussed with him has meant for me a scientific and human enrichment of invaluable worth.

I am very grateful to Prof. Wolfgang Nagel for the huge quantities of CPU time he reserved for me on the supercomputers of the Center for High Performance Computing in Dresden. I think there is no other university in the world where a single user has more than 250.000 CPU-hours/year at his disposal. Jarmila Nyderle, Stefanie Maletti, Wolfram Heinrich, Claudia Schimdt and Stephan Seidl are kindly acknowledged for the administration and management of the supercomputers. Particular thanks to Rapunzel, Rapinzel, Ratbert and Romulus because they worked hard day and night under my supervision.

I would like to mention here (in a pseudo-random order) all other colleagues I had in Dresden. Sascha Tselev, who shared the office with me for three and a half years and has been a great friend. Burkhard Schmidt-Brücken, presently my roommate. Gerit Jänchen, Martin Tuckermann, Jens Bradt, Stefan Lampenscherf and Ingo Brasack, who are good *Kumpel*. Oliver Jost, Togmid Turmunkh, Jörg Möller and Uwe Thiele. André Gorbunoff, Brigitte Garske, Dieter Reiche, Hans-Achim Bahr, Martina Hentschel, and Rhena Krawietz. Joachim Förster, Ortrud Zieschang, and Jan Voigt. Johannes Rödel, Wieland Beckert, Manfred Bobeth, and Wolfgang Kreher. Michael Gelinsky, Reiner Burth, Karl Weiss, Andreas Sewing, Antje Reinstorf, Birgit Knepper-Nicolai, Anne Bernhardt, and Steffi Lenhard: The *Knochentruppe*. Ines and Jürgen Hofinger, Bettina Winzer, Sabine Matys, Annegret Benke, Astrid Börner, and Carsten Lau. André Gerbatsch and Albrecht Ullrich, the old and the new system manager, respectively. Albrecht is the type system manager every group would wish to have, thank you! Finally, especially acknowledged for their indispensable work are Ursula Feist, Ute Winkler and Margit Frenzel.

All funny people in knew in Lausanne are very kindly acknowledged, above all Massimiliano Stengel for his precious help in trying to solve the mysteries of

LAUTREC.

Among the many friends I found in Dresden, I would like to remember here all the volleyball players of the TU-Dresden team for the time I enjoyed with them all around Saxony and south-Germany.

Special thanks to Roberta for special reasons, to Federica and Giuliano, and to all old Italian friends. A loving thank you to my family: my mother Lucia, my sister Aurelia and my brother-in-law Roland. Finally, very particular thanks to Marleen, whom I owe most of the joy of living in Dresden.

HSSS AdminTools (c) 2001, last visited: Fri Aug 02 11:19:13 GMT+02:00 2002